PROTEIN SEPARATION IN PLASTIC MICROFLUIDIC DEVICES

By

CHAMPAK DAS

A DISSERTATION PRESENTED TO THE GRADUATE SCHOOL
OF THE UNIVERSITY OF FLORIDA IN PARTIAL FULFILLMENT
OF THE REQUIREMENTS FOR THE DEGREE OF
DOCTOR OF PHILOSOPHY

UNIVERSITY OF FLORIDA

2007

To my Parents

ACKNOWLEDGMENT

I would like to take this opportunity to express my deepest gratitude to my graduate advisor, Dr. Hugh Fan, for guiding me in my research work and his patience in going through every draft I gave him. Special thanks go to Dr. Cattafesta, Dr. Chauhan, Dr.Hahn, and Dr. Denslow for serving in my committee and providing valuable suggestion to me for my dissertation. I would like to thank Mr. Zheng Xia for fabricating silicon and glass masters, Mr. Carl Fredrickson for plastic device optimization, undergraduate students Mr. Fernando Tavares and Mr. Andrew Simon for helping me with device fabrication. I also would like to thank Dr. Alexander Stoyanov and Dr. Jiyou Zhang for helping me in understanding the fine points in electrophoresis and surface coating, as well as fruitful discussion on improving the resolution in two-dimensional separation. Special thanks go to my fellow graduate students Qian Mei, Ruba Knouf, Karthik Pitchaimani, Jackie Viren and undergraduate students Corey Walker and Joey Wilson for the wonderful time I had with them in the lab. Thanks are also due to my friends Anales, Alpana, Jaya and Nadim.

Finally, I would like to thank my family for their endless love, support and encouragement in the process of my learning.

This work was supported in part by Dr. Fan's startup fund from University of Florida and the grant from Army Research Office (ARO).

TABLE OF CONTENTS

page

ACKNOWLEDGMENT....4

LIST OF TABLES....7

LIST OF FIGURES....8

ABSTRACT....11

CHAPTER

1 INTRODUCTION....13

1.1 MEMS....13
1.2 Microfluidics....15
1.3 Electrophoresis....19
1.3.1 Isoelectric Focusing....19
1.3.2 SDS-PAGE Separation....21
1.4 Electrophoresis in a Chip....21
1.5 Current Challenges....23
1.6 Objectives....25

2 INSTRUMENTATION AND DEVICE FABRICATION....28

2.1 LIF Setup and Characterization....28
2.1.1 Introduction....28
2.1.2 Instrumentation....29
2.1.3 Photo Bleaching Effects....30
2.1.3.1 Detection limit....34
2.1.3.2 Optical correction....35
2.2 Device Fabrication....37
2.2.1 Introduction....37
2.2.2 Design and Fabrication....38
2.3 Conclusion....39

3 THEORITICAL AND EXPERIMENTAL RESULTS OF IEF....46

3.1 Introduction....46
3.2 Materials and Methods....46
3.3 Theory of IEF....47
3.4 Experimental Results....54
3.4.1 Effects of Separation Medium....55
3.4.2 Effects of Separation Length....57
3.4.3 Effects of Separation Voltage....59
3.4.4 Focusing Time....59

3.4.5 pH Gradient Compression 61
3.5 Conclusion 62

4 TWO DIMENSIONAL SEPARATION OF PROTEINS 71

4.1 Introduction 71
4.2 Materials and Methods 72
4.3 Polyacrylamide Gel Valve 74
4.4 IEF in First Dimension 76
4.5 Numerical Simulation 78
4.7 SDS-PAGE Separation 83
4.8 Two-dimensional Separation 84
4.9 Conclusion 89

5 CONCLUSION AND FUTURE DIRECTIONS 108

5.1 Conclusion 108
5.2 Future Direction 109

APPENDIX TRANSIENT SOLUTION OF IEF 112

LIST OF REFERENCES 123

BIOGRAPHICAL SKETCH 130

LIST OF TABLES

Table page

3-1 The effects of IEF distance on separation resolution. 63

4-1 Effects of gel thickness and mask width on photo polymerization process. 90

4-2 Comparison of resolution between different channel lengths and 2-D device 90

4-3 Five different labeled proteins used for 2-D separation....91

LIST OF FIGURES

Figure		page
1-1	Representation of electrical double layer near a surface.	26
1-2	Illustration of basic process of IEF.	26
1-3	Typical microfluidic devices used for electrophoresis work.	27
1-4	Different microfluidic devices for 2-Dimensional separation.	27
2-1	LIF imaging system for protein separations.	40
2-2	The fluorescence intensity values measured in microchannels with different laser power. The exposure of CCD camera is 100 ms.	41
2-3	Temporal profile of photo bleaching effects.	41
2-4	The cylindrical lens compresses the beam in one axis	42
2-5	Spatial profile of photo bleaching effects.	42
2-7	Optical correction for removing Gaussian noise background	44
2-8	The layout of microfluidic devices for protein separation.	44
2-9	E-form used for this research.	45
2-10	General methods for plastic device fabrication.	45
3-1	Illustration of separation process for closely spaced peaks.	64
3-2	The temporal images of IEF separations of GFP in polyacrylamide gel.	65
3-3	IEF of different proteins in gel and linear polymer.	65
3-4	Comparison of front speed for different separation medium	66
3-5	IEF of GFP, RPE in HPC/HEC linear polymer.	66
3-6	The effects of the separation distance on IEF separation.	67
3-7	Separation resolution based on peak width and separation distance.	68
3-8	The effects of separation voltage on IEF.	69
3-9	The relationship between the focusing time and the inverse of the electric field strength	69

3-10 Comparison of IEF electropherograms of GFP and RPE between pH 3-10 and pH 4-6 gradients. 70

4-1 Layout of a microfluidic device for two-dimensional protein separation....91

4-2 Photo polymerization in microchannels....92

4-3 Polymerization time with acrylamide concentration. 92

4-4 Polymerization time with HCPK concentration. 93

4-5 The schematic of photo polymerization of acrylamide inside the microchannel.. 93

4-6 Micrograph of the valve arrays formed by *in situ* gel polymerization. Polymerized gels are dyed for easy visualization. 94

4-7 IEF in different microfluidic devices. 94

4-8 Isoelectric focusing of 4 proteins (Paralbumin, Ovalbumin, BSA, and GFP) in cross channel. 95

4-9 2-D device used for numerical simulation. 96

4-10 Transfer of negative species from cross channel to parallel channels due to an applied electric field of 100 V/cm. 97

4-11 Transfer of protein plugs into parallel channel due to application of electric field. 98

4-12 Protein migration pattern in all 29 parallel channels. 98

4-13 Electric field distributions at different location across the parallel channel. 99

4-14 Experimental results of location of protein front with respect to time. 100

4-15 SDS-protein complex migration pattern in Gel due to application of electric field. 101

4-16 IEF for RPE with and without SDS in 5 cm channel. The electric field is 500 V and pH gradient is 3-10....101

4-17 The transfer of GFP and RPE in second dimension after IEF is performed in first dimension. 102

4-18 2-Dimensional migration of a single protein. A) IEF of BSA in cross channel.. 102

4-19 2-Dimensional separation of three proteins. 103

4-20 2-Dimensional separation of three proteins (BSA, Ovalbumin and Trypsin) in lower pH gradient (3-5 pH) during IEF operation. 104

4-21 2-Dimensional separations of three proteins (BSA, Ovalbumin and Hemoglobin) in 3-10 pH during IEF operation. 105

4-22 2-Dimensional separation proteins for proteins BSA (1), carbonic anhydrase (2), ovalbumin(3) and trypsin (4). 106

4-23 2-D map for BSA, ovalbumin, hemoglobin and carbonic anhydrase in 10% acrylamide gel. 107

5-1 The mask size is increased such that 500 μm on both the sides of cross channel is left unpolymerized after UV exposure. 111

A-1 Assumed charge distribution for different CA/ proteins in IEF focusing process for nonlinear case 119

A-2 Assumed charge distribution for different CA/ proteins in IEF focusing process 119

A-3 Evolution of Gaussian peak with time for a particular ampholyte.. 120

A-4 Numerical results for front speed of CA/ proteins with time at different. applied electric field. 121

A-5 Conductivity plotted with respect to time at different electric fields. 122

Abstract of Dissertation Presented to the Graduate School
of the University of Florida in Partial Fulfillment of the
Requirements for the Degree of Doctor of Philosophy

PROTEIN SEPARATION IN PLASTIC MICROFLUIDIC DEVICES

By

Champak Das

August 2007

Chair: Hugh Fan
Major: Mechanical Engineering

Conventional two-dimensional gel electrophoresis has been extensively used for proteomics research, including discovering biomarkers associated with a disease. However, the process is time consuming and labor intensive. To address the limitation, a plastic microfluidic device (1"x 3") is developed that is capable of doing the same operation in a much shorter time with less labor. The devices are fabricated by compression molding, a similar technique for manufacturing compact discs. First two different separation mechanisms isoelectric focusing and polyacrylamide gel electrophoresis (PAGE) are separately demonstrated in microdevices. Isoelectric focusing (IEF) is optimized in terms of the applied voltage and separation medium. It is demonstrated that IEF is essentially independent of channel length, allowing miniaturization of separation apparatus. The time required for IEF is also drastically reduced when the channel length is reduced. It takes only 3–5 minutes in a 2 cm channel compared to 10–12 hours in conventional apparatus. Further integration is achieved by selective photo polymerization inside microchannels, obtaining a reliable interface that prevents one separation medium from contaminating with the other medium. PAGE takes another 5 minutes to perform. When these two separation mechanisms are integrated, it takes about 15 minutes from loading the samples to finishing the experiment whereas the conventional system takes more than a day to finish. A

laser induced whole channel fluorescence imaging system is assembled for detecting the proteins separated in the devices. The sequential images obtained from the imaging system helps in understanding the dynamic nature of protein separation such as IEF. The same imaging system can be used for single point detection for two–dimensional separation. The detection limit for this system was found to be around 1 nM of fluorescien solution and 0.03 ng/μl when Green fluorescent protein is used in isoelectric focusing. Fluorescently labeled proteins are used to demonstrate the viability of the miniaturized two–dimensional protein separation system.

CHAPTER 1
INTRODUCTION

Technology has come a long way from Eckert and Mauchy's 1946s 'Eniac', a 50-ton computer that filled an entire room, to a palmtop of today's world, many times powerful than its predecessor. System miniaturization has benefits, including less power required, portability and, in most cases, fast and reliable operation. Miniaturized systems can be optimally linked together in order to achieve specific mechanical, electrical, optical or chemical functions either one at a time or all combined together. In a broad sense, they take inputs from external stimulus, make decisions and give output.

Miniaturized systems, though very exciting in terms of size and integration of several functionalities in one small package, also prove to be a challenge to fabricate and integrate with other functional parts. As the parts get smaller, newer physical phenomena inapplicable or negligible to their larger counterparts start creating problems. Nevertheless, newer applications have been realized by finding an intelligent way to avoid these problems or making use of them. Although miniaturization has affected many facets of science, I will, in this thesis, focus on two areas, microelectromechanical systems (MEMS) and microfluidics. Subjects covered by these two terms overlap sometimes; but their definition and differences will be explained below. Since the application of this thesis is primarily related to electrophoresis, I will also review the technique briefly.

1.1 MEMS

A microelectromechanical system (MEMS) is an integration of sensors, actuators and other electrical or mechanical components, usually fabricated in a silicon substrate. This is achieved through microfabrication technology originally developed in the '60s for computer chips. With improvement of microelectronics, MEMS is poised to affect many parts of our life.

The fabrication of silicon devices is the most important part of MEMS and the process is well developed. A brief description of silicon fabrication relevant to this research is as follows. A silicon wafer is washed with tetrachloroethylene, acetone, methanol and deionized water before use. A photoresist is placed on the wafer and then spun at high speed to a thickness of a few microns and then baked. A pattern is exposed using a mask aligner with UV light and is then developed. The wafer is baked again, followed by deep reactive ion etching (DRIE), the left over photoresist after etching is removed by plasma etch. This etching process produces microchannels, which are used for most of the work described herein. Though silicon devices are not used directly for any experiment in this research, they are primarily used as a master to make plastic devices, which will be explained in later Chapters.

One of the most successful applications of MEMS is the inertial sensing technology.[1] Accelerometers in airbags are now used in millions of cars produced. Another important use of MEMS is micro mirrors, which can be used in a host of applications such as projection devices, scanners, laser printers and portable communication devices. More traditional MEMS-based devices are pressure sensors, which can be used in tire pressure sensing or in monitoring the pressure in the medical field. Radio frequency applications using MEMS are also proving to be popular nowadays. According to Nexus market analysis the market will grow at 16% per year from $12 billion in 2004 to $25 billion in 2009 for different MEMS products, with new fields of application coming up every year.

Another major application of MEMS is in the biomedical field. This has lead to emergence of a new field called biological microelectromechanical systems (BioMEMS).The inherent characteristics of BioMEMS lead to design and fabrication of miniature, smart and low cost biomedical devices which have potential to revolutionize the biomedical research and clinical

practice. The success of BioMEMS in industry is dependent on a few issues. First unlike MEMS, BioMEMS devices are mostly non-silicon based. While the silicon-based fabrication process is well understood and theoretical models are available for designing them, non silicon materials like PDMS, plastics and glasses are not. Hence device design and fabrication takes longer time. Second BioMEMS devices are cost-sensitive when compared to silicon devices, as for most of applications it is desirable to use disposable units. Other issues include biocompatibility, packaging, closed loop monitoring and controlling techniques, and power required for driving them. Important research thrusts related to BioMEMS include cell manipulation, cell separation, drug delivery on cellular level, retinal implants,[2] neural implants in central nervous systems, tissue engineering, and artificial organ creation. Cell separation among them is quite successful using BioMEMS.

There are several methods to achieve this, the most popular of which is di-electrophoresis.[3-5] Depending on the frequency of an alternating current and the size of the cell, the living and dead cells can be directed towards either the positive electrode or negative side of electrode. Other techniques include flow fractionations[6] based on electrophoresis, electroosmosis, pressure driven, optical switching[7] and using boundary layer manipulation.[8] A discussion on the topic will be provided in detail in Chapter 5.

1.2 Microfluidics

Microfluidics involves similar techniques of microfabrication, which is used to make microchannels and microfeatures in silicon, glass, or other materials. However the emphasis is on the fluid movement inside the channel as the name suggests. The research on microfluidics was first initiated about 30 years ago at Stanford University,[9] where miniaturization of a gas chromatograph was successfully implemented in a silicon wafer. Since then, more complex devices have been developed for many applications, for instance, chemical analysis to the benefit

of biochemists. Since movement of fluid is the underlying factor in microfluidics, great deal of research work has gone into modeling and understanding the various physical attributes of fluid behavior in the microscale.

Movement of fluid will invariably require some controls applied to it. Valves and pumps are most common ways to manipulate liquids inside the channel. The valves, due to planar nature of microchannel, tend to have 2-D structures. The small size of valve gives a faster response and has lower power requirement, but it tends to get clogged easily, and is very difficult to remove the clogs from the microchannels. Still there are many of designs available for valve actuations in literature including piezoelectric,[10] thermopneumatic,[11] electrostatic,[12, 13] electromagnetic[14, 15] and bimetallic.[16]

Similarly there are different types of propulsion system available for moving liquid inside the microchannel like thermocapillary,[17] electroosmosis,[18] electrohydrodynamics, magnetohydrodynamics,[19] pressure gradients etc. Micro pumps are also very common in these systems. Mechanical pumps have the same problems as valves and actuators, namely moving parts, clogging in addition to the problems of low flow rates and pressure. Pumps without any moving parts also have been designed, like diffuser/nozzle pumps,[20-22] electrohydrodynamic pumps[23] and electroosmotic pump.[24] Since this thesis will focus on electrophoresis (related to movement of charged particles under the influence of electric field), pumping using electroosmosis is discussed in detail below.

When a liquid is placed inside a microfluidic channel, the inner surface of the channel acquires charge. This is due to adsorption of ions from buffer onto the channel surface. In case of fused silica, the surface silanol (Si-OH) groups are ionized to negatively charged silanoate ($Si\text{-}O^-$) group. These negatively charged groups then attract the positively charged cations from the

buffer, which form an inner layer and are tightly held in position due to strong ionic interaction. But these cataions are not enough to achieve neutrality for the silanoate groups. Hence another outer layer of cation is formed, which is mobile in nature. When an electric field is applied, this mobile layer is attracted towards negatively charged chathode. Since this outer layer is not strongly attracted by silanoate group, it moves and drags the bulk fluid along with it. Figure 1 shows the schematic of such a double layer, where the wall is negatively charged. The first layer which is closest to the wall is immobile and is called the Stern layer. The next layer is called Gouy-Chapman layer, where the ions are free to diffuse into the bulk fluid. The plane separating these two layers is called shear plane. Figure 1b shows the sketch of the potential associated with this double layer. The potential at the shear plane is called the zeta potential.[25]

Electroosmotic flow (EOF) results when an electric field is applied through a liquid-filled microchannel having electrical double layer (EDL). The flow results from the ion drag on the fluid in the EDL.

The observed velocity of a particle in this system can be given by the following relationship

$$v_{Observed} = E\left(\mu_{EOF} + \mu_{EP}\right) \quad (1)$$

where $v_{Observed}$ is the velocity in cm/s, E is the electric field strength in V/cm, and μ_{EOF} and μ_{EP} are the electroosmotic and electrophoretic mobility, respectively, in units of $cm^2/s\ V$. The electroosmotic mobility is a measure of the speed of neutral material in the channel, and can be found by the relationship

$$\mu_{EOF} = \frac{\delta e}{\eta} \quad (2)$$

where δ is the thickness of the diffuse double layer in cm, *e* is the charge per unit surface area (coulomb/cm^2), and η is the viscosity in g/cm·s. It is desirable to reduce or eliminate EOF in some instances, and this can be accomplished by increasing the viscosity of the liquid in the channel. The electrophoretic mobility is a measure of the speed of charged particles in the channel (which are more attracted to the anode or cathode than a neutral particle), and is related to a particle's charge in coulombs, *q*, and radius in cm, *r*, by the equation

$$\mu_{EP} = \frac{q}{6\pi\eta r} \tag{3}$$

EOF is important when considering flow in microscale as it effects the flow condition. Some of the electrophoretic technique uses EOF to its advantage, while it is detrimental for some other techniques like isoelectric focusing (see Chapter 3). EOF is also used for development of EO pump in microchannels.

Overall, microfluidic systems are relatively new when compared to MEMS in terms of research work; however it has been successfully applied to quite a few commercial applications such as inkjet printing. The other application of microfluidics that has attracted immense importance is chemical analysis and separation technology The chemical analysis in microfluidic format can be traced back to the 1980's, much before the development of field of microfluidics itself. However the rapid development of microfluidics has immensely improved the chemical analysis system.

As the microfluidics technology has matured in last decade, many chemical processes like separation, detection and purification could be miniaturized in microfluidic format. In an analytical operation, there is sampling, preliminary treatment, separation, purification, measurement and interpretation. It is a dream of chemist to have all of them integrated in one platform. The microfluidics brings about several advantages including a) smaller size, b) faster

operation, c) lower reagent consumption, d) higher selectivity, e) lower detection limit, f) better precision and g) lower cost of fabricating a device. This has lead to a related concept called "lab on a chip" (LOC) where one can have total chemical analysis system (TAS) in miniaturized format. Manz et al.[26] first introduced the term μ-TAS based on this concept in 1990. One of the most important components of μ-TAS is separation of macromolecules in liquid medium. Electrophoresis is one such technique for separation of electrically charged macro molecules like proteins, peptides, deoxyribonucleic acids (DNA) or particles under the influence of electric field in a conductive medium. The general form of electrophoresis is very well developed and has been in practice for the last 100 years, and is usually done in the macro scale. Below is a brief history of electrophoresis techniques available.

1.3 Electrophoresis

Separation of different electrolyte phases under an electric field was first observed in the early nineteenth century and the first quantitative work was done by Friedrich Kohlrausch in 1897.[27] Thereafter significant work was done on the determination of ionic conductivities and the mobility of different electrophoretic systems. It was not until 1920's that Tiselius first adopted this process for separation of proteins and colloids. The use of polyacrylamide gel leads to dramatic improvements in separation technique because of its non-ionic nature, low protein adsorption, minimal electroosmosis and anti-convective nature of the gel. Svensson further refined the technique by using ampholytes for stabilizing the pH gradient under the electric field. This process is known as isoelectric focusing (IEF) and is discussed next.

1.3.1 Isoelectric Focusing

IEF is carried out in a pH gradient, which can be created by carrier ampholytes or an immobilized pH gradient. Under an electric field, a protein migrates along the pH gradient (pH

increases from anode to cathode) and is eventually focused at a location where the pH value is equal to its isoelectric point (pI), which is the pH at which the net charge of the protein is zero.[28, 29] At the pI location, a dynamic equilibrium between IEF focusing and diffusion keeps the protein remaining in place.[30] Since each protein has its unique pI, proteins can be separated along a pH gradient. Figure 1-2 shows the schematic of IEF.

In his first seminal paper, Svensson pointed out that formation of uniform pH gradient formation, there needs a large number of low-molecular-weight amopholytes with low buffering capacity and different isoelectric points. These ampholytes were first synthesized through a reaction of acrylic acid with oligoamines by Vesterberg (1969) and was made commercially under the name 'Ampholine'. This process was a huge success because of its very high resolution and was quickly adapted by labs around the world.

IEF is usually carried out in polyacrylamide gel (3% to 5% T, '%T' defines the total amount of polymer concentration in solution). This gel is a mesh-like structure and has very less electroosmotic flow, which is advantageous for IEF process. However there is one disadvantage of using polyacrylamide (PAA) gel, when it is used to separate high molecular weight proteins. When high molecular weight protein is bigger in size than the pore size of the mesh-like PAA gel, it will not be able to travel towards its pI point. Several researchers[31-33] have proposed agarose gel as a suitable alternative to PAA. This is also popular but this has some electroosmotic flow. Linear polymers are also popular among researchers since they are viscous, preventing convection with no sieving effects. Alongside Righetti et al.[34-36] invented a technique to covalently bond the pH gradient to the gel matrix and marketed it under the name "Immobilines." With an immobilized pH gradient, there will be very less electroosmotic flow

and also the resolution can be as high as 0.001 pH unit. All these mediums can be used for IEF process.

As mentioned above the sieving effect in PAA gel is used advantageously for protein separation on the basis of size. This topic is discussed next.

1.3.2 SDS-PAGE Separation

The separation of proteins can be achieved based on their sizes. Sodium dodecyl sulphate (SDS) is used to facilitate this purpose. SDS is highly anionic in nature and helps to denature the proteins. Merceptoethanol is used first to open up the di-sulphide bonds of the proteins. The negatively charged SDS then attaches to proteins to form complexes with similar charge-to-size ratio. The resultant electrostatic repulsion tends to make the proteins rod-like structures. These proteins are then subjected to the electric field. While they move through the mesh-like polyacrylamide gel structure, they get separated based on the size of complexes. Usually the migration velocity shows an inverse relationship to logarithm of molecular weight.

O'Farrell[37] designed a methodology of combining IEF and SDS-PAGE gel electrophoresis and his protocol is still widely followed with minor modifications. This method uses the samples in fully denatured condition and the second dimension used different gradient of polyacrylamide gel for improved resolution.

1.4 Electrophoresis in a Chip

Electrophoresis in microscale glass devices was first reported in 1993 by Harrison et al.[38] Early work was based on glass or silicon. Each microfluidic device was individually fabricated, requiring time consuming fabricating procedures.[39] Nowadays materials like plastic and flexible polymer are used to fabricate devices, which can be batch produced, taking less time. The fabrication process for glass is discussed here in brief. Thin layers of metal and photoresist are applied to the surface of glass. The photoresist is masked and exposed to UV light to form a

pattern, which is then etched to define the channels. The channels are sealed by thermally bonding a glass cover sheet. Flexible polymers such as polydimethylsiloxane (PDMS) have made the fabrication comparatively easy.[40, 41] A pattern can be made in SU-8 on a glass or silicon substrate, and it is used as master, from which PDMS can be cast. Due to flexible nature of PDMS, it is easy to peel off from master, and the master can be used for a number of times.

More recently plastic microfluidic devices[42, 43] have become popular because a) they can be made in bulk, b) raw materials are comparatively cheap, c) have very good optical properties for UV/Visible detectors, d) have structural rigidity and e) most importantly, the materials are almost inert to most of the macromolecules. Compared to silicon or PDMS, these plastic devices are more rigid thereby ensuring ease of handling and also cheap to fabricate. Usually the plastic devices are made by embossing or injection molding, though other fabrication techniques such as laser ablation and compression molding have been reported in laboratory settings. This research work uses plastic device that are fabricated using compression molding, whereby resin pellets are pressed against a nickel mold. The fabrication technique will be discussed further in detail in Chapter 2.

Usually in microscale electrophoresis, the device consists of a main channel for separation with side channels for sample introduction. The entry to those channels is done by creating wells as can be seen in a typical device shown in Figure 1-3.

The main channel (AB) is usually filled with buffer/separation solution; the sample to be separated is injected either by pressure or EOF through a side channel (CD). An electric field is then applied to main channel (AB) to perform electrophoresis. Once the constituents are separated, they can be detected by a detection system. Different types of excitation sources like UV illumination or laser induced fluorescence (LIF) are available. UV detection can be applied

to many compounds, but its sensitivity is low, whereas LIF is applied only to fluorescent molecules but has very high sensitivity. For those compounds that are not naturally fluorescent, they may be tagged by fluorescent molecules for LIF.

Microscale electrophoresis has proved to be so successful that a few commercial products are available in the market, including instruments for electrophoresis from Agilient and Bio-Rad. Extensive research work is going to integrate multidimensional separation in chip format. This research focuses mainly in this aspect, and is discussed briefly in objective section below.

1.5 Current Challenges

The objective of this research is to miniaturize 2-D slab gel electrophoresis system into microfluidic chip format, study the separation process and develop an optical detection setup for the same. A short review on the work done so far in scientific community is discussed with current challenges that need to be solved before it can put into regular use instead of slab gel system.

1.5.1 Literature Review and Challenges: The grand challenge in microfluidics is to integrate the different components like valves, pumps, different separation mechanism, detection system etc. in one compact system. There have been several reports of standalone separation systems like isoelectric focusing[44, 45], free solution electrophoresis[46], SDS-PAGE[47], but very few attempts have been made to integrate them. While it is comparatively easy to perform standalone systems, it is extremely difficult to integrate them because of chemical incompatibility, physical problems related to flow or difficulty in pumping the reagents from one location to others. The first effort in 2-dimensional protein separation was reported by Chen et. al.[48] in 2002. They fabricated a complicated 3-dimensional structure of PDMS as can be seen from Figure 1-4.

The device design is very complicated and involved six layers of PDMS. The device consists of a 25 mm long horizontal channel for IEF and several parallel channels (60 mm long).

The fabrication of this device requires alignment, bonding, removal, realignment and rebonding. The feasibility of such device is demonstrated with limited experiments. This system has a problem of proteins traveling in multiple channels in SDS-PAGE separation.

More recently in 2004 Li et. al.[49] tried to do the 2-D separation in plastic microfluidic device. They had one cross channel and several parallel channels embossed in polycarbonate substrate. The cross channel is used for IEF and parallel channels are used for SDS-PAGE. Figure 1-5 shows the device they have used for their experiment.

The main problem for this experiment is that they have used liquid medium for both the separations. Parallel channels are filled up with one liquid medium (SDS-PAGE) and cross channel with another liquid medium (IEF). This gives a serious problem of cross contamination of the liquids at the junction of cross channels with parallel channels. Since there is no solid physical boundary at the junction of cross channel with parallel channels, the proteins may diffuse into the parallel channels even before they are focused. These diffused proteins will then be present in all the parallel channels and will give false peaks in the second dimension separation. Also the parallel channels are spaced 1 mm apart. This reduces the resolution of the effective resolution of IEF quite appreciably as even if the proteins are separated in IEF channel; the separated proteins in between two parallel channels will go to one single channel. So there still remains a major challenge of integrating the two separation mechanism (IEF and SDS-PAGE) with proper resolution in a single device. The simplicity in device fabrication will ensure lower cost and disposability. Plastic is both rigid and cheap and optically transparent for detection when compared with PDMS. Hence plastic is chosen for my research work. Simple design of one cross channel and multiple parallel channels are chosen for easy sample loading and ease of experiment. However instead of using liquid medium for both the separation

mechanism (as in Li et.al.), second dimension separations in parallel channels are performed in gel. All the channels except the cross channel is polymerized. This will prevent the cross contamination of two separation medium. Presence of gel on the junction of cross channel with parallel channel will prevent easy diffusion of proteins onto the parallel channels. The parallel channels are also designed to be closer than previous designs as it will make the separation more precise. Both IEF and SDS-PAGE are separately evaluated in plastic microfluidic device and their parameters are optimized before the integration of both of them is tried. IEF is optimized with respect to channel length and electric field to find out the best parameters and SDS-PAGE is optimized with respect to gel strength, buffer concentration and electric field. These conditions are then used to integrate the two separation mechanism in one device. The outlines of the subsequent Chapters are given in the following paragraphs.

1.6 Objectives

Chapter 2 discusses a whole channel image detection system for IEF in a microfluidic chip. Laser induced fluorescence detection is used. The photo bleaching effect of the fluorophore molecules due to laser illumination is investigated and an optimum condition with minimum photo bleaching was found for IEF. In addition device fabrication for plastic microfluidic chips is also discussed.

Chapter 3 describes the dynamics of isoelectric focusing of proteins in microfluidic devices. Theory for isoelectric focusing process is discussed and the experimental results are compared with theoretical results.

Once the IEF process is optimized in microfluidic devices, a device consisting of one cross-channel for IEF process and several parallel channels for SDS-PAGE separation is designed and fabricated as discussed in Chapter 4. The device is then tested for two separation mechanism (IEF and SDS-PAGE). IEF is performed first on the cross channels followed by

SDS-PAGE in parallel channels. Critical parameters are discussed; optimization is done to attain the high separation resolution in both the separation mechanism.

Chapter 5 discusses the conclusion and future of the work.

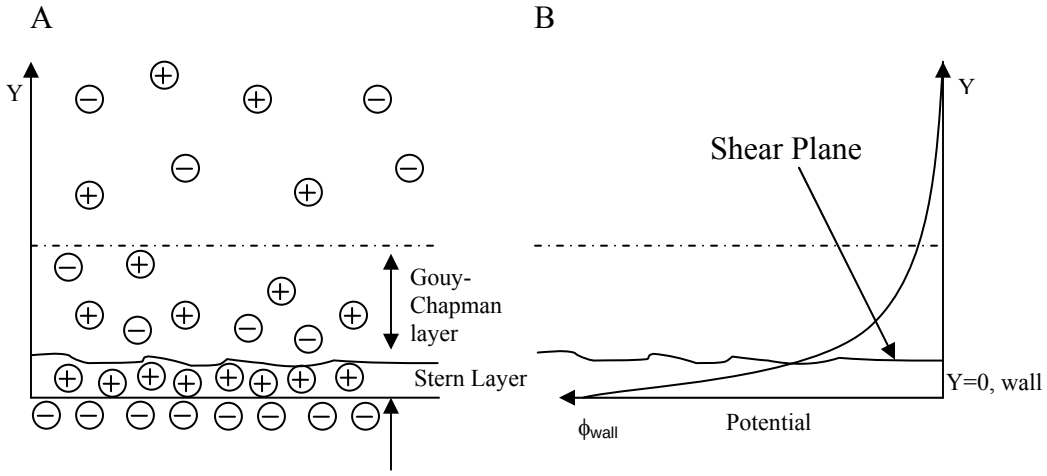

Figure 1-1. Representation of electrical double layer near a surface. A) The distribution of ions near the surface can be divided into two layers, closely packed ions in stern layer, and more freely moving ions in Gouy-Chapman layer. B) Plot of potential near the wall of a negatively charged wall showing zeta potential, wall potential and shear plane.

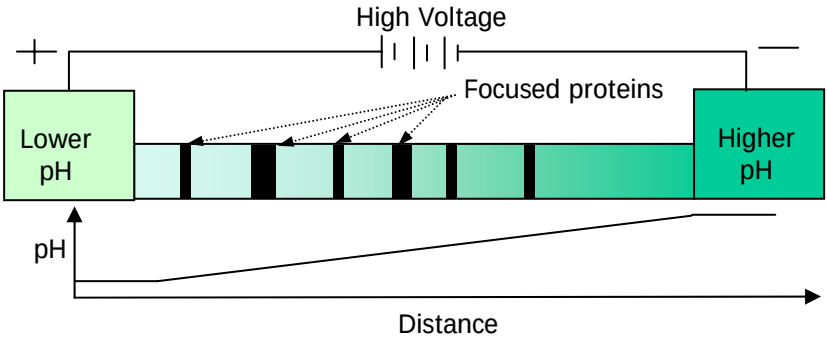

Figure 1-2. Illustration of basic process of IEF, ampholytes gets focused with application of electric field, creating uniform pH gradient in which protein migrate to their pI point and remain there in dynamic equilibrium. The focused proteins can be seen as dark bands.

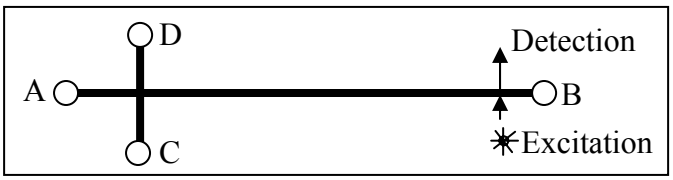

Figure 1-3. Typical microfluidic devices used for electrophoresis work. AB is the main channel where the electrophoresis is performed. The sample is introduced from side channel CD. The detection shown here is one point detection where an excitation source illuminates a single point and the detector detects the change in intensity due to either absorption or emission by samples.

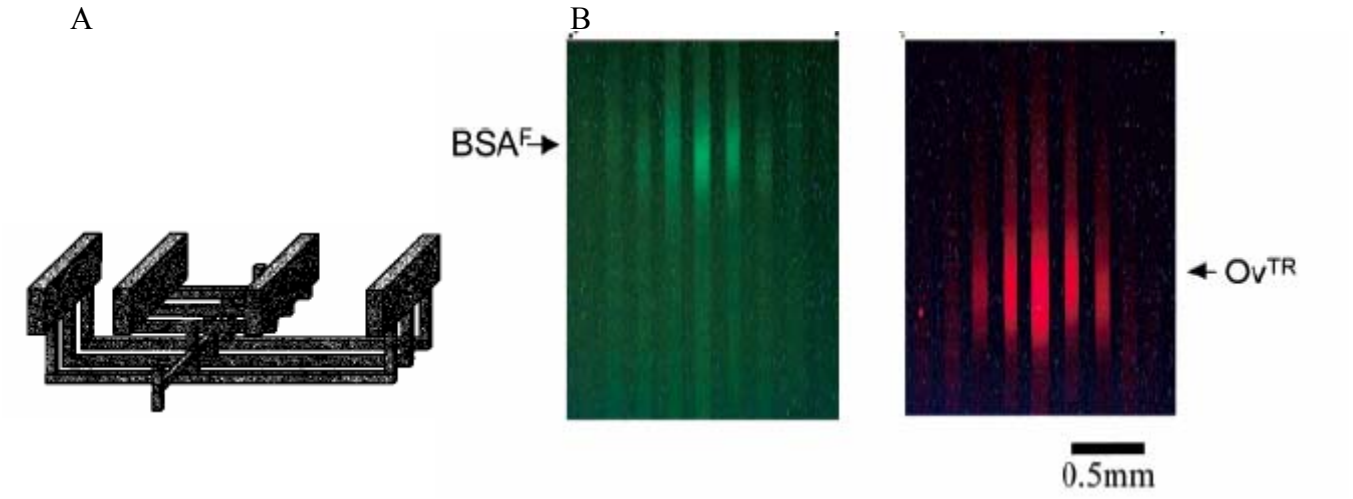

Figure 1-4. Different microfluidic devices for 2-Dimensional separation. A) 3-Dimensional structure in PDMS. B) Separation of BSA and ovalbumin in the PDMS device. [Reprinted with permission from Chen, X.; Wu, H.; Mao, C.; Whitesides, G. M. *Anal Chem* **2002**, *74*, 1772-1778]

CHAPTER 2
INSTRUMENTATION AND DEVICE FABRICATION*

2.1 LIF Setup and Characterization

2.1.1 Introduction

Fluorescence is an optical phenomenon, where a fluorophore molecule absorbs a high energy photon and re-emits it as a low energy photon. The absorption of energy leads to the electronic transition of an electron to an excited state. The excited electron then drops back to its ground state emitting energy in form of fluorescence. The energy difference between the absorbed and emitted light is expressed in the form of molecular vibration (heat energy). The wavelength emitted is dependent on the absorbance curve and Stokes shift of a particular fluorophore molecule.[50] Use of a laser as an exciting source is popular because of the selectivity of the wavelength and high energy density availability.

Laser-Induced Fluorescence (LIF) detection is a widely used method in capillary electrophoresis (CE) and microfluidic devices because of its high sensitivity. Most LIF systems use one point detection, in which a laser beam continuously illuminates a fixed point along the separation capillary (or channel) to detect the signal when fluorescent molecules pass by.[51] For IEF applications, however a considerable length of channel needs to be illuminated and imaged because proteins do not move after focusing and any effort to move them for single point detection results in distortion of peak resolution, destruction of pH gradient and longer analysis time. This whole-channel imaging is important because it can also give dynamic information of separation process like protein-protein interaction and protein front evolution with time.

* A part of this Chapter has been published: Das, C.; Xia, Z.; Stoyanov, A.; Fan, Z. H. *Instrumentation Science and Technology*, 33, 379-389,2005

Sensitivity and detection limit of the LIF system depends on the efficiency of fluorescence emission and selective collection of that emission from background noise. The fluorescence emission depends on laser intensity, uniformity of the line beam, and photo bleaching of fluorophore molecules. The impact of photo bleaching has been studied using single-point detector and the study suggested that photo bleaching process takes place in accordance with a first-order rate Equation in its simplest form.[51] This Chapter is to investigate photobleaching in microchannels using the whole channel imaging scheme. Also studied are the effects of laser intensity, uniformity of the line beam, and photo bleaching on the detection sensitivity and characterization of the imaging system for protein separations.

2.1.2 Instrumentation

A LIF imaging system is assembled in house and it is schematically illustrated in Figure 2-1. The light source is an Ar^+-ion laser (488 nm, 30 mW, JDS Uniphase, Model no: 2214-30sl, 0.69 mm beam diameter @ $1/e^2$), which is directed by mirrors to a beam expander (HB-20X, Newport). For isoelectric focusing, an average power of 3 amps (~ 6 mW) is used whereas for second dimension separation, power up to 20 mW is used. The laser has to be run for at least 5 minutes prior to any experiments to stabilize. The beam expander (Newport: HB 20 XAR.14) converts the laser into a column of light, which is focused into a line beam (15 mm) using a cylindrical lens. A capillary or a microfluidic device is mounted via a holder onto an XYZ translation stage, which is used for aligning the device to the position of the beam. It is tricky to adjust the beam expander with the laser line. The laser is adjusted with the help of mirrors to shine a spot on the microfluidic device. The device is kept on fixture so the final laser position is fixed. The beam expander is adjusted in such a way that laser beam glances the external surface of the beam expander. Since the beam expander is circular cylinder, when the beam glances the outside surface it should be parallel to the cylinder surface giving the indication that the angle of

beam expander is right. The expander then moved and then placed exactly in the right position so that the laser beam comes out as expanded beam with Gaussian intensity distribution. The slight adjustment needed can be done by changing the mirror angle and the adjusting the knobs in the expander itself. A scientific-grade, cooled charge-coupled device (CCD) camera (14 bit digital, 2184 x 1472 pixels, Apogee) is mounted vertically above the microfluidic device. The fluorescence emission is collected by the camera after passing through a band pass filter (HQ535/50 nm, Chroma Technology, Rockingham, VT). The CCD array size is 6.8 μm x 6.8 μm. The dynamic range of the camera is 77 dB.

For IEF, a high voltage power supply (0-3 kV, Glassman High Voltage Inc., High Bridge, NJ) is used. The power supply is controlled by a computer using software written in Labview (National Instrument, Austin, Texas). A 10-KΩ resistor is connected in series between the channel and ground electrode so that the current in the device can be monitored by measuring the voltage drop across the resistor. The set-up is first studied for photo-bleaching effects, detection limit and optical characterization.

2.1.3 Photo Bleaching Effects

Continuous excitation of fluorophore molecules causes a reduction in their ability to absorb and re-emit light, resulting in permanent or temporary bleaching of them. As a result, the effect of photo bleaching must be taken into account when a solution is subjected to a prolonged exposure of laser illumination because it will affect the sensitivity of the imaging system.

The theoretical formulation for photo bleaching can be expressed as a first-order rate process. Therefore, the concentration of unbleached dye molecules, *c(t)*, remaining after continuous illumination from time t_0 to time t, can be expressed as [51, 52]

$$c(t) = c_0 \exp\left[-Q_b \sigma \phi (t - t_0)\right] \qquad [1]$$

where c_0 is the concentration of the dye at time t_0, Q_b is the quantum bleaching efficiency, σ is the absorption cross section, and ϕ is the photon flux of the excitation source. Q_b is defined as the number of dye molecules that are bleached per absorbed photon, and can vary with the type of dye solvent, the dye concentration, the excitation wavelength, and the photon flux.[51] The photon flux is given by $\phi = I/h\upsilon$, where I and ν are the intensity and frequency of the monochromatic excitation source, respectively, and h is Planck's constant.

Since Q_b and σ are a function of dye concentration, excitation wavelength and photon flux. In reality however absorption of photons from the incident laser flux promotes some flurophores to the first excitation state, which may also absorb and go to second excited state[53, 54]. These excitation states will have different absorption cross section and total absorption coefficient (α) will depend on population density in each excitation state. The absorption coefficient in that case is:

$$\alpha = \rho_0\sigma_0 + \rho_1\sigma_1 \qquad [2]$$

where $\rho_0 \, and \, \rho_1$ are the population densities of fluorophores in first and second excited states. $\sigma_0 \, and \, \sigma_1$ are the absorption cross section for first and second excited states. The temporal evolution of these population densities:

$$\rho_0 = \rho \exp\left[-\int_0^t \sigma_1 I \, dt \right] \qquad [3]$$

It is difficult to get any estimate of population density from the above Equation without knowing the value of absorption cross section. This variation in the absorptive properties of fluorophores are however not significant when power is very low. A simple experiment (Figure 2-2) is done to show the there is a linear relationship between laser power and fluorescence intensity, so that it can be assumed that the fluorphores are not saturated and a single excitation

state will be sufficient. The laser power used for most of the experiments in subsequent Chapters is around 6 mW. The actual energy delivered is still less as the laser beam is expanded 20 times.

Therefore, the above condition can be simplified by assuming[51] that the coefficient $Q_b\sigma\theta$ can be mathematically described by $Q_b\sigma\phi = f(c_0, \nu, I)$. For our experiment ν and *I* are constant, this equation reduces to $Q_b\sigma\phi = f(c_0)$. At any given time, *t*, the fluorescence, *F*, is proportional to intensity, *I*, and the concentration of the remaining, unbleached dye molecules, *c(t)*. Therefore, F can be described as

$$F = \alpha I c_0 \exp\left[-\beta f(c_0)(t - t_0)\right], \qquad [4]$$

where α and β are constants.

Using Equation [2] as the theoretical model, the fluorescence intensity is studied as a function of time. The temporal intensity profiles observed in experiments generally agree with mathematical values calculated using the model, as shown in Figure 2-3. The data indicates that photo bleaching is very significant for higher concentrations of fluorescein, reducing the intensity by 12% in 100 s and by 48% in 500 s for 1 μM fluorescein solution. The results also suggest that the effect of photo bleaching drastically decreases with concentration. The photo bleaching is negligible for a fluorescein solution at a concentration of 0.01 μM.

Since the profile of the laser light is gaussian, the beam shape after the beam expander should have a similar envelope, i.e., stronger intensity at the center than on the edge as in Figure 2-4. Therefore the effect of spatial variation must also be taken into account. Assuming the power is conserved during expansion, the intensity profile can be described by

$$I = e^{-(x^2+y^2)/2\sigma^2}, \qquad [5]$$

where x and y are orthogonal axes and σ is the standard deviation of gaussian profile of the beam. The cylindrical lens compresses one axis to make a line beam, so that the intensity in x-axis can be found by integrating intensity in y-direction.

$$I = \int_0^y e^{-(x^2+y^2)/2\sigma^2} dy = \sqrt{\frac{\pi}{2}}\sigma\, e^{-x^2/2\sigma^2} erf\left(\frac{\sqrt{r^2-x^2}}{\sqrt{2}\,\sigma}\right) \qquad [6]$$

where *r* is radius of the expanded beam. Substituting *I* into Equation [4] gives

$$F = \alpha\sqrt{\frac{\pi}{2}}\sigma\, e^{-x^2/2\sigma^2} erf\left(\frac{\sqrt{r^2-x^2}}{\sqrt{2}\,\sigma}\right) c_0 \exp\left(-\beta\sqrt{\frac{\pi}{2}}\sigma\, e^{-x^2/2\sigma^2} erf\left(\frac{\sqrt{r^2-x^2}}{\sqrt{2}\,\sigma}\right)(t-t_0)\, f(c_0)\right) \qquad [7]$$

The Equation [7] has both spatial and temporal dependency. As a result, both spatial and temporal effects of photo bleaching can be investigated.

Figure 2-5.A shows spatial intensity profiles of fluorescence, imaged at different times for 1 μM fluorescein solution in a 200 μm diameter capillary. The intensity values are normalized against the maximum intensity value after one minute exposure. The results indicate that fluorescence decreases both spatially and temporally. For longer exposure times, the dye molecules at the center of gaussian irradiation undergo significant photo bleaching, apparently due to stronger light intensity. As a result, a dip forms at the center of the intensity profile while two side lobes have relatively higher intensity. A similar result is obtained using numerical simulation according to Equation 5, as shown in Figure 2-5.B. The agreement between the numerical values with experimental data suggests that the simple theoretical model used, can be employed to predict the degree of photo bleaching and help to find optimum experimental conditions.

It should be pointed out that photo bleaching is significantly reduced for lower concentrations of fluorescein as suggested in Figure 2-2. Equations [4] and [7] also predict that

the effect of photo bleaching is reduced for lower concentrations of fluorophores and lower laser power. It was found that the effect of photo bleaching is negligible when the laser power is less than 3 mW and the exposure time is less than 60 seconds for a fluorescein solution at a concentration of 1 μM or less. These results help in determining detection sensitivity of the imaging system and applying the apparatus for protein separations in capillaries or micro fabricated devices.

2.1.3.1 Detection limit

After studying photo bleaching and finding out the conditions in which there is negligible photo bleaching, the sensitivity and detection limit of the imaging system was investigated. The limit of detection is found out by estimating the S/N ratio. This is defined as the ratio of the mean value of the signal ($\bar{E}$) to rms noise (s_E). Mean value of signal is defined as arithmetic mean of 'n' observations (E).

$$\bar{E} = \frac{\sum_{i=1}^{n} E_i}{n} \qquad [8]$$

The rms noise is the standard deviation of the signal derived from 'n' measurements.

$$s_E = \left[\frac{\sum_{i=1}^{n} \left(E_i - \bar{E} \right)}{n-1} \right]^{1/2} \qquad [9]$$

The S/N ratio of 2 is taken as the limit of detection. Proper care is taken while analyzing the data as the signal is gaussian in shape and the noise is over this gaussian signal. So one particular spatial point (usually the maximum intensity) is chosen along the gaussian beam and data is obtained for n repeated experiments. The detection limit of the imaging system is determined to be 1 nM (nanomolar) of fluorescein (S/N ratio is 2.45), as suggested by the

calibration between fluorescence intensity and fluorescein concentration in Figure 2-6 A. The calibration curve is linear over five orders of magnitude at an incident laser power of 3 mW with an exposure time of 50 seconds. The data collected is averaged over entire width of the channel to eliminate possible surface irregularities.

Using fluorescein for calibration helps in understanding the limit of detection of the system. However separation processes like IEF leads to focusing of proteins and as the proteins get concentrated, very low initial concentration can be used. Figure 2-6 B shows the calibration curve using GFP in IEF. The minimum detection limit is 0.03 ng/μl and is much lower than the case when fluorescein was used. For higher concentrations (more than 1 μM) of fluorescein, the nonlinear effect of photo bleaching is prominent even at this power and exposure time. This can be avoided by having less exposure time. Very low intensity fluorescence measurement has a different problem. The gaussian nature of the laser line induces similar gaussian characteristics in fluoresecence emission. Hence the intensity is maximum at center and gradually reduces on two sides. This requires mathematical correction of the profile and is discussed next.

2.1.3.2 Optical correction

The sensitivity of the detection system is inversely proportional to the square of the distance between the object and the camera. The shorter the distance is, the better the sensitivity is. The shorter distance also increases the spatial resolution; however, it reduces the field of view. A trade-off between the maximum field of view and the best sensitivity is chosen depending on the application. Due to spatial difference in the laser intensity, there is a dependence of the fluorescence intensity on the location of a protein. If a protein is focused near the center of a gaussian beam, the protein exhibits maximum fluorescence. If a protein is

focused near the edge of the gaussian beam, the protein exhibits less fluorescence. As a result, a visual distortion exists in terms of relative intensities of the focused proteins.

This distortion can be corrected by refractive beam shaper or mathematically. A refractive beam shaper though commercially available is very expensive and still tend to have some distortion at the edges. Mathematically it can be corrected by taking into account the original intensity profile of the laser beam. At any given time, fluorescence intensity can be approximated by $F = \alpha IC$, where α is a proportionality constant, *I* is the laser intensity, and *C* is the concentration of protein. Assuming the initial concentration of the sample is uniform along the channel, the initial light intensity can be described by $F = \alpha I_0 I(x) C_0$, where I_o is the maximum intensity at the center and *I(x)* is a normalization function along the channel. In other words, a normalized intensity profile between 0 to 1 will give a profile of *I(x)*, i.e., $F_{normalized}^{start} = I(x)$. After IEF and proteins are focused, the fluorescence can be described as $F = \alpha I_0 I(x) C_0 C(x)$, where

C(x) is also a normalization function along the channel, but for the variation in concentration. The normalized intensity profile between 0 to 1 will give a profile of $I(x)C(x)$, i.e. $F_{normalized}^{final} = I(x)C(x)$. Therefore *C(x)* in the image can be correctly represented by

$$C(x) = \frac{F_{normilzed}^{final}}{F_{normalized}^{start}}.$$

Figure 2-7 shows an electropherogram of different proteins before and after mathematical correction. At the beginning of experiment, the protein is uniformly distributed along the channel. Initial intensity profile shows a gaussian distribution, which is consistent with that of laser beam profile as discussed earlier. After IEF, the protein is focused at its isoelectric point, represented by a peak in the electropherogram. The raw data for Figure 2-7 A shows the effect

of gaussian beam profile. The profile is flat after removing the gaussian effect. Similar correction shows a clear shoulder peak in Figure 2-7 B. This shoulder peak is expected due to microheterogeneity of GFP, which refers to slight structure differences among isoforms of a protein synthesized biologically. GFP is often observed having a large portion of the primary component with a small portion of other isoforms as discussed in the literature.[55] Slight increase of intensity in the corrected profile at both ends is probably due to amplification of noise near the edge of the gaussian beam.

2.2 Device Fabrication

2.2.1 Introduction

A growing amount of research is being devoted to the study of microfluidic devices for a number of applications, including DNA analysis, protein separations, and cell manipulation. While many researchers use PDMS, glass, or silicon to fabricate their microfluidic devices, others choose thermoplastics due to the following advantages. First, plastic devices are potentially inexpensive, resulting from low-cost raw materials and vast experience in manufacturing high-volume plastic parts. For example, the manufacturing cost of a compact disc (CD), a two-layer structure made from acrylic or polycarbonate and containing micro scale features, is less than 40¢. [42] As a result, it will probably be affordable for plastic devices to be disposed off after a single use. Being disposable could have tremendous impact in applications where cross-contamination of sequential samples is of concern, including point-of-care clinical diagnostics, drug screening, and forensic analysis. In addition, plastic devices are compatible with biological and chemical reagents, evident from the extensive use of plastic labware such as micro centrifuge tubes and micro plates.

The plastic materials investigated for micro-fabrication and micro fluidics include polymethyl-methacrylate (PMMA),[56-62] polycarbonate (PC),[62-65] cyclic olefin copolymers

(COC),[66-71] polyester, fluorinated ethylene propylene, and poly(ethylene terephthalate). COC is used since it offers a number of advantages, including increased solvent resistance, higher optical clarity, and reduced absorption of moisture.[66]

The major techniques for fabricating plastic microfluidic devices include hot embossing, injection molding, and laser ablation. Casting is another approach that is almost exclusively used for PDMS.[72] The general methods for fabricating plastic devices have appeared in literature and have been reviewed. [42, 73, 74] In the following sections the device fabrication and design parameters adopted for producing microfluidic devices for this work is described.

2.2.2 Design and Fabrication

The device was designed using AutoCAD and the layout is shown in Figure 2-8. The 6-channel device (Figure 2-8A) is fabricated for isoelectric focusing. The channel length ranges from 1 cm to 6.5 cm, with a side channel approximately 5 mm in length and 5 mm away from one end of channel. The side channel is designed for sample injection. The channels are approximately 120 μm wide and 30 μm deep. The second device (Figure 2-8 B) consists of one vertical channel (AB) for the first dimensional separation (IEF) and 29 horizontal channels (CD) for the second dimensional separation (PAGE). The feature size of etched channels is approximately 120 μm wide while the CD channels are separated by 240 μm.

Plastic microfluidic devices were produced using the procedure similar to what has been reported in the literature.[42, 66] A glass master with the desired pattern was defined by photolithography. Chemical isotropic etching was exploited to create glass masters with channels approximately 30 μm deep and 120 μm wide. Electroplating against the master created a metal electroform[42] and it was carried out by Optical ElectroForming (Clearwater, FL). The

electroplating material is nickel alloy and the thickness of the electroform is about 1 mm (Figure 2-9).

The topology of the electroform is exactly the opposite of the glass master; a channel in the master becomes a ridge in the electroform. This electroform served as a molding die that would produce plastic parts from Topas® 8007 resin (Ticona, Florence, KY) using a hydraulic press (Carver, Wabash, WI). The molding temperature is around 257 ^{o}F and the compression force is 5000 lbs. About 15 gm of Topas® 8007 resin is sandwiched between E-form and a 6"x 6" inch glass plate and placed inside the press as illustrated in Figure 2-10A.

After preheating for 5 minutes at 257 ^{o}F, the lower platen is raised to compress the resin at 5000 lbs and kept at that pressure for 5 minutes for pressure molding. Then the molded plastic is cooled at controlled temperature of 70 ^{o}C for 5 minutes and is removed from the E-form. Holes were drilled at the end of channels using a computer numerically controlled (CNC) mill (Flashcut 2100; Flashcut, Menlo Park, CA) to function as reservoirs. The device is completed by sealing the plastic substrate with a cover film (~70 μm thick Topas 8007 film) using thermal lamination.[42] Figure 2-9 B shows the schematic of lamination process. The plastic device and film sandwiched between two Mylar films (2 mil thick) are initially preheated for 1 minute at 85 ^{o}C, and then is run through a laminator (Catena 35, GBC). The roller temperature for the laminator is set at 110 ^{o}C.

The devices thus fabricated are checked for any channel blockage, which can happen due to variation in lamination temperature and applied pressure.[75] These devices are then surface treated for carrying out electrophoresis, the detail of which is discussed in next Chapter.

2.3 Conclusion

A laser-induced fluorescence imaging system was assembled for viewing the full length of microchannels. The advantage of the system is that its ability to study the protein separation

dynamics as a function of time since the sequential images can be obtained. This method is useful for studying IEF process, as proteins need not be moved after focusing, thereby preventing the loss of resolution of protein peaks. The detection limit for this system was found to be around 1 nM of fluorescien solution. Photobleaching was found to be an issue, when the fluorophore concentration is higher above 1 μM of concentration. As a result care is taken to carry out all the subsequent experiments within that range, though the degree of photobleaching effect may differ in different types of fluorophore molecules. For very low intensity fluorescence measurement, gaussian beam profile correction needs to be done. In addition, I discussed the fabrication process of microfluidic devices. The compression molding has good reproducibility, and hundreds of devices can be fabricated from one master.

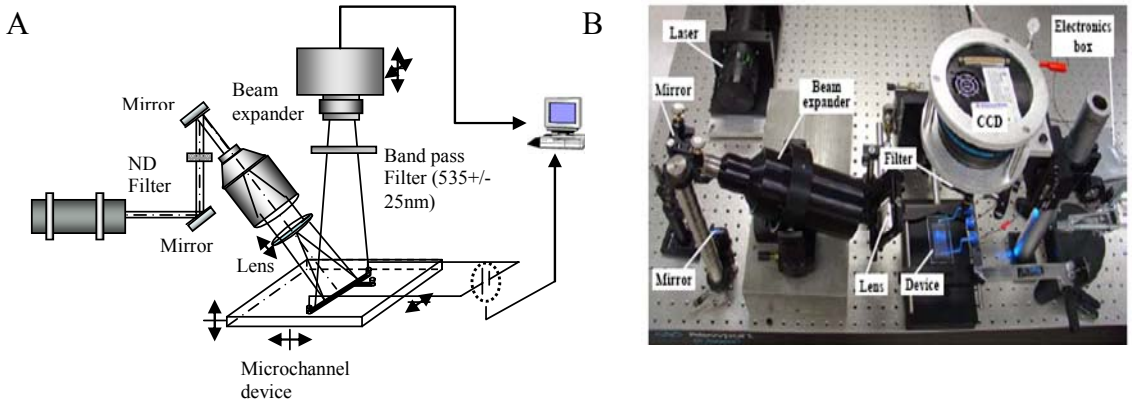

Figure 2-1. LIF imaging system for protein separations. A) The laser beam is transformed into a line beam using a beam expander and cylindrical lens. A line beam is needed to illuminate and image an entire channel during isoelectric focusing of proteins. B) Photograph of the set-up in an optic table.

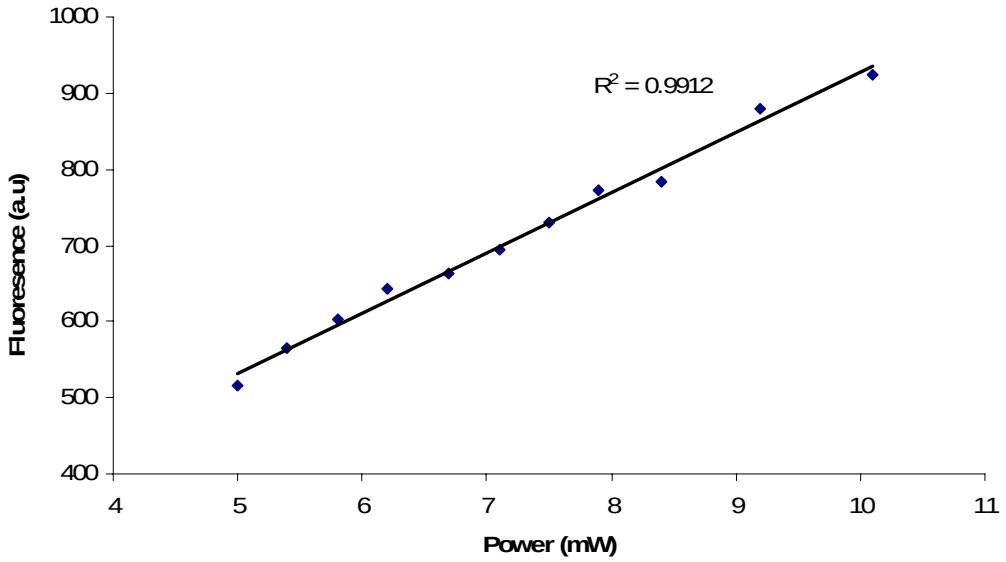

Figure 2-2. The fluorescence intensity values measured in microchannels with different laser power. The exposure of CCD camera is 100 ms.

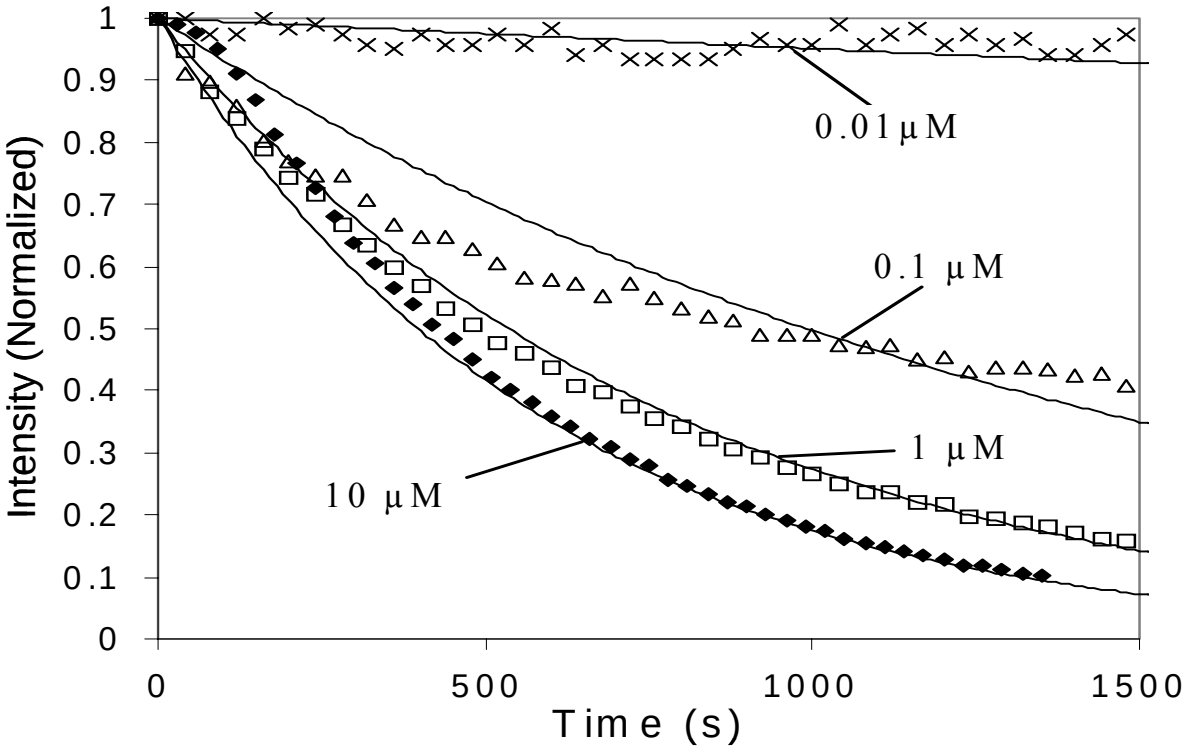

Figure 2-3. Temporal profile of photo bleaching effects. The data points are experimental results, whereas the solid lines are numerical calculation using Equation [4]. The concentration of fluorescein solution is indicated. The fluorescence intensity values are normalized with their respective maximum values, so that the gradients can be compared in the same plot. The power of laser line is 3 mW.

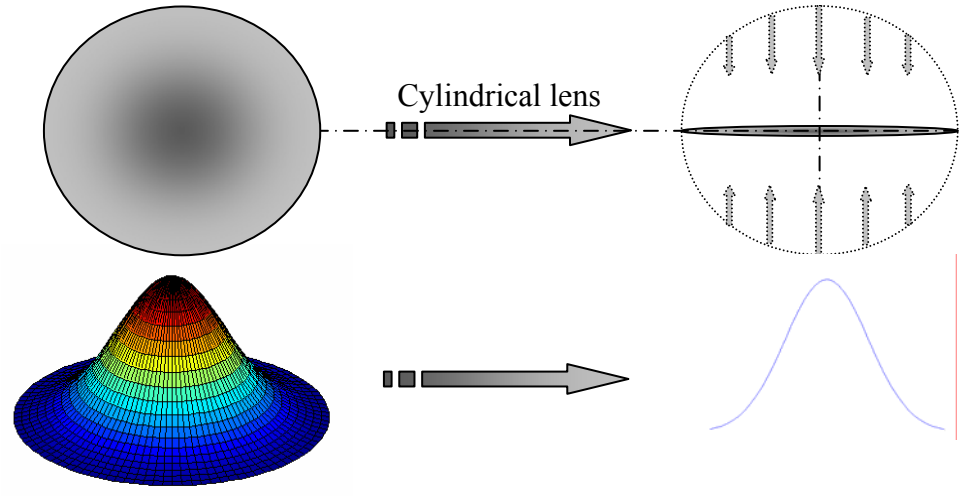

Figure 2-4. The cylindrical lens compresses the beam in one axis

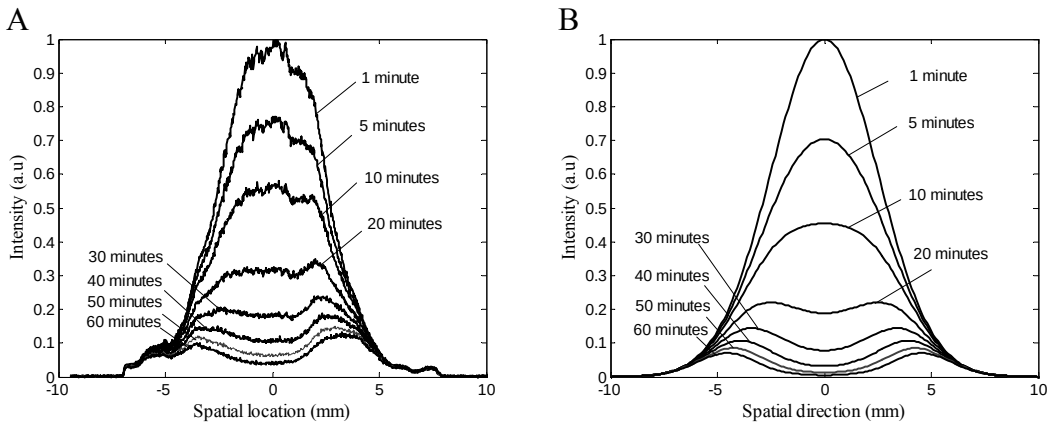

Figure 2-5. Spatial profile of photo bleaching effects. A) Experimental results for sample of 1 µM concentration of fluorescein solution. The length of laser line is 20 mm. The intensity values are normalized with the maximum value of intensity of the first minute profile. B) Numerical simulation for photo bleaching effects using the same parameters as in A.

A

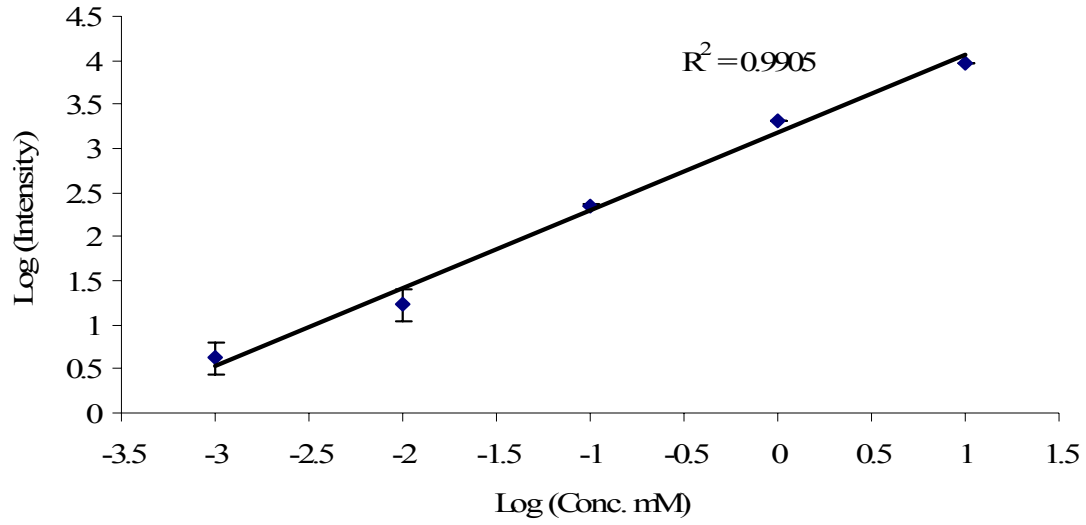

B

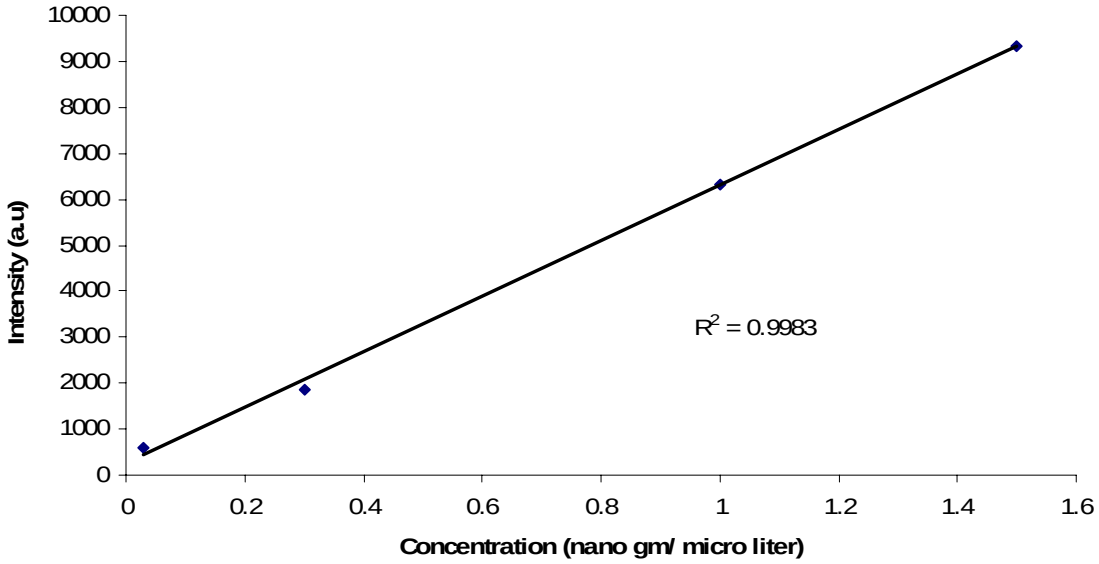

Figure 2-6. Calibration curve for the detection system. A) Calibration curve of fluorescein solution in a glass capillary using the imaging system in Figure 2-1. Both axes are in log scale. B) Similar calibration of the system using GFP in Isoelectric focusing. The channel length used is 4 cm at 100 V/cm.

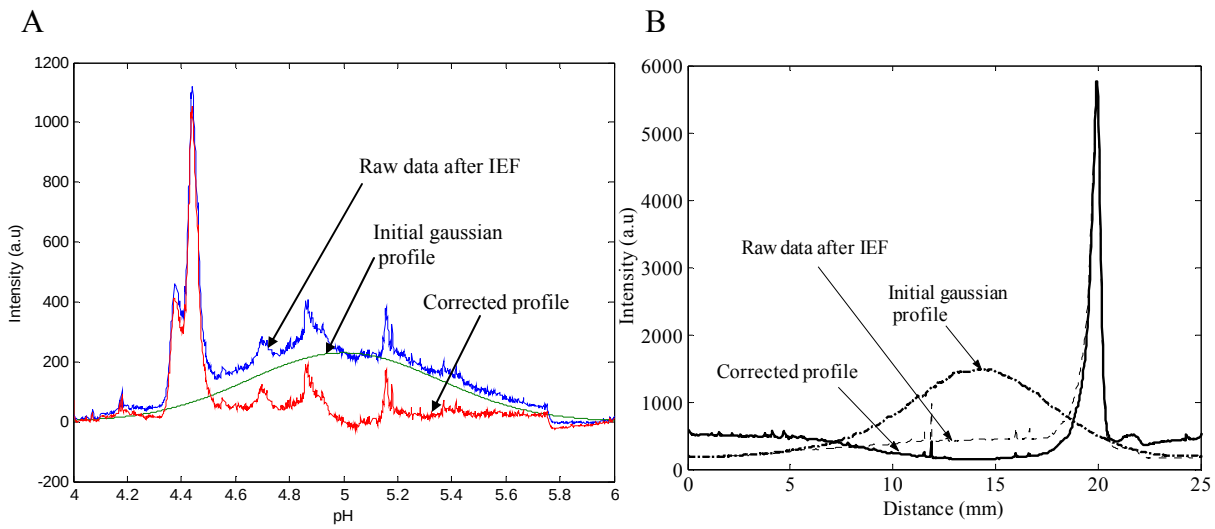

Figure 2-7. Optical correction for removing Gaussian noise background. A) Isoelectric focusing of four proteins green fluorescent protein, R-phycoerythrin, B-phycoerythrin and phycocyanin in pH gradient of 4-6. B) IEF for GFP in pH gradient of 3-10 formed in channel of length 2 cm. The electropherogram is mathematically corrected in both cases by taking into account of spatial laser intensity variation. The raw data in left image (blue) after correction (red) shows a flat intensity profile. Similarly for right one, a small hump for isoform of GFP is visible after correction.

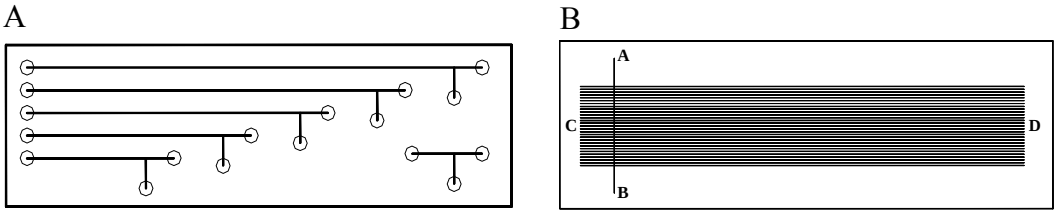

Figure 2-8. The layout of microfluidic devices for protein separation. The size of the device in general is 1" x 3". A) Device used for isoelectric focusing of proteins. B) Device used for 2-dimensional electrophoresis. Cross channel AB is to be used for IEF whereas parallel channels CD are used for separation based on sizes.

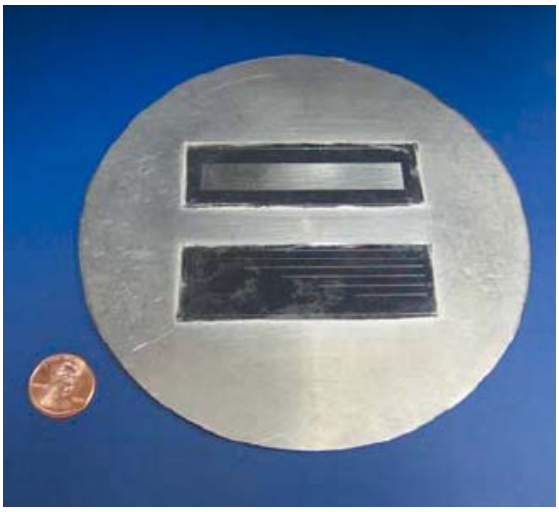

Figure 2-9. E-form used for this research.

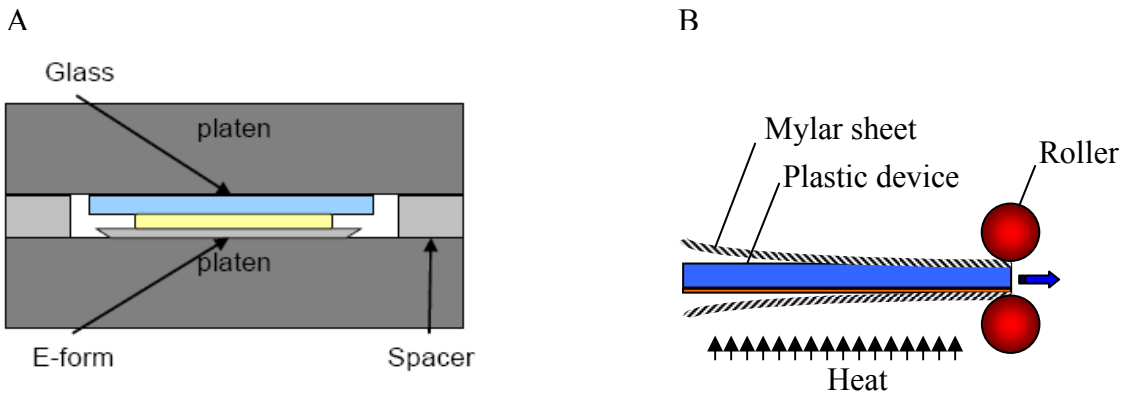

Figure 2-10. General methods for plastic device fabrication. A) The schematic of molding operation for plastic device using E-Form. B) The plastic device and film is initially heated and then run through laminator at 230 ^{o}C

CHAPTER 3
THEORITICAL AND EXPERIMENTAL RESULTS OF IEF[†]

3.1 Introduction

With the advent of microfluidics, efforts were made to miniaturize electrophoretic processes to the microfluidic chip format. IEF has been adapted to the microfluidic format due to potential advantages of miniaturization.[59, 64, 76-85] Possible advantages include less sample amount, faster analysis, higher separation efficiency, potentially lower cost, and the ability to integrate with other components including a detector. In this Chapter, I will discuss IEF in the 6 channel device described in Chapter 2, and a comparative study between theory and experimental results. The details of experimentation will be first described, followed by theoretical and experimental results.

3.2 Materials and Methods

Carrier Ampholytes (CA) (pH 3-10, 4-6) were purchased from Bio-Rad Laboratories (Hercules, CA) while ethanolamine, 2-hydroxyethyl cellulose (HEC, MW 90,000, 150 cps @ 5% w/w in water), hydroxypropyl cellulose (HPC, MW 80,000, 150-700 cps @ 10% w/w in water), Myoglobin and Bovine Serum Albumin (BSA) were from Aldrich-Sigma (St. Louis, MO). Myoglobin and BSA were labeled with Alexa488 Protein Labeling Kit (A-10235) from Molecular Probes (Eugene, OR). Green Fluorescent Protein (GFP, 1 mg/mL stock) was obtained from BD Biosciences Clontech (Palo Alto, CA) and R-phycoerythrin (RPE, 10 mg/mL stock) was obtained from Cyanotech (Kailua-kona, HI). Acrylamide:bis-acrylamide (electrophoretic grade, 5%C), TEMED (N, N, N', N'-tetramethylethylenediamine), glycerin, acetic acid, and microscope slides were purchased from Fisher Scientific (Atlanta, GA). All solutions were prepared using water purified from Barnstead Nanopure Water System (Model: D11911,

[†] A part of this Chapter has been published: Das, C.; Fan, Z. H. *Electrophoresis,* 27, 3619-3626, 2006

Dubuque, Iowa). Solutions of 10 mM acetic acid and 10 mM ethanolamine served as the anolytes and the catholytes, respectively.

All experiments were performed either in glass or plastic microfluidic devices. The channels in the device were first cleaned with 1% (0.18 M) potassium hydroxide (KOH). The solution is allowed to stay for 5 minutes inside the channel and then flushed out with water. The channel is then filled with IEF separation medium, which consists of 5% ampholytes (pH 3-10) stock solution (at 40% supplied by the vendor), 10% glycerol stock solution (80% v/v in water), and 85% HPC/HEC stock solution (1.83% HPC and 0.73% HEC in water, except where specified otherwise). A mock IEF is performed with all the constituents (including proteins) in the presence of an electric field, followed by flushing out with water. This step helps to block all the active sites in the surface of channel, thereby preventing protein adsorptions in future experiments and helps conditioning the wall surfaces under an electric field. It has been reported that most plastics, including poly(cyclic olefin), possess much smaller EOF, typically a factor of five or so smaller than silica/glass.[42] Electroosmotic flow (EOF) are further suppressed by dynamic coating of HPC/HEC contained in the IEF separation medium, as reported in the literature.[86-88] Nevertheless, a minute amount of EO flow was observed, especially when the electric field strength was high.

A protein sample can be introduced into a microfluidic device by using two approaches. One is to fill proteins in an entire channel [59, 76, 78, 79] whereas the other is to inject a plug of protein samples into the IEF channel [89] as demonstrated in many microfluidic CE devices.[90, 91] It is chosen in this work to fill an entire channel with analytes to ensure uniformity in pH gradient.

3.3 Theory of IEF

Electrophoresis in a microchannel is a complicated three dimensional problem. The analytical electrophoretic model used here is assumed to be one-dimensional in nature. The

motive of this analysis is to find out the physical factors behind the focusing characteristics and relation of time of completion with that of conductivity drop in the system due to IEF process.

Several simple assumptions are made for the following semi-analytical solution. The process of IEF in a typical microfluidic device or capillary can be viewed as follows. The channels are initially filled with carrier ampholytes and proteins (both are charged macromolecules). As the electric field is applied, a pH gradient is established. Once the pH gradient is established the proteins (macromolecules) starts migrating towards their pI point where their net charge is zero. At a steady state the proteins stay stagnant at their pI points.

Standard transient electrophoretic process can be defined as[2,3,4,92]

$$\frac{\partial C(x,t)}{\partial t} + \frac{\partial \left[C(x,t)u(x)\right]}{\partial x} = D\frac{\partial^2 C(x,t)}{\partial x^2} \qquad [1]$$

where *u* and *D* are the velocity and diffusion coefficient of the component, *t* and *x* are time and distance variables, and *C(x,t)* is the concentration of the component, which is a function of location and time. The equation is the Fick's diffusion law[93] modified with an additional term for electrophoresis.

Both the transient process and final steady state is of importance in separation science. The transient solution shows the dynamics of protein front evolution, how the finer structures of proteins evolve with time and that the process proceeds towards completion asymptotically. The transient equation is difficult to solve, but if certain assumptions are made, the underlying physics of the problem can be understood. The equation is non-dimensionalised for the purpose with following variables.

$$x^* = \frac{x}{l}; \quad t^* = \frac{tu_0}{l}; \quad u^* = \frac{u}{u_0}; \quad C^* = \frac{C}{C_0}$$

where l is the length of channel, u_0 is the initial velocity and C_0 is the initial concentration of the species/proteins. The corresponding non-dimensional equation is of the following form

$$\frac{\partial C^*}{\partial t^*} + \frac{\partial \left[C^* u^* \right]}{\partial x^*} = \left(\frac{1}{Pe} \right) \frac{\partial^2 C^*}{\partial x^{*2}} \qquad [2]$$

where $Pe = \frac{l u_0}{D}$ is defined as the Peclet number. This is defined as the ratio of product of length and fluid velocity to that of diffusion. When the Peclet number is small, the diffusion is dominant in the system, whereas when it is high, diffusion can be neglected when considered with the size. Let us consider the case when diffusion dominates, the equation simplifies to:

If $Pe << 1$

$$\frac{\partial^2 C^*}{\partial x^{*2}} = 0 \qquad [3]$$

$$C^* = Ax^* + B \qquad [4]$$

Hence the concentration is a linear function of distance. The channel length is very short when compared to diffusion of species. The species will diffuse into the channel very fast and IEF will fail in this condition. The limiting conditions for this case can be taken as the theoretical limit for electrophoresis. $Pe = \frac{l u_0}{D} << 1$

$$l << \frac{D}{u_0} << \frac{D}{\mu E} \qquad [5]$$

Where μ is the electrophoretic mobility for IEF and E is the applied electric field.

Using diffusion constant for a model protein[94] (BSA in this case) $D = 7.75 \times 10^{-7} cm^2 / s$, electrophoretic mobility $\mu = 4 \times 10^{-4} s^{-1} V^{-1} cm^2$, E= 100 V/cm, the length of channel is calculated to be:

$$l <<\sim 10^{-5} cm \quad (0.1\ \mu m) \qquad [6]$$

The above phenomenon occurs when the channel length is less than 0.1 □m. It can be assumed that IEF can be safely performed for longer channel length. However as it will be demonstrated, there is practical limitation to the minimum size beyond which it becomes practically impossible to perform IEF. The other extreme of the above equation is to have very high peclet number.

$$Pe >> 1$$

Equation 2 then changes to

$$\frac{\partial C^*}{\partial t^*} + \frac{\partial \left[C^* u^* \right]}{\partial x^*} = 0 \qquad [7]$$

This equation can be solved analytically with additional information for velocity from IEF. For general electrophoretic movement the velocity is dependent on electric field as:

$$u = \mu(x) E \qquad [8]$$

Svensson [95] made an assumption that the pH gradient, d(pH)/dx, and the mobility difference at pI value, d□/d(pH), are constant. Then the mobility can be expressed by

$$\mu_x = \frac{d\mu}{d(pH)} \frac{d(pH)}{dx} x \qquad [9]$$

Hence u can be written as a linear function of x

$$u = kx^* + d \qquad [10]$$

Where k, d are the constants. The final solution for this case can be written as

$$C^* = Ae^{-\beta t^*} . \left[kx^* + d \right]^{\frac{\beta - k}{k}} \qquad [11]$$

Where β is also a constant. This however gives very sharp concentration gradient which decays exponentially with time. The sharp concentration gradient is because of very high peclet

number. The full equation is solved though with some assumptions and can be found in literature[96, 97]. The final analytical solution is given here and the full solution can be seen in Appendix A:

$$C(x,t) = \frac{1}{s(t)\sqrt{2\pi}} \exp\left[-\frac{\left(x - x_{pI}\left[1 - \exp\left(-t/t_0\right)\right]\right)^2}{2s^2(t)} \right] \quad [12]$$

This solution gives a moving front of peak with Gaussian concentration profile which moves towards its isoelectric point and ultimately stops there.

Equation 12 can be analyzed for different conditions

At time t = 0, $g(t) = \sigma$, $\langle x(t) \rangle = 0$, the center of mass for the CA/protein is at x=0

$$C(x,0) = \frac{1}{\sigma\sqrt{2\pi}} \exp\left[-\frac{(x)^2}{2\sigma^2} \right] \quad [13]$$

At time $t = \infty$, $g(t) = \sqrt{Dt_0}$, $\langle x(t) \rangle = x_{pI}$, So at very long time the CA/protein peaks center of mass will be exactly at their pI point.

$$C(x,\infty) = \frac{1}{\sqrt{2\pi D t_0}} \exp\left[-\frac{\left(x - x_{pI}\right)^2}{2Dt_0} \right] \quad [14]$$

Equation 12 has the spatial location of center of mass of protein peak. Differentiating with respect to time will give the front velocity. The front speed thus can be defined as:

$$\langle v(t) \rangle = \frac{x_{pI}}{t_0} \exp\left(-\frac{t}{t_0} \right) \quad [15]$$

This front speed can be monitored in real time by the imaging system developed for whole channel viewing and the numerical results can be experimentally verified. However the steady state analysis gives us the various experimental conditions required for successful completion of IEF.

For IEF, a steady state is presumably reached at the completion of focusing, i.e, $\frac{\partial C(x,t)}{\partial t} = 0$. Then the concentration is a function of location, *x*, only. The velocity of a component can be calculated from its electrophoretic mobility at its location, $\mu(x)$, and the electrical field, *E*, i.e., $u = \mu(x)E$ (assuming zero electroosmotic flow). As a result, Equation 1 is simplified to Equation 16,

$$C(x)\mu(x)E = D\frac{dC(x)}{dx} \qquad [16]$$

where *x* is now defined as being *x = 0* at the concentration maximum of a peak. To solve this Equation [16], Svensson [95] made an assumption that the pH gradient, $d(pH)/dx$, and the mobility difference at pI value, $d\mu/d(pH)$, are constant. Then the mobility can be expressed as:

$$\mu_x = \frac{d\mu}{d(pH)}\frac{d(pH)}{dx}x \qquad [17]$$

After substituting $\mu(x)$ into Equation 16, the equation can be integrated on both sides as follows,

$$\frac{d\mu}{d(pH)}\frac{d(pH)}{dx}\frac{E}{D}\int_0^x x dx = \int_{C_0}^{C_x}\frac{dC(x)}{C(x)} \qquad [18]$$

where C_0 is the concentration of the component at the peak maximum. Solving this equation will give Equation 19

$$C_x = C_0 \exp\left[\frac{x^2}{2}\frac{d\mu}{d(pH)}\frac{d(pH)}{dx}\frac{E}{D}\right] \qquad [19]$$

To fit with the traditional gaussian distribution of a peak, Equation 19 can be rewritten as Equation 6,[95, 98]

$$C_x = C_0 \exp\left[\frac{-x^2}{2\sigma^2}\right] \qquad [20]$$

where σ is defined by $\sigma = \sqrt{\frac{D}{E}\frac{dx/d(pH)}{-d\mu/d(pH)}}$, and its physical meaning is the standard deviation of the gaussian peak.

The IEF resolution can be described by the minimum pI difference required to separate two proteins. In order to distinguish two peaks, the distance between them must be at least 3σ. Figure 3-1b shows graphically the requirement for 3σ between the peaks for proper resolution.

The superimposition of the two gaussian profile if separated by 2□, gives only a single peak, whereas 3σ separation resolves them. Therefore, the minimum pH difference required is

$$\Delta(pI)_{\min} = 3\sigma\frac{d(pH)}{dx} = 3\sqrt{\frac{D}{E}\frac{d(pH)/dx}{\left[-d\mu/d(pH)\right]}} \qquad [21]$$

When a constant voltage, *V* is applied and a uniform *pH* gradient is used, then *E = V/L* and $\frac{d(pH)}{dx} = \frac{\Delta pH}{L}$, where *L* is the separation distance. Equation 7 is simplified to Equation 8,

$$\Delta(pI)_{\min} = 3\sqrt{\frac{D}{V}\frac{\Delta pH}{-d\mu/d(pH)}} \qquad [22]$$

in which there is no term related to the distance. Equation 8 clearly indicates that the minimum pI difference required for two proteins to be separated by IEF is independent of the separation distance. As a result, a short focusing length is advantageous, especially for a microfabricated device, since it should provide more rapid analysis without sacrificing the resolving power. It should be noted, however, that a few assumptions are made during derivations, and they (e.g., negligible EO flow) may not be true in some experimental conditions. In addition, the separation voltage must remain the same while reducing the separation distance. As a result, the electric

field strength and current will increase; possibly producing Joule heating that is not negligible anymore.

From the theoretical results above, the factors that need to be optimized for miniaturization are a) electric field strength, b) length of channel, c) time of separation for proper optimization. The theory predicts that length of channel should not be a factor in separation, as the minimum pI difference required for proper resolution of protein peaks is independent of channel length. So a very long capillary needed for electrophoresis can be shrunk into a small chip like a microfluidic device. Since the time of completion of IEF is inversely proportional to electric field, if proper heat dissipation from the chip can be designed, high electric field can ensure the IEF can be completed with in minutes. Since the channel length is reduced the high field strength can be maintained very easily without need for very high voltage power source. There are several other parameters that come directly from practical standpoint and experimental issues. All these will be discussed in next sections with emphasis on channel length independency, the effects of field strength, focusing time and pH gradient compression.

3.4 Experimental Results

The theory described above is idealized and has many assumptions, which will lead to mismatch between experimental results and theoretical calculation. Correctly analyzing those anomalies will lead to better understanding of process and thus improving the theoretical analysis. The first set of experiments were carried out by focusing one protein at a time and then gradually making the system more complicated by adding more proteins. The whole-channel imaging system designed and characterized before is used for detecting proteins after their separation by IEF. Since GFP is naturally fluorescent, it has been used for characterization of the system. The dynamics of IEF was investigated and the temporal images of GFP separation are shown in Figure 3-2. This result indicates that a front starts focusing from each end after

applying a voltage across a separation channel. Focusing fronts start to be observed at the fourth minute. Both fronts progressively move towards the middle, and finally combine together at the focusing point after about forty minutes. The cathode front is rather wide and faint during focusing whereas the anode front is sharper. Protein bands at the anode front are clearly visible soon after the front appears (after ~5 min at 200 V). The conductivity of system drops while the pH gradient is being established. As a result, a higher electric field may be applied after initial focusing. For example, the applied voltage was increased up to 500 V for final zone compression and better resolution. The separation medium for this case was polyacrylamide gel.

3.4.1 Effects of Separation Medium

The separation medium used is either polyacrylamide gel or linear polymer; both of them have been successfully implemented in either microfluidic channels or glass capillaries. The polyacrylamide significantly reduces electroosmotic flow (EOF), especially when the gel form is used. However polymerization inside a microchannel is a significant problem. Introducing the solution inside the channel becomes difficult if the chemical polymerization is started beforehand. UV polymerization can be done *in situ*, but it destroys the fluorescence of proteins and thus can not be detected. Elimination of EOF flow keeps the focused protein bands in place, as well as enhances separation resolution. The cross linked polymer (for polyacrylamide) is a mesh like structure and it has sieving properties for proteins moving across it. This leads to increased drag and hence longer separation time. Mesh like structure also hampers separation of large molecular weight proteins. The linear polymer on the other hand is a viscous liquid and does not have mesh like structure. So it is easy to introduce inside the channels and does not restrict the flow of bigger proteins.

Next three different proteins are focused in the microchannel. They are GFP, BSA, and Myoglobin. Both BSA and Myoglobin are labeled with Alexa 488 dye, so that they can be

visible when illuminated by argon laser. Figure 3-3 shows the separation of these proteins in both linear polymer in Figure 3-3a and polyacrylamide gel in Figure 3-3 b.

The results in Figure 3-3 suggest that the resolution in the linear polymer is slightly better than in cross linked polymer. The images recorded at regular interval by CCD camera are analyzed to track the protein front with time. Figure 3-4 shows the protein front speed comparison with time for the case above (Figure 3-3). Time required for separation is less for linear polymer (40 minutes for gel and 20 minutes for linear polymer). It is also observed linear polymer can withstand higher level of electrical field without appreciable heat generation when compared with polyacrylamide gel. The reason behind maybe of convective cooling possible with linear polymer but not with cross linked gel. The sample prepared can be used multiple times in case of linear polymer, whereas the polyacrylamide gel can be used only once. Hence it is chosen for all subsequent work.

Since BSA, and Myoglobin labeled with Alexa488 gave broad peaks due to heterogeneity in labeling,[99] we did not use them for studying the IEF process. It is necessary to know the exact pI point of the proteins for evaluating the completion of IEF. Also the dyed peaks have broad irregular shapes which make it difficult to study the resolution issues in IEF, as it is easier to assume the clean peaks as gaussian in nature and then calculate the resolution thereof. GFP and RPE are two naturally fluorescent proteins with well defined pI point. They can be excited with same wavelength (488 nm) and have similar emission spectrum. So these two naturally fluorescent proteins are chosen, whose pI points are well characterized.

The next sets of experiments were started similarly by uniformly filling a channel with a mixture containing ampholytes, linear polymers (HPC/HEC) and proteins. The ampholytes with a pH gradient of 3-10 were used and the separation voltage was 500 V (other voltages were also

studied as discussed below). As mentioned previously,[100] the protein peaks were observed almost immediately after an electric field was applied. These peaks traveled from the anode side toward the middle of the channel. The intensity of the protein peaks was initially very low, and then increased as they traveled along the channel while more proteins were focused and accumulated in the peaks. Figure 3-5 shows IEF of these proteins at 100 V/cm. The GFP is having one dominant peak flanked by two small peaks. These small peaks are due to micro heterogeneity of GFP. The pI points for these peaks are 4.88, 5.0 and 5.19. Similarly for RPE three peaks are visible; the pI for the dominant peak is 4.2.

The length of the channel is 5 cm and protein concentration is 5 μg/ml. The proteins thus optimally focused inside the microchannel and being detected by the CCD camera indicated that this setup can be used for further studying the effect of channel length, electric field and other parameters.

3.4.2 Effects of Separation Length

According to Equation 8, the minimum pI difference between two proteins separated in IEF should be independent of the separation distance if the voltage is maintained and all assumptions are met. Figure 3-6 shows the IEF electropherograms of GFP and RPE in channels II-V with different separation distances (2.1, 3.2, 4.3 and 5.4 cm respectively). The channels of length 1 cm and 6 cm were not used due to their too short or too long a channel. All three peaks of GFP in all four separation distances were observed, thus it can be claimed that all of them have capability to separate proteins with pI difference of 0.1 pH units. However, it is clear that the degree of separation between these peaks is less when the separation distance shortens. The concept of separation resolution is used to analyze the results further as discussed below.

Separation resolution (R) can be calculated by dividing the separation distance of two adjacent peaks by their average width, i.e.,

$$R = \frac{(x_2 - x_1)}{\frac{1}{2}(w_1 + w_2)} \qquad [9]$$

where x_1 and x_2 are the location of two peaks and w_1 and w_2 are the width of the peak at the base, measured between the tangent lines of the peak sides.[101, 102] Larger values of R mean better separation, and smaller values of R poorer separation. In order to maintain the separation resolution when the separation distance shortens (i.e., $x_2 - x_1$ becomes smaller), peaks must be sharper (i.e., w_1 and w_2 also become smaller). This is theoretically possible because a higher electric field results when a shorter channel is used while the separation voltage remains the same; a higher electric field likely leads to sharper peaks. Figure 3-7 shows the comparison between different resolution values. Also shown is the effect of superposition of two peaks of different peak heights. Comparing the case for R=1, the superimposed image of different peak heights (1:0.75) appears to be barely resolved, whereas same peak height looks better visually. As discussed above, separation resolution (R) can be calculated by using Equation 1. The R values between peaks 1 and 2 of GFP (can be seen in Figure 3-8) as a function of the separation length at different separation voltages are tabulated in Table 3-1.

Statistical analysis using ANOVA (analysis of variance) indicates that the resolution values at 300 V and 500 V in Table 1 are the same at the 95% confidence level for different separation lengths. The resolution values at 200 V and 400 V are statistically different based on ANOVA, but the trend of the change is not clear, especially for those at 200 V. Relatively large standard deviation in these values is primarily due to the fact that each peak corresponds to 15 to 25 pixels of CCD. One pixel variation will result in 4-6% deviation. The results indicate that the

separation resolution is independent, within the experimental errors, of the separation length, which is in agreement with the theory predicated. It is should be pointed out that the conclusion is true for the most experiments when the separation voltage changed from 200 V to 500 V, which correspond to the electric field strength of 38 to 263 V/cm.

3.4.3 Effects of Separation Voltage

Effects of the separation voltage on IEF by applying different separation voltages across 5.2 cm channel are investigated. Figure 3-8 shows a few representative IEF electropherograms of GFP and RPE when different separation voltages were used.

There is little difference in the electropherogram, though it showed sharper peaks when voltage increased initially. The initial increase in the peak sharpness is also evident from the increase of separation resolution listed in the Table 3-1. This is also the basis of the theoretical prediction that the separation resolution is independent of the separation distance, as discussed above. On the other hand, higher electric fields could also result in Joule heating, which increases peak dispersion. This may explain the general trend that the separation resolution increase initially, level off, and then decrease later on as indicated in Table 1 and Figure 3-8.The key advantage of using a higher separation voltage is a shorter analysis time, as discussed below.

3.4.4 Focusing Time

A short analysis time is one of major motivations to go for miniaturization. Obviously, the IEF focusing time will be affected by both the separation length and voltage. When the separation resolution is minimally affected, a shorter separation length and higher separation voltage, thus higher electrical field strength, will be preferred as they will lead to a shorter analysis.

However, IEF analysis time is difficult to measure. Theoretically in IEF, the proteins will reach its pI point asymptotically and hence will take almost infinite time towards total

completion. Experimentally, completion of a conventional IEF in a slab gel or a tube is facilitated by a dye contained in a sample when ampholytes are used. When the dye reaches to the end of the capillary tube or slab gel, it is regarded as the point to stop. It is likely that the property of the dye is different from proteins in the sample. IEF experiments are often helped by empirical experience and the protocols supplied by manufacturers. For immobilized pH gradients (IPG), protocols often recommend an overnight IEF since the pH gradient will not move away.

The whole-channel imaging detection (WCID) system described in Chapter 2 allows us to monitor IEF dynamically. Temporal profiles of protein separations provide the information about the time when the peaks do not move any further, and IEF is considered to be completed. However, EOF was not completely eliminated as mentioned above, especially when a higher voltage was used. Therefore the completion of IEF is determined by the significant slowing-down of peak moving, and it gave a very good idea after a certain amount of experience. The completion of IEF is confirmed by the expected pI location assuming the pH gradient is uniform and linear in the channel.

Figure 3-9 shows the relationship between the focusing time and the electrical field strength when a variety of separation voltages were used in different separation lengths.

The standard deviations represented by the error bars were obtained from three sets of repetitive experiments. A voltage range of 200 V to 1000 V was used for channel V as in Figure 3-8 whereas a smaller range of 200 V to 500 V was used for channels II and IV. The focusing time ranged from 1.5 to 46 minutes depending on the separation length and electrical field used. The data suggest that the focusing time decreases with the electrical field strength and there is a

linear relationship between the time and the inverse of the electric field strength. In addition, the focusing time decreased with the separation length as expected.

3.4.5 pH Gradient Compression

Recently Cui et al. reported that the pH gradient in a microfluidic device is compressed to the middle of a channel, rather than in the whole channel starting from the anode and ending at the cathode.[79] Similar compression phenomenon was found to be existed in these experiments. For the electropherograms in Figure 3-2, the compression ratio is 83, 84, 88 and 93% for channels II-V, respectively. The compression ratio was the actual distance (in pixel) between two major peaks of GFP and RPE divided by the calculated distance from their pI difference and the pH gradient. The results suggest that catholytes and anolytes entered into IEF channel for a short distance (7-17% of the channel) to facilitate the formation of pH gradient. The degree of compression decreased with the length of separation channel.

The effects of different pH gradients, pH 4-6 and pH 3-10 on IEF focusing and gradient compression was also investigated. As expected, the peaks were better resolved in the pH 4-6 gradient, having larger peak separation than that of the pH 3-10 gradient, as shown in Figure 3-10. Both experiments were run in 5.2 cm channel. The separation voltage was 1000 V. Their compression ratios were calculated 56% and 61% for the pH 3-10 gradient and the pH 4-6 gradient, respectively. The results suggest that catholytes and anolytes entered about the same level for both pH gradients.

Cui et al. suggested that an increase in the viscosity of catholytes and anolytes may reduce the compression of pH gradient.[79] This was studied by adding different concentration of glycerol in both catholytes and anolytes (glycerol concentration at 25%, 50% and 65%). There was no evidence of any decrease in pH gradient compression. In fact, it was observed that there was decrease in the peak distance between GFP and RPE (137, 122, and 98 pixels for 25, 50, and

65% glycerol, respectively), indicating an increase in the compression. Also observed was an increase in the focusing time at a higher viscosity, suggesting a longer time is required to form a pH gradient.

3.5 Conclusion

IEF theory predicts that the IEF resolution is independent of separation length under the conditions that meet the assumptions in the derivation. The assumptions include (1) negligible EOF; (2) negligible Joule heating; (3) constant pH gradient, d(pH)/dx,; and (4) constant mobility difference at pI value, dμ/d(pH). The conclusion is significant since it supports the use of IEF in a microfabricated device without sacrificing the resolving power, and at the same time the analysis time is significantly reduced due to shorter channels and higher electric field strengths. Although IEF was performed in channels III-V for separation of GFP peaks with a pI difference of 0.1 pH units, there was a slight increase of separation resolution with the separation length. The deviation of the experimental results from the theory is possibly due to the presence of EOF and/or Joule heating as discussed above.

The LIF whole-channel imaging detection (WCID) system is a very useful tool for studying IEF dynamics. Simultaneous illumination of an entire channel with an expanded laser line and collection of fluorescence emission by a CCD camera enable elimination of the mobilization step that is often practiced in capillary or channel IEF. In addition, WCID provides useful information about the dynamic behavior of protein migration during the process of IEF, and the temporal information could be used for determining the shortest focusing time as demonstrated in this work.

pH gradient compression reported recently by Cui et al.,[79] that is, the pH gradient is compressed to the middle of a channel exits, rather than crossing the whole channel from the

anode to cathode. This phenomenon is important because it conveys the exact distance of a pH gradient actually formed, rather than the assumed capillary or slab length. In addition, presence of EOF also affects the actual distance of a pH gradient since some separation medium might flow out of the separation channel or capillary. These factors suggest an immobilized pH gradient is probably a direction for future work,[103-105] especially considering the claim that a true steady state in absence of immobilized pH gradients cannot be achieved experimentally at all according to theoretical simulation.[30]

The IEF process performed in 6 channel device gave an idea of process parameters. These are now used to perform the first dimension separation in 2-D microfluidic device and are discussed in later Chapters.

Table 3-1. The effects of IEF distance on separation resolution. Separation resolution was calculated as discussed in the text. The standard deviation was obtained from three repeating experiments. The separation voltage for each row was listed in the first column while other experimental conditions were the same as in Figure 2.

	Channel II	Channel III	Channel IV	Channel V
Separation Length (cm)	1.9	3.0	4.1	5.2
Resolution (200V)	0.95 $\pm$ 0.07	1.1 $\pm$ 0.2	0.7 $\pm$ 0.1	1.5 $\pm$ 0.4
Resolution (300V)	1.1 $\pm$ 0.4	1.2 $\pm$ 0.1	1.4 $\pm$ 0.2	1.6 $\pm$ 0.3
Resolution (400V)	1.0 $\pm$ 0.1	1.5 $\pm$ 0.3	1.7 $\pm$ 0.2	2.1 $\pm$ 0.2
Resolution (500V)	1.2 $\pm$ 0.3	1.4 $\pm$ 0.3	1.6 $\pm$ 0.9	1.7 $\pm$ 0.4

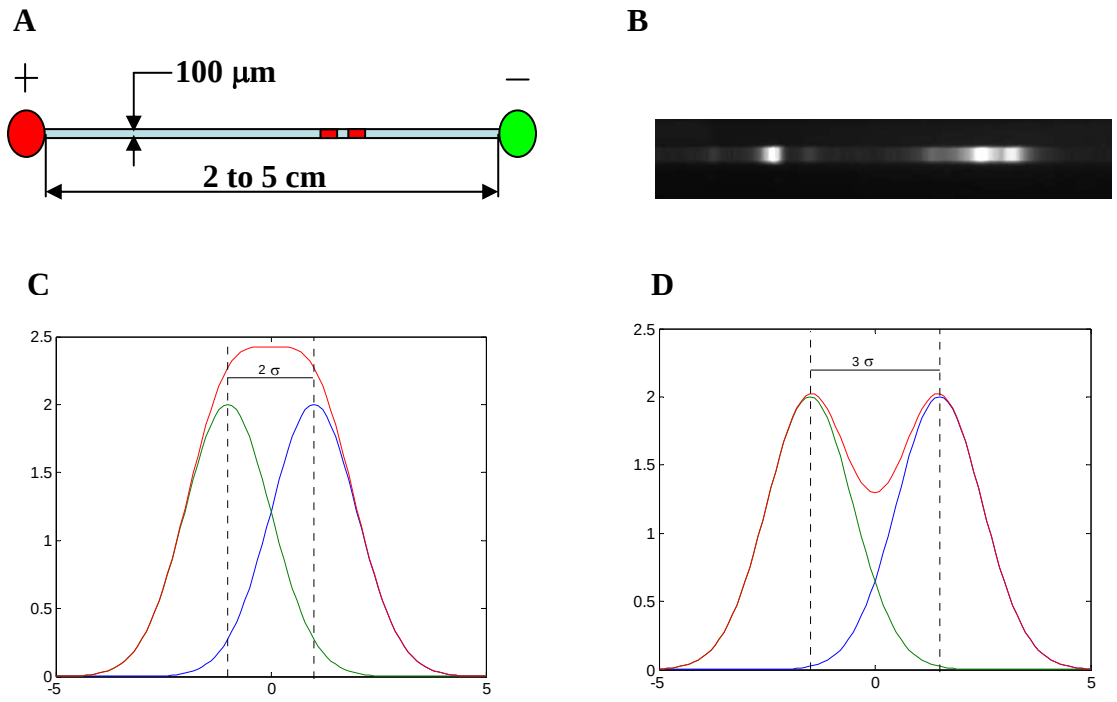

Figure 3-1. Illustration of separation process for closely spaced peaks. A) Representative diagram of channel with two closely spaced proteins. B) The real picture of two proteins GFP and RPE focused in microchannel. RPE on the right has two closely spaced peaks which are barely resolved. C and D) Illustration of minimum spatial difference required between two peaks to be resolved properly. Two closely spaced Gaussian peaks (green and blue, both have same characteristics) are separated by 2σ in picture C and 3σ in picture D. It should be at least 3σ of the gaussian curvature of the peaks for them to be resolved. The red line is superposition of two gaussian lines green and blue.

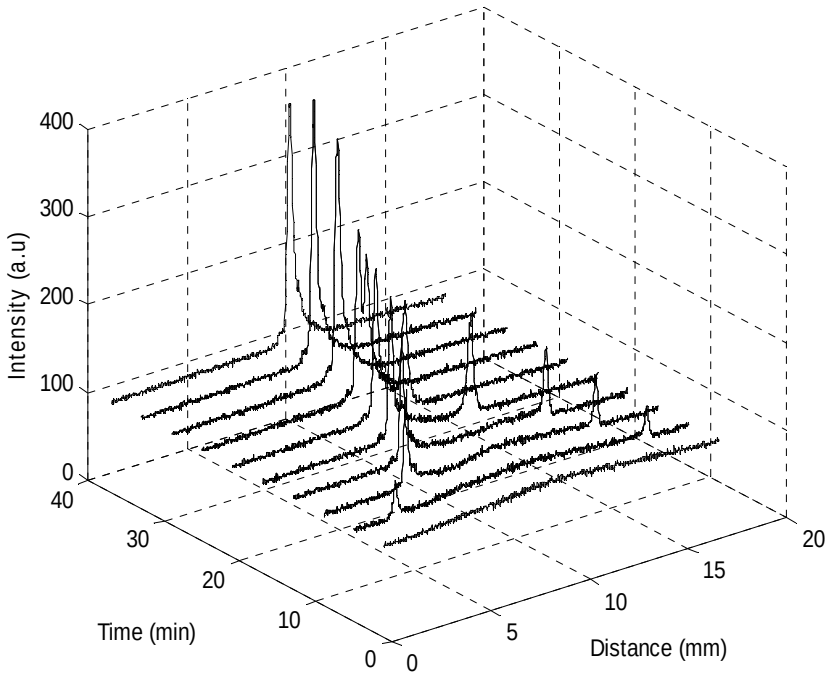

Figure 3-2. The temporal images of IEF separations of GFP in polyacrylamide gel. The length of channel is 3 cm. The electric field applied is 200 volts and total time for focusing is 40 minutes. The device used was made in glass.

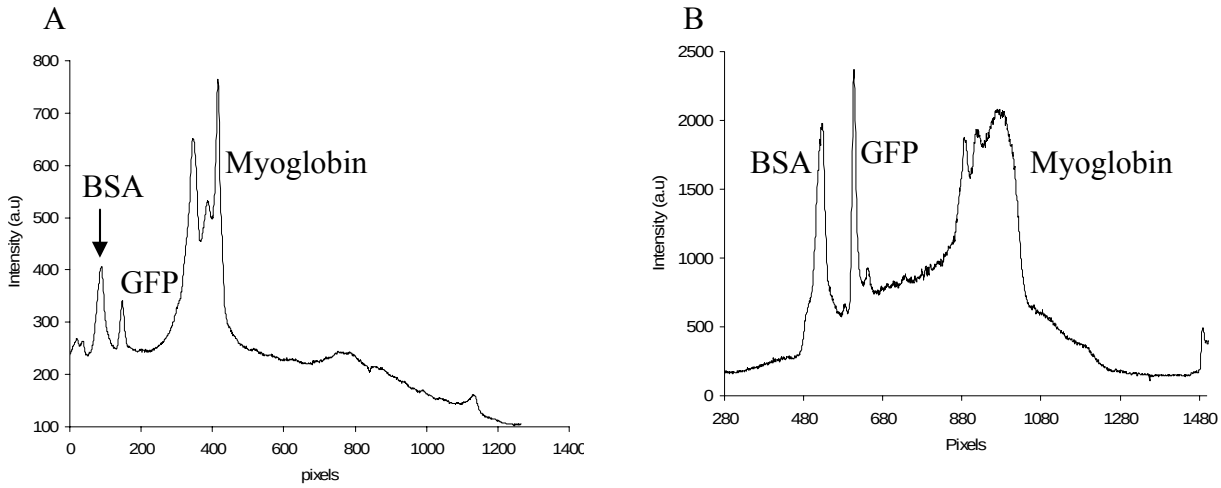

Figure 3-3. IEF of different proteins in gel and linear polymer. A) IEF of GFP, BSA and Myoglobin in linear polymer. B) in polyacrylamide gel. The electric field strength in both the cases is 66 V/cm. Time of completion for linear polymer is 20 minutes whereas for gel is 40 minutes.

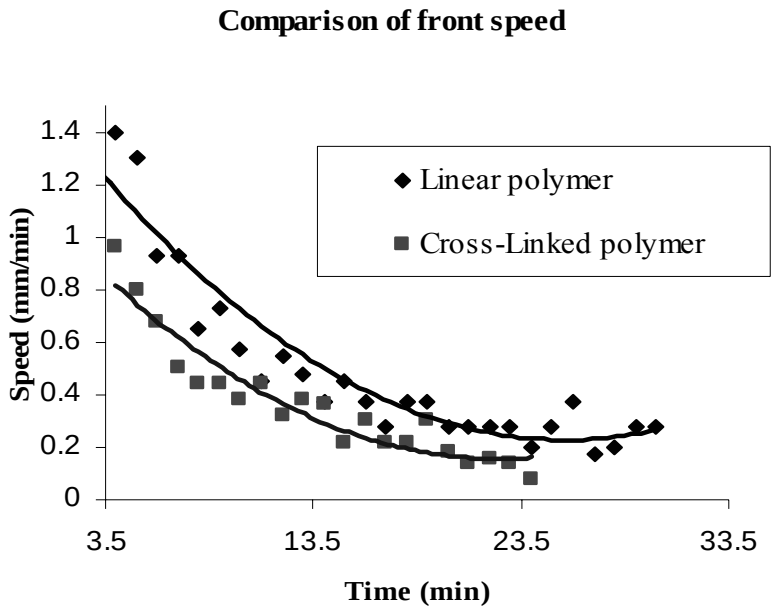

Figure 3-4. Comparison of front speed for different separation medium

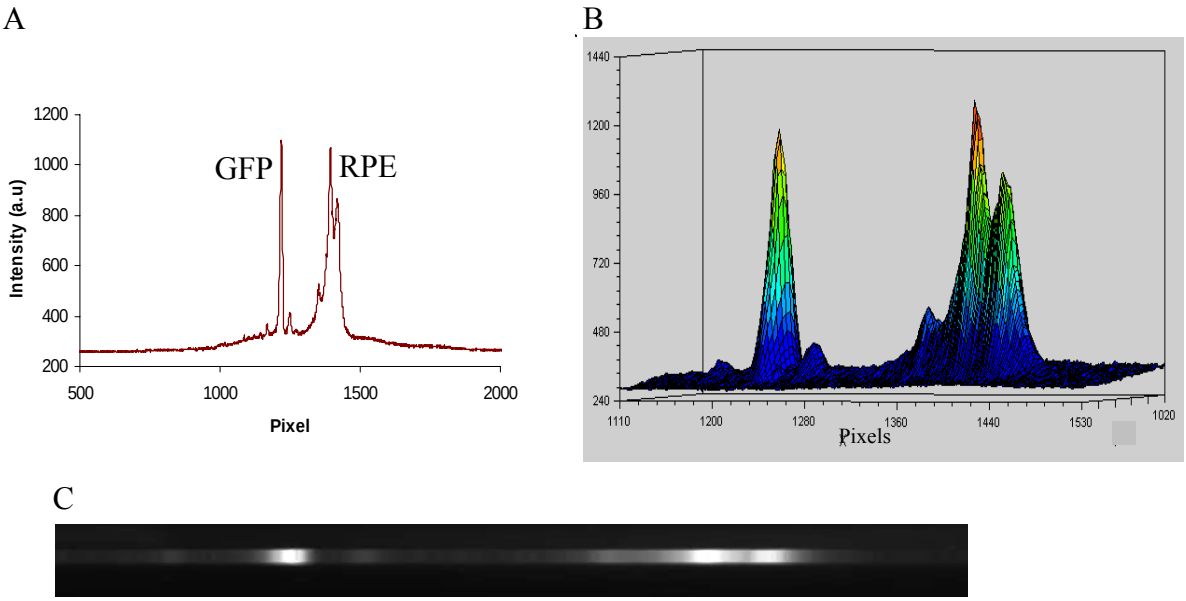

Figure 3-5. IEF of GFP, RPE in HPC/HEC linear polymer. A) line intensity profile at the center of the channel. B) Full channel intensity profile in the software where the intensity is plotted over the region of interest. C) The image acquired by the CCD camera. The minor peaks of GFP are lost when the image is converted to JPEG format.

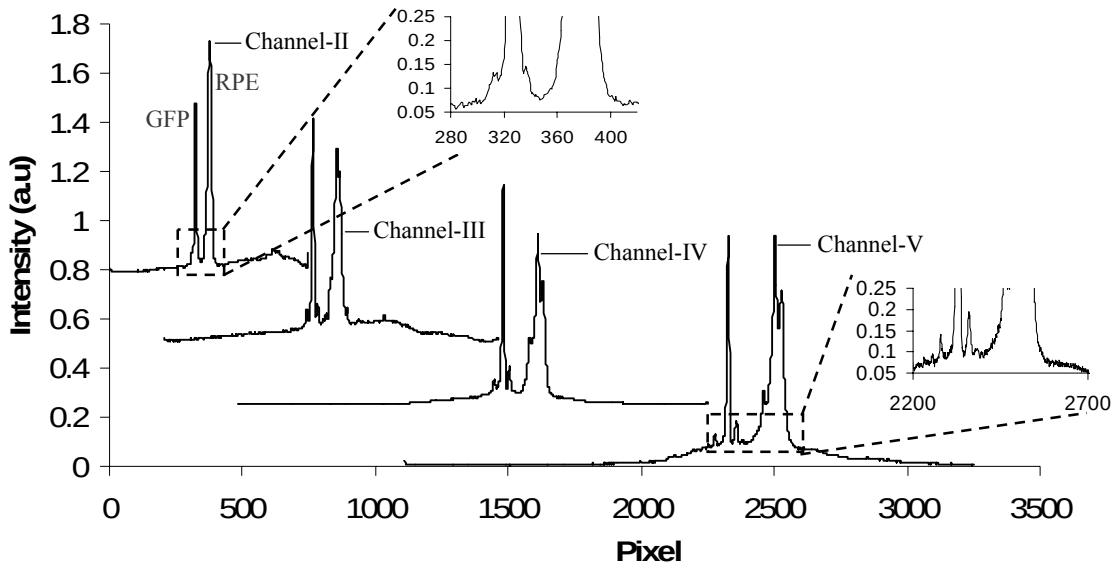

Figure 3-6. The effects of the separation distance on IEF separation. GFP (5 ng/µl) and RPE (3.85 ng/µl) were separated in IEF with channel length of 2.1, 3.2, 4.3 and 5.4 cm. Minor peaks of GFP are shown in the expanded views of a part of electropherograms for 2.1 cm and 5.4 cm channel. A voltage of 500 V was applied to all channels; and the cathode was on the left and the anode was on the right. The pH gradient was 3-10, and the separation medium was prepared from 1.83% HPC/0.93% HEC stock solution. The IEF times were 3, 6, 11, and 18 minutes for channels of length 2.1, 3.2, 4.3 and 5.4 cm, respectively. Each pixel in x axis approximately corresponds to 20 µm. The IEF electropherograms were shifted in both axis for clarity, the degree of up-shift is indicated by the background intensity and that of right-shift is by the starting point.

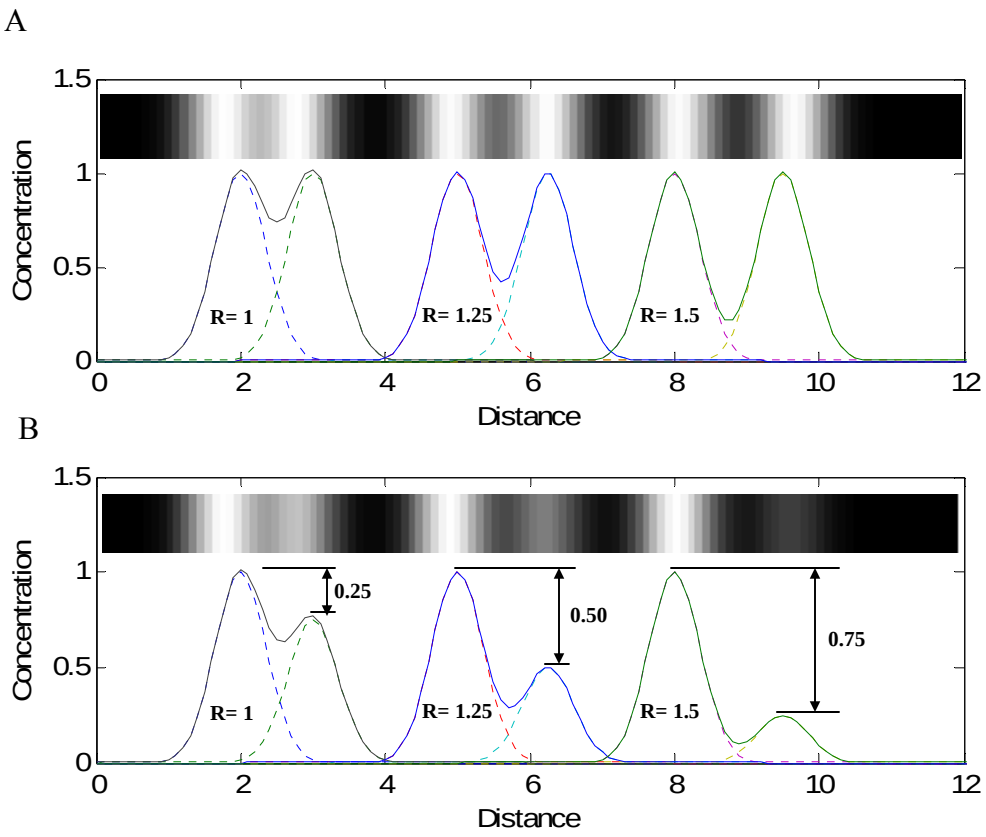

Figure 3-7. Separation resolution based on peak width and separation distance. A) Three different resolution 'R' values (1, 1.25, and 1.5) and its corresponding grey scale image is shown. The relative peak heights are same. Dotted lines represent the original pulses whereas the firm lines are after superposition. B) Same as in A, but the relative peak heights are at a ratio of 1:0.75, 1:0.5, and 1:0.25.

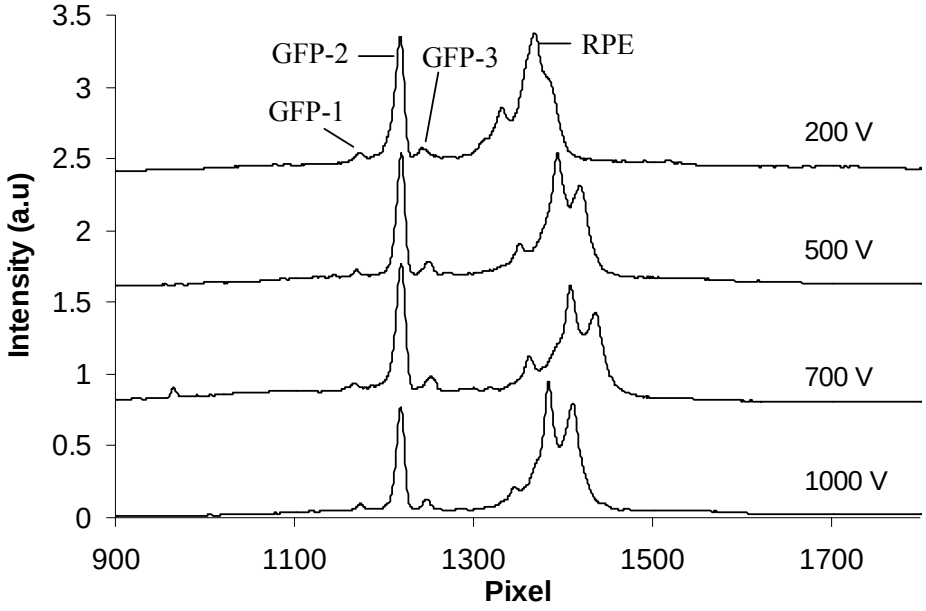

Figure 3-8. The effects of separation voltage on IEF. IEF electropherograms at separation voltages indicated. 5.2 cm channel was used for all experiments. Other conditions were the same as in Figure 3-6.

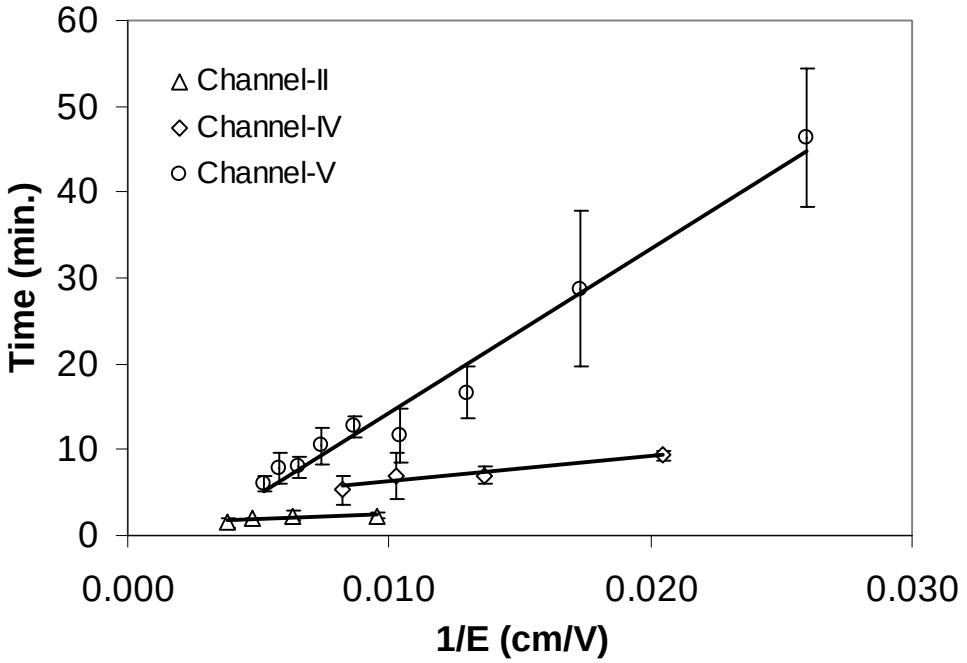

Figure 3-9. The relationship between the focusing time and the inverse of the electric field strength. The pH gradient used was 3-10. The separation length is represented by the channel number while the separation voltages were indicated by the electrical field strength. Other conditions were the same as in Figure 3-7

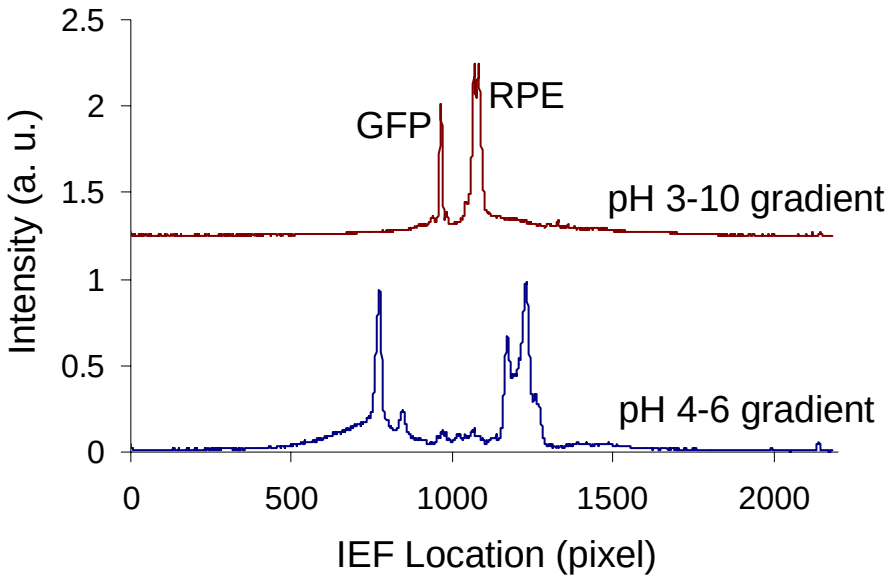

Figure 3-10. Comparison of IEF electropherograms of GFP and RPE between pH 3-10 and pH 4-6 gradients. Channel V was used with a separation voltage of 1000 V. Other conditions were the same as in Figure 3-2.

CHAPTER 4
TWO DIMENSIONAL SEPARATION OF PROTEINS[‡]

4.1 Introduction

Two dimensional protein separation in the slab gel format is well developed and has been around for almost half a century. Although this method provides very high resolution, it has a few drawbacks. The process involves complex handling procedures. First IEF is performed separately and then transferred in gel for second dimension separation. Thereafter a tedious staining process is required to visualize the separated proteins. The time involved is also very long, more than ten hours. Several groups have explored the application of microfluidics for multidimensional separation of proteins/peptides because of faster operation and other advantages offered by microfluidics as described previously. Chen et al.[48] had used 6 layers of PDMS for performing IEF and SDS-PAGE, but this process involves alignment, bonding, debonding and realignment of PDMS layers which is also very tedious process. Li et al.[49] had used plastic microfluidic device to couple IEF and SDS-PAGE using one cross channel and 10 parallel channels that are orthogonal to the cross channel. The cross channel is used for IEF whereas the orthogonal channels are used for SDS-PAGE. The medium of separation is viscous liquid. This is a pretty novel technique, but there is a problem of contaminating first dimensional constituents with the second dimension. The cross-talking between different media is of important concern when performing this type of multidimensional separation. In this research, an array of microfluidic valves is created to obtain a reliable interface which prevents one separation medium from contaminating with the other separation medium.

[‡] A part of this Chapter has been published : Das, C.; Fredrickson, C.K.; Xia, Z., Fan, Z.H. *Sensors and Actuators A*, 134, 271-277, 2007

4.2 Materials and Methods

The reagents used for IEF is already described in Chapter 3. The additional chemicals required are as follows. Sodium dodecyl sulphate (SDS), Tris-HCl (1M) and Tricine is purchased from Fisher scientific (Atlanta, GA). Hydroxycyclohexylphenyl-ketone (HCPK) and acrylamide monomers (acrylamide / bisacrylamide, 19:1 ratio in 40% stock solution) are purchased from Sigma (St. Louis, MO). The SDS-PAGE medium is made of polyacrylamide (8-12% T), whereas IEF medium is made of linear polymer, constituents of which are same as discussed in Chapter 3. '%T' defines the total amount of polymer concentration in solution (the amount in gram of acrylamide + gram of Bis per 100 ml of solution). An acrylamide concentration of 8-12%T is generally used depending on the type of proteins separated. For exclusive SDS-PAGE, the proteins are precomplexed with SDS (1%) at 95 ^{0}C for 5 minutes before separation (section 4.7). Similarly 0.1% SDS is electro kinetically injected inside the acrylamide gel before IEF and then 10% SDS solution in slot for SDS-PAGE only in Figure 4-2. For all other cases, 10% SDS is injected inside the gel from slot only after IEF is performed. Following are the detailed steps required to be performed for a standard 2-D separation.

1. Photopolymerization: The monomer solution for photopolymerization is prepared by adding 125 µl of acrylamide/bis-acrylamide monomer solution (19:1), 20 µl of Tris-HCl (1 M concentration), 20 µl of Tricine (1 M concentration), 65 µl of HCPK (100 mM in propanol) to 260 µl of DI water in a vial. The contents are mixed well and kept under cover to prevent it from room light. The 2-D device is then placed under microscope and the monomer solution is added to the top slot and two reservoirs (for IEF). Vacuum is used to suck the monomer solution into the parallel channels and cross channel. Care should be taken such that there are no bubbles anywhere inside the channel. The remaining liquid is then drained. DI water (2 µl) is added in each circular reservoir. Since it is impossible to drain the monomer solution totally from IEF reservoirs, so adding DI water dilutes the remaining monomer solution and will not polymerize in the reservoirs. The monomer solution is also drained from the two slots but it is ensured a thin layer of solution is present near the junction of parallel channels with slot such that no air bubble is trapped inside the channel during polymerization. The device is then flipped over and the mask is placed carefully on the top of the device. The mask is carefully placed such that the cross channel is completely covered by the mask. The device thus made ready with mask covering the cross channel, is exposed to

UV light. The high intensity of UV light (75 Watt lamp) polymerizes the parallel channels within 50 seconds. The diameter of UV light is around 2.5 cm. So during photopolymerization only 19.6 square cm area of the device is polymerized. The device is then removed from UV source. The mask is removed. The cross channel did not polymerize due to presence of mask. One of the IEF reservoirs is filled up with DI water and contents of the cross channel is sucked out of the other reservoir. The water is added to the reservoir is to ensure air does not go inside the cross channel when monomer solution is removed from the cross channel. Now both the slots are filled up with monomer solution and the device is again exposed to UV light for further polymerization, but this time without the mask. The whole device is polymerized for about 5 minutes. The device is again removed from the UV source and gel from the slot is removed. All the slots and reservoirs are filled up with DI water and the device is kept under DI water for future use.

2. IEF in cross channel: The next step is to perform IEF in cross channel. The IEF medium is prepared as described previously. 5 μl of this medium is pipetted into one of the reservoirs of cross channel. The liquid is sucked into the cross channel and the remaining liquid is removed. Anolytes and catholytes are loaded onto two reservoirs. The negative electrode slot is filled with 10% SDS solution whereas the positive electrode slot is filled up with TrisHCl buffer (20 mM). The device is then placed in the platform where the experiment is performed. 4 electrodes required for the 2-D separation is carefully lowered into the reservoirs and slots of the device. The electrodes used for IEF is 0.5 mm thick platinum wire whereas flat 2 cm platinum foil (0.05 mm thick) is used for SDS-PAGE electrodes in slots. The laser line is focused onto the cross channel and 100 V/cm is applied to the cross channel whereas the slot electrodes are kept floating. Proteins will focus inside the cross channel and will be visible as distinct fluorescent peaks. It takes around 5 minutes to perform IEF.

3. SDS-PAGE: The laser line (20 mW) is now shifted from the cross channel towards the parallel channel. The laser line is usually placed either at 6.5 mm or 2 cm away from the cross channel. After IEF operation is over, 1200 V is applied across the parallel channels through the slot electrodes. 10% SDS inside the negative slot is electro kinetically injected inside the gel. It meets with the proteins already focused on the basis of charge inside the cross channel. The SDS then binds with respective proteins to form the negatively charged complexes inside the parallel channels. These proteins as they travel inside the parallel channels get separated on the basis of molecular weight. These separated proteins can be seen arriving at different times to the zone where they are detected by a laser line. The whole process is continuously recorded by the CCD camera (exposure time 1 second with full analog gain). The images are later processed in MATLAB to obtain a 2-D map. It takes around 5-8 minutes to perform SDS-PAGE.

Figure 4-1 A) shows the schematic of two types of devices used for the 2-D separation. The first design consists of one cross channel and several parallel channels. The cross channel AoBo is for IEF process. Once the IEF is completed, the second dimension separation is done in orthogonal parallel channels CD. Two different separation medium is used for IEF and SDS-

PAGE. Figure 4-1 B) shows the similar layouts of device but a part of the CD channels are staggered with each other. These staggered intersections ensure all samples in the first dimension flow into the second dimension. These devices are made through a glass master, and the channel is 100 μm wide while the CD channels are separated by 360 μm (center to center). The number of orthogonal channels is 29 for both design, but there is an additional channel on the left for the staggered design to realize the staggering arrangement. The most important aspect of 2-D separation is to achieve reliable gel valve, which is discussed next.

4.3 Polyacrylamide Gel Valve

An array of pseudo valves is designed by having *in situ* gel polymerization for all parallel channels. The solution for making gel valves is prepared by mixing HCPK, a photo-initiator (100 mM in propanol) with acrylamide monomers (8%T), and DI water in a volumetric ratio of 1:3:6. A mask is used to define the physical location of gel such that the IEF channel is left unpolymerized. Figure 4-2A shows the mask pattern used to check the fidelity of pattern transfer to gel. The gel is formed by introducing monomer solution of acrylamide between two glass slides separated by a spacer of measured thickness (Figure 4-2B). The spacer is made by spinning photoresist SU-8 at a certain speed to give the desired thickness. Then it is exposed to UV light with a mask to form the desired gel pattern. The lines on the mask will block UV light exposure and lead to no polymerization in the region. Table 4.1 shows the effects of mask dimension as well as gel thickness on the width of gel formed. The fidelity of pattern transfer is better for thinner gels when all experimental conditions (exposure time, energy density of UV light and gel composition) are kept constant. Mask widths are the actual line thickness printed out.

Another aspect of photopolymerization is to reduce the time required for exposure to UV light. Photopolymerization is not strictly defined by direction of light. With long time of exposure to UV, solution will polymerize nearby even in the presence of mask as the reaction initiated by HCPK can propagate in all the direction. Monomer and photoinitiator concentrations are varied to investigate their effect on time of exposure. Figure 4-3 shows the plot of polymerization time with respect to acrylamide concentration, keeping photo initiator ratio concentration constant. The plot is linear in nature, suggesting the exposure time should be reduced for higher concentration. Below 4% T, monomer is still a viscous liquid after polymerization. Above 8% T the polymerization process takes less than 5 seconds.

The percentage of photoinitiator also affects the polymerization time. Figure 4-4 shows the rate of polymerization as a function of the concentration of HCPK at a constant acrylamide concentration (6% T). The polymerization process is almost independent of time below a certain concentration of HCPK (< 4%), as with very long time of exposure even very small concentration of photo initiator (HCPK) will ultimately polymerize the whole liquid.

These results discussed above are obtained by performing experiments on a glass substrate. The optical depth of glass slides and plastic devices are different. Hence the time of polymerization will be different in plastic device, but the overall trend will remain the same. The UV exposure time and power required is arrived at by performing a series of experiments at different power and exposure time. For higher powers the polymerization is fast but bubbles tend to form inside the channel due to heat from UV light, whereas at low power the required time of exposure is long, and it tends to dry up the wells and air goes inside the channel. The optimum condition of polymerization in plastic device is as follows:

Acrylamide / bisacrylamide: HCPK = 2:1

a. UV-energy density @ 365 nm wavelength = 40 mW/cm^2

b. Time for polymerization = 50 seconds

Next step is to perform selective polymerization in parallel channels in 2-D device. All the channels in the device in Figure 4-1 are filled with the solution. The device is then turned upside down and a chrome mask with a 100 μm line is placed on the top (the film side) of the device. To make gel valves at precise locations, an alignment is made between the line in the mask and AB channel in the device. Then the device is exposed to UV light for about 50 seconds. Figure 4-5 shows the schematic of the UV-polymerization process.

Photo-initiated polymerization took place in all parallel channels (CD from Figure 4-1 A) because they are exposed to light, whereas the solution in the cross channel (AoBo from Figure 4-1 A) channel did not polymerize since UV light is blocked by the mask. Non-polymerized solution in the AoBo channel is removed by vacuum and replaced with the first dimensional separation medium. Figure 4-6 shows the selective polymerization of acrylamide in microchannel. The gel is dyed with congo red. Monomer solution in the proximity of the region exposed to UV light tends to polymerize as well. This obstacle is overcome by adjusting the size of the mask line and UV exposure time.

Once the selective photopolymerization is completed, the nonpolymerized cross channel (AoBo) monomer solution is sucked out. IEF solution is then introduced in that channel and IEF is performed in first dimension, details of which are discussed in next section.

4.4 IEF in First Dimension

IEF in first dimension is performed by applying 200 V across the channel AoBo filled with IEF medium as shown in Figure 4-7 B. The parallel channels are polymerized with polyacrylamide gel as discussed above. The IEF medium is linear polymer of 1.83% HPC / HEC and all other constituents are same as the experiments performed in the 6 channel device. Figure

4-7 B shows the separation of GFP and RPE in cross channel whereas Figure 4-7 A shows similar separation in 6 channel device. They are very similar in nature.

As seen from Figure 4-7 the PAA gel in the parallel channel did not contaminate the IEF medium. Also the IEF medium did not penetrate inside the gel, resulting in clean separation of two proteins. However these two proteins can not be used for SDS-PAGE separation as they lose their fluorescence after complexation with SDS. This will be discussed in detail later. So new fluorescently labeled proteins are also used to demonstrate the robustness of the gel valve in the cross channel. Figure 4-8 shows IEF of four proteins (three labeled and one naturally fluorescent protein) in the cross channel. The proteins used are paralbumin (pI 4.10), ovalbumin (pI 4.6), BSA (pI 4.6) and GFP (pI 5.0). The Figure 4-8 shows three distinct peaks because BSA and ovalbumin share the same isoelectric point and they could not be separated in IEF.

The linear polymer for IEF medium is increased to 2.75% HPC to reduce the effect of hydrostatic imbalance. The separation is achieved by applying 300 V across the cross channel.Table 3 shows the comparison of resolution between the cross channel of 2-D device and that of 2, 3 and 4 cm channels. The resolution of 2-D device (calculated for major peaks of GFP and RPE) is 1.95 whereas for 2 cm channel it is 2.12. The peak widths and distance between the peaks for two proteins are also similar. The experimental conditions like field strength (100 V/cm) and IEF medium (similar concentration of linear polymer and CA and protein concentration) are same for all the cases. The resolution for 3 cm (2.38) and 4 cm (2.64) is however better than 2D device (1.95) mainly because of channel length. The increase in channel length leads to better control of hydrodynamic flow and less effect of pH gradient compression.[79, 106] However these two proteins can not be used for SDS-PAGE separation as they lose their fluorescence after complexation with SDS. So fluorescently labeled proteins are

also used to demonstrate the robustness of the gel valve in the cross channel. Figure 4-8 A shows IEF of four proteins (three labeled and one naturally fluorescent protein) in the cross channel. The proteins used are paralbumin (pI 4.10), ovalbumin (pI 4.6), BSA (pI 4.6) and GFP (pI 6.0). Three distinct peaks (electropherogram in Figure 4-8 B) are only visible because BSA and ovalbumin share the same isoelectric point and they could not be separated in IEF. Figure 4D shows the plot of isoelectric point of the above proteins with respect to their physical location inside the cross channel. The linear trend (R^2=0.99) of the plot is very important as it shows the pH gradient generated in IEF is uniform and linear in nature. However if the data is further analyzed, it reveals a high compression of pH gradient.[79, 106] The cross channel is 15 mm long and if it is assumed that the pH gradient is established uniformly along the entire channel length, 1 pH unit will span a length of 2.14 mm of the cross channel. But the experiment shows a length of only 0.8 mm of cross channel is used for 1 unit pH gradient. This translates to a pH gradient compression of around 60%. This suggest some amount of catholytes and anolytes have entered inside the cross channel to facilitate the gradient formation. This fact can however be advantageously used in design of the device. The cross channel can be made longer without increasing the number of parallel channels or spacing between them for the similar resolution. The increase in length will also ensure less hydrodynamic instability and less effect on IEF due to electroosmotic flow.

4.5 Numerical Simulation

Integrated microfluidic systems with complex network like the 2-D device needs optimizations before being put to real experiments. CFD simulation can accelerate the design, development and optimization of these integrated microfluidic devices. Though it is still impossible to simulate the exact conditions prevailing in experimental conditions for 2-D device,

appropriate assumptions can make the problem definition simpler and results thereof can be used to understand the underlying physics of the problem.

One of the most important issues of the 2-D separation is the transfer of protein from cross channel to parallel channels. The relative position and blob size of proteins with respect to parallel channel will decide the way the protein will move while getting transferred. In order to understand this transfer phenomenon CFD-ACE multiphysics software is used for simulation. The problem description is defined below, followed by the methodology used for simulation.

Geometry: Two dimensional planar. Rectangular grid is generated by CFD-ACE software. Figure 4-9 shows the geometry. The full scale of the device is used for modeling. The parallel channel has a total length of 6.5 cm while the cross channel length is 1.7 cm. An individual channel is 100 μm wide and the distance between the parallel channels is 360 μm.This is a problem of transient electrophoresis of charged molecules/species. To do that all the parallel channels are divided into small segments, so that a particular species can be initially placed anywhere in the channel and its migration under an electric field can be studied. In order to simulate this type of problem, there is a feature in CFD-ACE which allows the electrical conductivity to be calculated as a function of ion concentration. Two different types of species are selected with different mass diffusivities ($2.5 \times 10^{-9} – 5.5 \times 10^{-9}$ m^2/s) and one or both the species are selected as negatively charged. The reason behind selecting the negative charge for species is that the protein in SDS-PAGE separation becomes negatively charged after complexation with SDS. The common buffer strength is $4x\ 10^{-6}$ 1/Ohm-m. Usually an electric field of 1000 V is applied across the electrodes. A time step of 0.001 s and Euler first order scheme is chosen for the transient solution with 20 iterations in each step.

4.5.1 Results and Discussion: The cross channel is filled up with one species whereas the parallel channel are filled up with a different species. An electric field of 100 V/cm is applied to the parallel channels via the slot. The negative cross channel species are gradually seen to move into the parallel channels. Figure 4-10 shows such a transfer of species from cross channel. The numerical results in Figure 4-10 A matches pretty well with experimental results shown in 4.10 B. The fluorescent proteins are seen to split less uniformly in one direction. Two possible reasons can be given, A) The parallel channels are staggered, so the electric field can not travel straight from parallel channels above the cross channel to the staggered ones below the cross channel. Two possible cases of electric field orientations are shown in 4.10 C and D. In first case the electric field splits equally into channels whereas the second case shows that the field does not split but follows a tortuous line. Either of the cases can happen. So for this experiment, proteins split preferentially in the direction of least resistance of flow path (electrical field) as in Figure D. It is difficult to justify similar preferential movement in numerical simulation. B) Presence of continuous hydrostatic flow in the cross channel, which may have moved the proteins in one particular direction in cross channel. This condition however is not present in numerical simulation.

If IEF is performed in cross channel first, the proteins will focus as bands in the cross channel and when these bands of proteins are transferred in the parallel channels, they will transfer either into a single channel or into multiple channels depending on the position and size of the bands. A few cases are simulated as shown in Figure 4-11. Figure 4-11 A shows the case where the protein after IEF is focused in between two parallel channels (topside) but since the parallel channels are staggered, the proteins are trifurcated into three channels while it is transferred. Figure 4-11 B shows the similar case, but here the protein plug is shifted in such a

way that it is in between two lower parallel channels. So during transfer the protein gets bifurcated neatly into two channels. Figure 4-11 C and D shows a smaller plug size. The plug is just above one lower parallel channel and gets entirely transferred in that channel (Figure C) whereas for Figure D the plug position is shifted and it gets bifurcated again. Figure 4-11 E shows the experiment result for protein plug transfer from cross channel to parallel channel.

The position of electrode in the slot of parallel channels can distort the electric field distribution inside the different parallel channels, which will in turn effect the electrophoretic movement of charged species. If a conventional pointed electrode is used, the channels near the electrode will have higher electric field whereas the channels away from the electrode will have less electric field. The difference in electric field distribution will lead to uneven electrophoretic speed of the charged species. The second dimension separation is based on the electrophoretic mobility of SDS complexed proteins. The detection of these proteins is done by illuminating the channels with a laser line at one particular location near the end of the parallel channels. As the proteins move past the detection zone, the CCD camera collects the signal with time. Proteins of different molecular weight will travel with different electrophoretic mobility (due to same charge to mass ratio attained during complexation of SDS with proteins, higher molecular weight proteins will have higher resistance to flow in gel due to bigger physical size and will have lower mobility) in the gel filled channels. Any artificial change of that mobility due to different electric field will cause the proteins to travel faster or slower than their counterparts in different channels. This will cause an error in the migration. An experiment is performed to demonstrate the problem. The parallel channels are polymerized with gel and the cross channel is then filled with a protein (GFP 1μg/ml) solution. Two pointed electrodes are placed on the two slots (at the center of slot) at the end of the parallel channels and an electric field is applied. Figure 4-12

shows the irregular positions of protein plug (GFP in this case) in different channels due to distortion of electric field. Non uniformity of gel can also be a reason for this behavior. It is difficult to ensure the uniformity of gel, so greater control on electric field uniformity is applied.

It is very important to ensure that the electric field is constant across all the channels. This can be ensured by using an electrode which covers the entire slot. Full scale simulation is carried out in CFD-ACE to evaluate the effects of electrode size and position on the transfer of plugs in parallel channels.

Three cases are evaluated, a) pointed electrode at center of slot b) pointed electrode at one corner of slot c) a flat electrode which covers the entire slot. The purpose is to evaluate the distortion of electric field at different condition. Electric field of 1000 V is applied across the electrodes. The buffer conductivity is 4×10^{-6} 1/Ohm-m and the mass diffusivities are 2.5×10^{-9} m^2/s for parallel channels and 5.5×10^{-9} m^2/s for cross channel. The mobility of the proteins or any other charged species will depend directly on the magnitude of the electric field. Figure 4-13A shows the field distribution for all the three case and as expected the distortion of electric field is more for the pointed electrode when compared with flat electrode. Figure 4-13 B shows the approximate field strength at a particular location across all the parallel channels. The configuration where the pointed electrode is at one corner shows maximum distortion in field of around 8% between two extreme channels. This will lead to an error of around 9 % in time taken by proteins to travel the same distance in channels. The center electrode configuration will lead to an error of around 2% on time. The flat electrode shows almost no variation in electric field. The CCD camera used for LIF detection can also used to monitor the protein front movement inside the parallel channels. Since SDS complexation renders uniform charges to mass ratio to the proteins, the protein of one particular mass will travel with constant velocity inside the parallel channels at constant electric

field.[107] Experimental results for pointed electrodes show a bow shaped (deviation $\pm 133\ \mu m$) migration pattern. This results in error of $\pm 1.2 kDa$ in the estimate of molecular weight of ovalbumin. The same experiment when performed with flat electrodes, gives more uniform field strength across the channels and results in similar migration velocity and hence flat shaped (deviation $\pm 23\ \mu m$)migration pattern in all the channels. The resultant error will be much less at $\pm 0.2\ kDa$. Figure 4-14 shows the plot for location of the protein peak with respect to time and the trend is very linear (R^2 =0.999). The inset plot shows almost constant velocity profile of the same data (4 pixels/s or 80 μm/s) with second order accuracy. Next different electrode configurations to control the two dimensional separations are discussed.

4.7 SDS-PAGE Separation

In conventional SDS-PAGE technique, proteins are allowed to bind with SDS through hydrophobic interaction. A constant amount of approximately 1.4 gram of SDS is complexed by each gram of protein to form the negatively charged complexes, with similar charge to size ratio. The gel used for this separation is a random meshwork of cross linked individual polyacrylamide mesh and has sieving effect on proteins during the separation procedure. When SDS-PAGE is performed by applying electric field the complexes migrate with a velocity which is dependent only on size of complex.[108] Hence this process can separate the proteins based on their sizes. The linear relationship between the logarithm of molecular weight and mobility allows one to determine unknown sample molecular weight by comparing with standards.

SDS-PAGE separation is first tried on two dimensional devices. The proteins are first complexed off chip with 1% SDS at 95 ^{0}C for 5 minutes. Four proteins are used a) trypsin Inhibitor (20 kDa), carbonic Anhydrase (31 kDa), ovalbumin (45 kDa) and bovine serum albumin (66 kDa). The device is filled with monomer solution and UV photopolymerization is

performed to form gel. The cross channel is covered with a mask as discussed before and is not polymerized. Two different gel strengths are used (10 & 12%).

The gel also contains Tris HCl (40 mM) and tricine buffer (40 mM) for supporting the electric field required for PAGE operation. The precomplexed proteins are loaded into the cross channel and an electric field of 1200 V is applied across the parallel channels. The proteins traveled from cross channel into the parallel channel and got separated due to difference in molecular weight. They are observed as separate peaks by the CCD camera when the channels are illuminated by a laser line at a distance of 6 mm from the cross channel. As seen from the Figure 4-15 the proteins separated shows consistent linear trend when their molecular weight is compared with their electrophoretic mobility. This is a very important characteristic for SDS-PAGE separation as proteins of unknown molecular weight can be separated and its molecular weight can be found out from the linear relationship with its electrophoretic mobility.

4.8 Two-dimensional Separation

The next step is to integrate both IEF and SDS-PAGE separation in 2-D device. In flat bed SDS-PAGE system, the gel medium contains about 1% SDS, so that when the proteins are transferred to the second dimension, the SDS inside the gel can form complexes. However in 2-D device, since the polymerization of parallel channel are done before IEF, any SDS in the cross channel can severely effect the IEF process. So the cross channel needs to be thoroughly cleaned before the IEF separation is tried. Also the gel inside the parallel channel should be well polymerized so that SDS does not leak out from the parallel channel into the cross channel.

To study the effect of SDS on IEF, a separate experiment is performed in 6 channel device. A small amount of SDS (0.1%) is added to IEF solution. As seen from the Figure 4-16, the SDS, even in small quantity, can affect the focusing process. RPE

forms a sharp peak without SDS. With SDS, however, a broad peak is visible just at the beginning of the experiment but became more and more diffused as the experiment progressed. Same effect is also observed when the experiment is performed in 2-D device with SDS in PAA gel in cross channel.

Next a different approach is tried, where the parallel channels are polymerized without SDS, so that there is no chance of IEF medium coming in contact with SDS. After the IEF is performed in cross channel, SDS is introduced in negative electrode slot of parallel channels. Thereafter an electric field (800 V) is applied and SDS is electrokinetically injected into the parallel channel. As the SDS went and interacted with proteins, they formed complexes and started traveling along the parallel channels. Figure 4-17 shows the results of IEF and corresponding transfer of proteins in the second dimension. The laser line for illumination in the second dimension is kept very close to the cross channel (5 mm away) to observe the transfer of proteins. As seen from the Figure the proteins are seen are transferred smoothly into the parallel channels (GFP in 7^{th} and RPE in 10^{th} Channel). Since the detection is made very close to cross channel, it is difficult to ascertain about the SDS complexation with proteins.

Though GFP and RPE are naturally fluorescent proteins and gives good peaks in IEF, they are not very useful for second dimension separation as the proteins loose their fluorescence as soon as they form complex. Although the proteins are seen traveling in the parallel channels, they gradually disappear and if the laser line is placed further down the channel, no fluorescence is detected. However there will be no such problem with labeled proteins as the SDS will not react with fluorescence of the labeling dye. Hence it is decide to label non fluorescent protein with a fluorescent dye.

Molecular probes' fluorescent labeling kit is chosen for labeling the proteins. The dye is insensitive to pH gradient of 4-10 and is ideally suited for our application. The absorption and fluorescence emission maxima are 494 nm and 519 nm respectively. The labeling procedure is well documented in literature and is discussed here in brief. The proteins are all separately labeled. The protein of concentration of 2 mg/ml is mixed with sodium bicarbonate solution (~ pH 8.3) to raise the pH of reaction mixture as the dye reacts efficiently at pH 7.5-8.5. The solution is then mixed with the dye and stirred with a magnetic stirrer for 1 hr at room temperature. After the reaction is over the labeled protein is purified from excess dye by passing it through a resin column and PBS (phosphate buffer) elution buffer. As the protein solution passes through the column, it gets separated into two fluorescent bands. The first band is that of protein and the following band is that of unlabeled dye. The protein is collected and stored at -20 ^{0}C. Five proteins are labeled in this way. The proteins are tabulated below in the Table 4.3. The labeled proteins are used to for all subsequent experiments. First a single protein is used to demonstrate the IEF and SDS-PAGE together. The protein is first focused in IEF and then transferred in second dimension for PAGE. Figure 4-18 A and B shows the focused peak of BSA in both IEF and SDS-PAGE. The protein is focused in IEF and then is nicely transferred to one of the parallel channels.

Next three proteins are tried together. The proteins are so chosen that all proteins can not be separated alone in any one dimension. Separation of BSA, trypsin and hemoglobin is tried as in Figure 4-19. The experimental conditions are same as described before. The three proteins are focused in IEF first. Since BSA and Trypsin are having same isoelectric point, they are not

separated in IEF. So there are two major bands in IEF. The band towards the acidic side contains both BSA and trypsin whereas the other band contains hemoglobin.

The second dimension (SDS-PAGE) however separates the BSA and trypsin as they differ in their molecular mass. Trypsin being the smallest in terms of molecular weight travels the fastest in gel followed by hemoglobin and BSA. Hemoglobin is already separated in IEF itself and it travels in separate parallel channel. IEF for most of the cases are done at 3-10 pH gradient, but there may be specific need to do the IEF at less pH gradient. One of them is improving the resolution in IEF. The next experiment is performed with 3-5 pH gradient in IEF but with different set of proteins (BSA, ovalbumin and trypsin).

The proteins got separated as expected based on their molecular weight as in Figure 4-20. But there is some discrepancies regarding the isoelectric point of the proteins. All the proteins have same pI point and hence can not be separated in the cross channel in IEF. However SDS-PAGE should separate all three because of difference in molecular weight. Trypsin and ovalbumin got separated in the same channels but BSA is seen traveling in the channel far away from the other two proteins. One possible explanation is the change of pI point of BSA due to labeling. The correlation between molecular weight and electrophoretic mobility is quite high ($R^2 = 0.9928$). Further experiments are performed with three or four proteins to characterize the system at different molecular weight and isoelectric point.

The above Figure 4-21 shows the 2-D map using three different proteins (BSA, ovalbumin and hemoglobin) in 3-10 pH gradient. Hemoglobin is more basic protein and hence is focused towards the right side and transferred to the extreme right channels. Trypsin is more acidic (pI 4.6) and has lower molecular weight (20 kDa) and got focused to wards left side and traveled

fastest down the parallel channels. Carbonic anhydrase has pI of around 5.9 and molecular weight of 31 kDa and hence is in the middle with respect to other two proteins.

There after four proteins are tried. They are BSA, ovalbumin, trypsin inhibitor and carbonic anhydrase. First three proteins have same isoelectric point (4.6) whereas the last one has isoelectric point of 5.9. So ideally first three proteins should get separated only in second dimension and in same perpendicular channel.

One of the important parameter for 2-D separation is to ensure proper on-chip complexation of SDS with protein. Presence of SDS already in gel enhances the complexation process. However it is difficult to photopolymerize gel inside the channels with SDS in monomer solution. So SDS (0.1%) is electrokinetically injected after polymerization into the gel before IEF. IEF in cross channel is not heavily affected because of very low concentration of SDS in gel. The injection time is about 10 minute to ensure uniformity of concentration of SDS though out the entire length of parallel channels. Figure 4-22 shows the separation of all four proteins. The proteins are well separated and the peak shape is very good and there are very less spurious peaks due to leaking of proteins in all different proteins during IEF. However there is very high amount of pH gradient compression observed in the cross channel. The total length of cross channel is around 17 mm and since a pH gradient of 7 units is used (Carrier ampholytes of pH 3-10), the entire channel should have linear pH gradient starting with pH of 3 at the anode end and pH of 10 at the cathode end. In that case the minimum difference between the proteins BSA (pI 4.6) and carbonic anhydrase (pI 5.9) should be 3.15 mm; otherwise the proteins will be atleast 8 channels apart. The difference observed in actual experiment is only around one channel gap or around 0.3 mm. This gives an approximate 10 times pH gradient compression.

The proteins thus compressed in IEF, got transferred in parallel channels. Another important aspect of IEF in linear polymer is the presence of electro-osmotic flow. The presence of electro-osmotic flow from anode to cathode tends to shift the focusing action more towards the right side of the cross channel. The electroosmotic flow is irregular due to highly random structure of gel on the interface of parallel channels. Some times presence of gel structure in cross channel and geometry enhances or reduces the electro osmotic flow. Figure 4-23 shows the similar focusing of four proteins (BSA, ovalbumin, hemoglobin and carbonic anhydrase) where the proteins are well distributed along the cross channel and
got transferred in the parallel channels. Though hemoglobin has lower molecular weight that BSA, yet it traveled slower in the parallel channels. The probable reason may the gel inconsistency between different channels. BSA and ovalbumin have similar pI (4.6) but different molecular weight. The map is not very clean as proteins seem to have leaked into different channels.

4.9 Conclusion

Gel valve array for introduction of two types of separation media in orthogonal channels for implementing two-dimensional protein separation is studied in a microfluidic device. The valve arrays are fabricated by using photo-definable, *in situ* gel polymerization. The precise location is provided by the photomask and optical alignment. The locally-polymerized gels function as pseudo-valves, leading to a fluidic network that allows (1) the first dimension based on IEF and the second dimension based on PAGE; (2) full sample transfer from the first to second dimension; and (3) negligible disturbance between two dimensions.

Isoelectric focusing of two proteins, green fluorescent protein and R-phycoerythrin, in the first dimension is demonstrated after gel valves are formed in the second-dimension channels. This result further showed the function of the gel valve array, verifying the overall concept of the

fluidic interface designed for two-dimensional protein separation in a microfluidic device. Different fluorescently labeled proteins are used apart from naturally fluorescent protein to study the viability of 2-D separation. The proteins are separated both on basis of charge (IEF) and molecular weight (SDS-PAGE). The separation based on mass showed a linear correlation when molecular weight is compared with electrophoretic mobility. The data matches well with literature. The separation in first dimension (IEF) takes around 5 minutes at 100 V/cm whereas the second dimension takes around 2-8 minutes depending electric field (120 V/cm-185 V/cm) and detection zone (distance away from cross channel). Presence of SDS in the gel helps on-chip protein complexation with SDS better.

Table 4-1. Effects of gel thickness and mask width on photo polymerization process.

Gel thickness (μm)		Mask width (μm)		
		56	66	68
25	Non-polymerized gel width (μm)	54	68	75
50		52	61	66
80		47	47	52

Table 4-2. Comparison of resolution between different channel lengths and 2-D device

	Peak width		Distance between peaks	Resolution
	GFP	RPE		
2-D device (1.7 cm channel)	39	46	83	1.95
2 cm channel	28	53	86	2.12
3 cm channel	37	83	143	2.38
4 cm channel	41	105	193	2.64

Table 4-3. Five different labeled proteins used for 2-D separation

No.	Protein	Isoelectric point	Molecular weight (kDa)
1	Trypsin Inhibitor	4.6	20
2	Carbonic Anhydrase	5.9	31
3	Ovalbumin	4.6	45
4	Hemoglobin	7.1	65.5
5	Bovine serum albumin	4.6	66

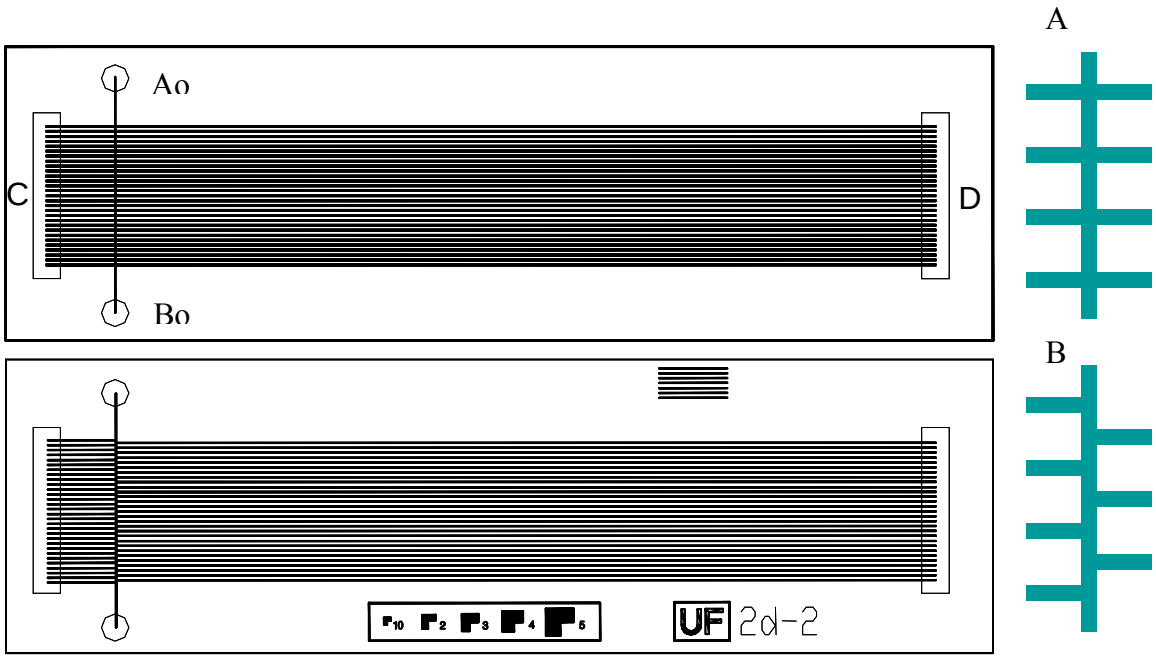

Figure 4-1. Layout of a microfluidic device for two-dimensional protein separation. It consists of one vertical channel (AoBo) and 29 horizontal channels (CD). An exploded view of the intersections of each device is illustrated on the right. The size of the device is 1" x 3". A) The device with intersections of aligned CD channels. B) The device with intersections of staggered CD channels.

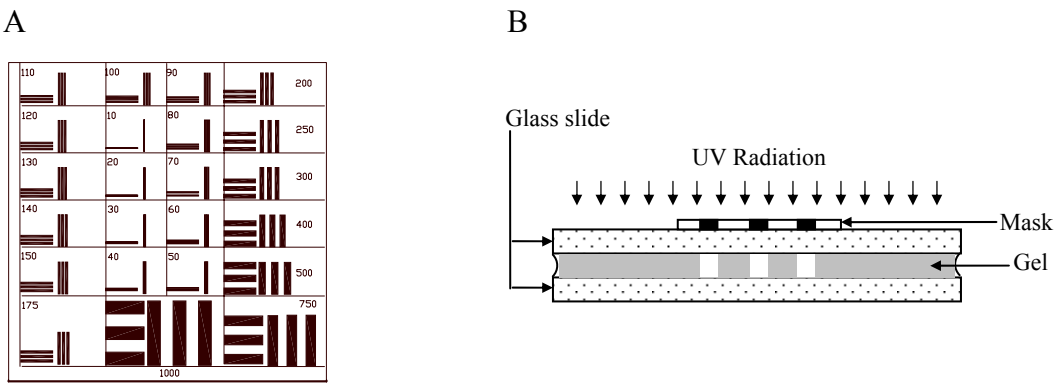

Figure 4-2. Photo polymerization in microchannels. A) The photomask printed out in transparency. The minimum line thickness is 10 μm, but while it is printed using commercial printer, minimum resolved line is 50 μm. B) The schematic of experiment for gel polymerization between two glass slides.

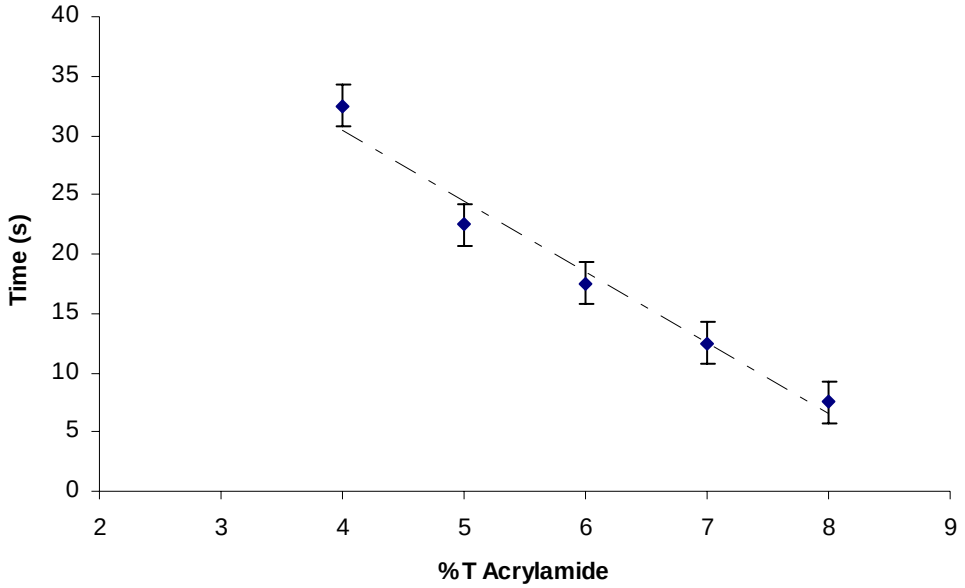

Figure 4-3. Polymerization time with acrylamide concentration.

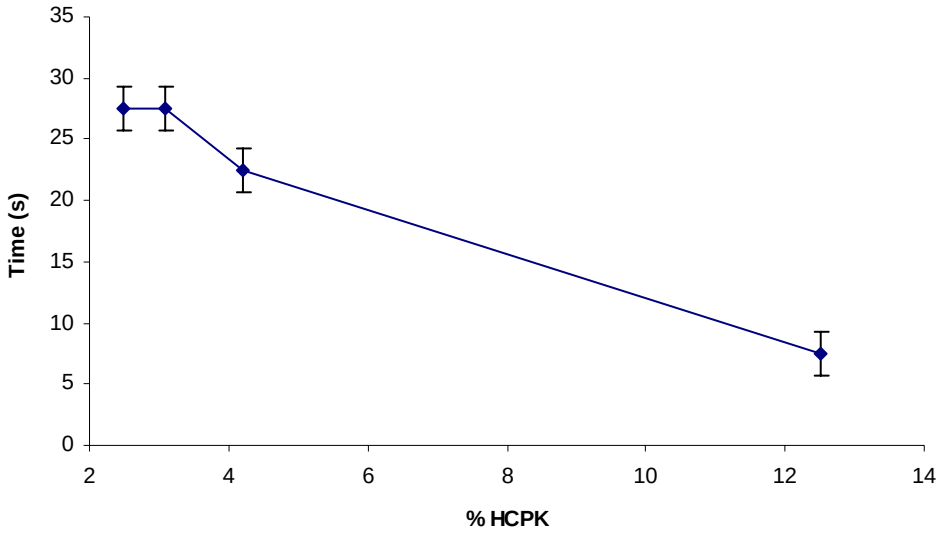

Figure 4-4. Polymerization time with HCPK concentration.

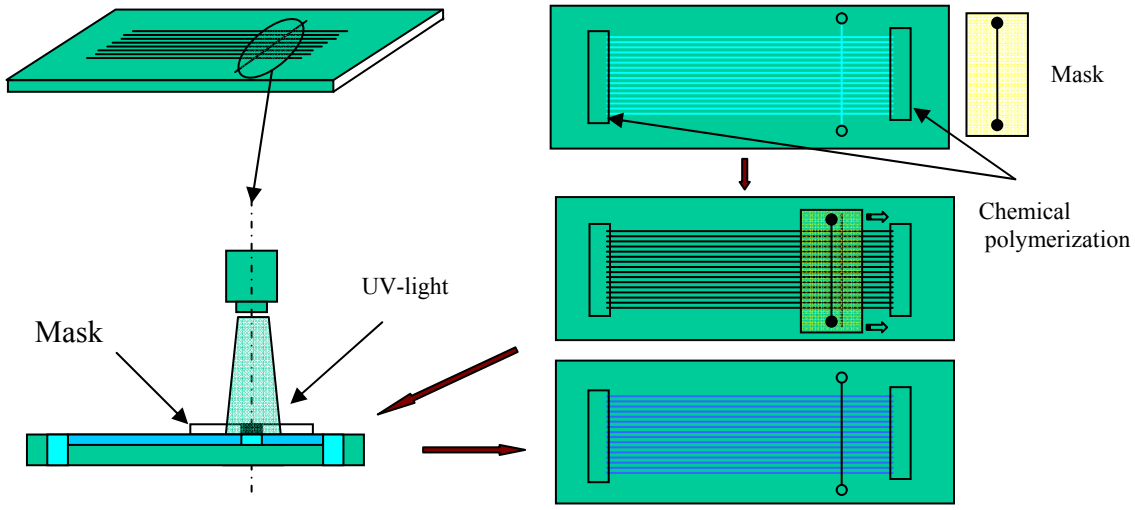

Figure 4-5. The schematic of photo polymerization of acrylamide inside the microchannel. The channels are first filled with the monomer solution. The two slots at the extreme end of parallel channels are chemically polymerized, so that during UV polymerization, air does not enter inside the channels from open slots. Chemical polymerization is not required for the end wells of the cross channel, since the liquid present inside the cross channel is sucked out after polymerization. The device is then flipped over and mask is carefully placed on top of the cross channel. Thereafter it is exposed to UV light for about 50 seconds. The mask is then removed, and the unpolymerized monomer solution is removed and replaced by the IEF solution.

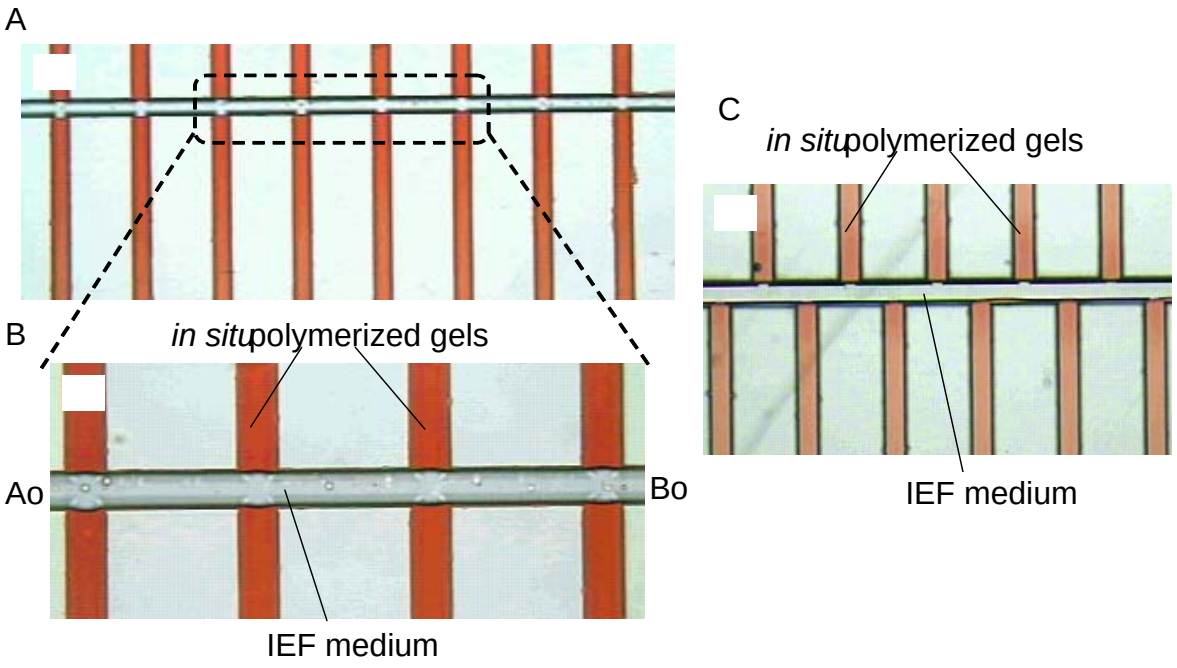

Figure 4-6. Micrograph of the valve arrays formed by *in situ* gel polymerization. Polymerized gels are dyed for easy visualization. A) From a device shown in Figure 4-1 A. B) An exploded view of the marked area in A. C) From a device shown in Figure 4-1 B.

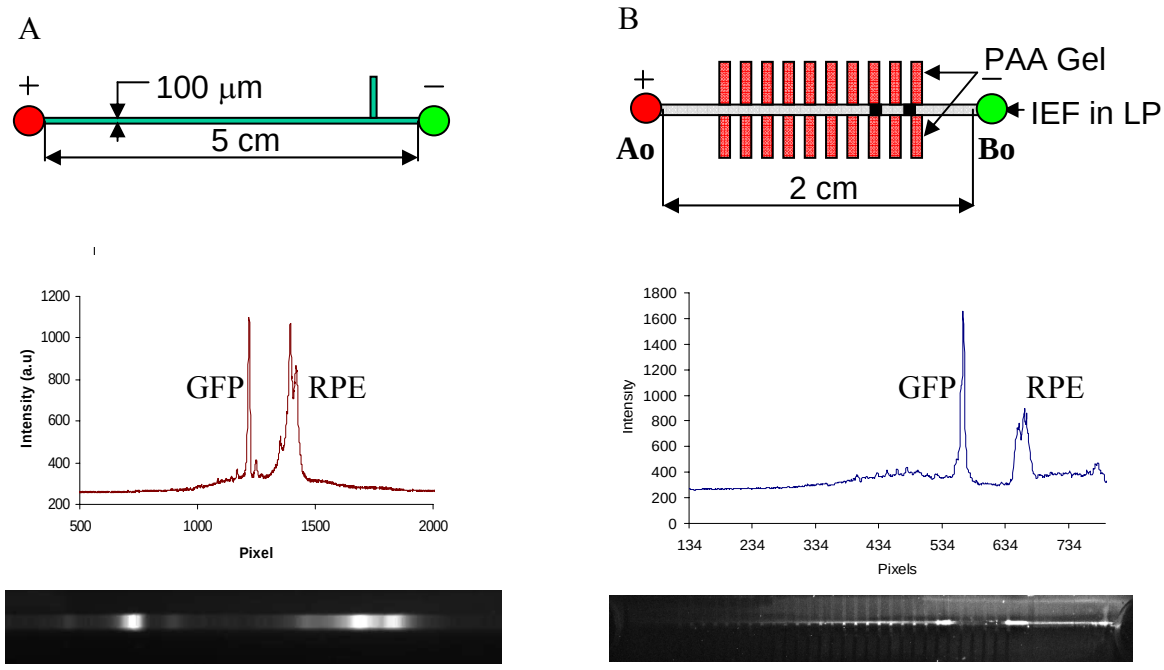

Figure 4-7. IEF in different microfluidic devices. A) IEF in 5 cm channel at 500 V. B) IEF performed in cross channel AoBo of 2-D device, while the parallel channels are polymerized with polyacrylamide gel using same experimental condition as in A.

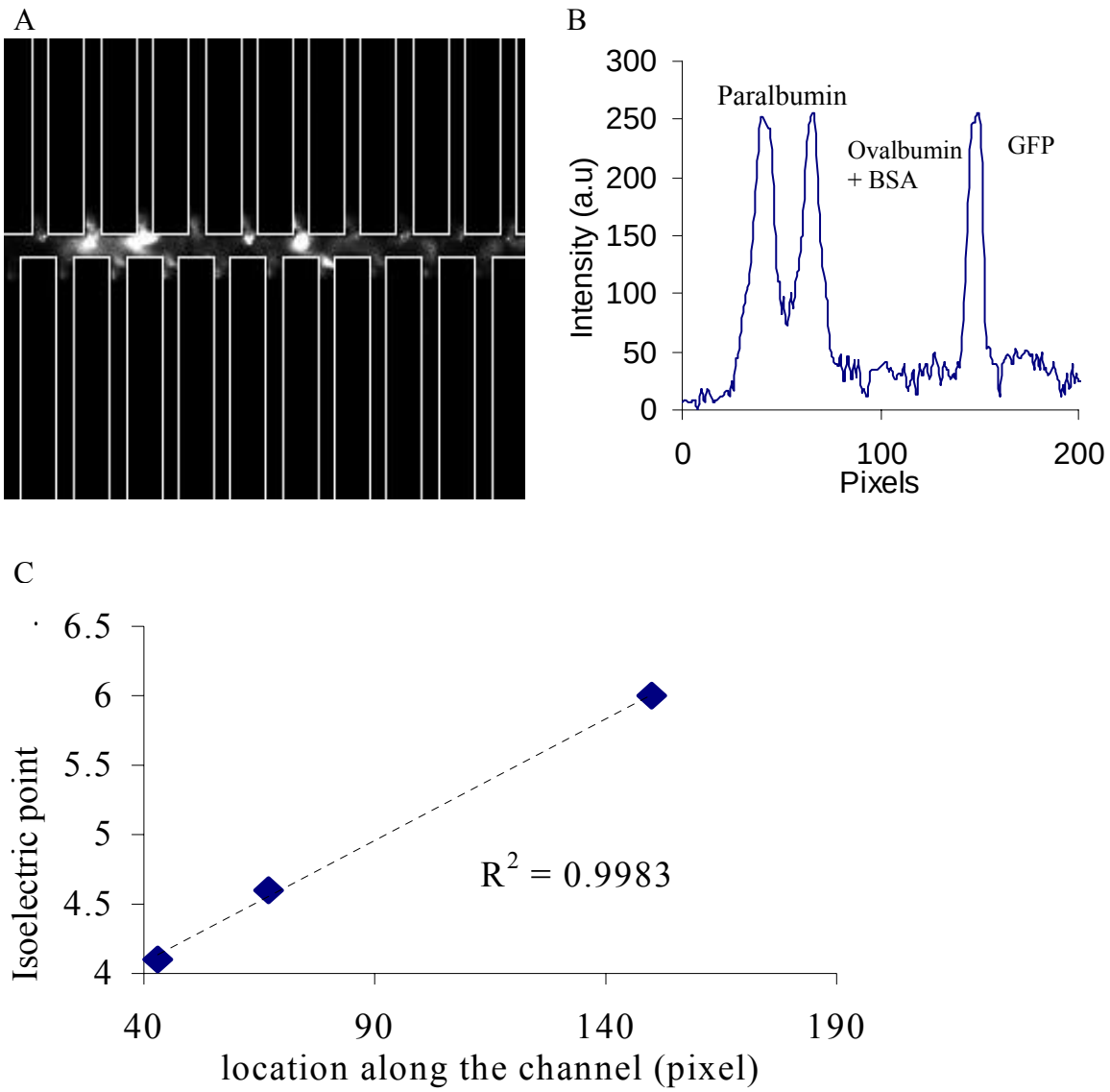

Figure 4-8. Isoelectric focusing of 4 proteins (Paralbumin, Ovalbumin, BSA, and GFP) in cross channel. A) Raw image. Experimental conditions: 300 V, 2.75% HPC in IEF medium, 10% T acrylamide polymer in parallel channels. Ovalbumin and BSA could not be separated because they have same isoelectric point. B) Electropherogram of A. C) Plot of isoelectric point of proteins in B with their physical location in cross channel. The linear trend of the plot indicates the uniform and linear pH gradient of IEF.

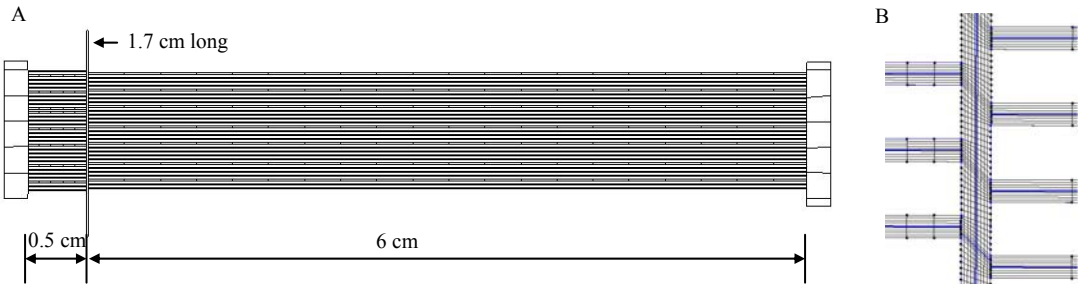

Figure 4-9. 2-D device used for numerical simulation. A) The length of parallel channels is 6.5 cm and that of cross channel is 1.7 cm. B) Close up view of cross channel with staggered parallel channel with quadrilateral mesh. The channel width is 100 μm and distance between parallel channels is 360 μm.

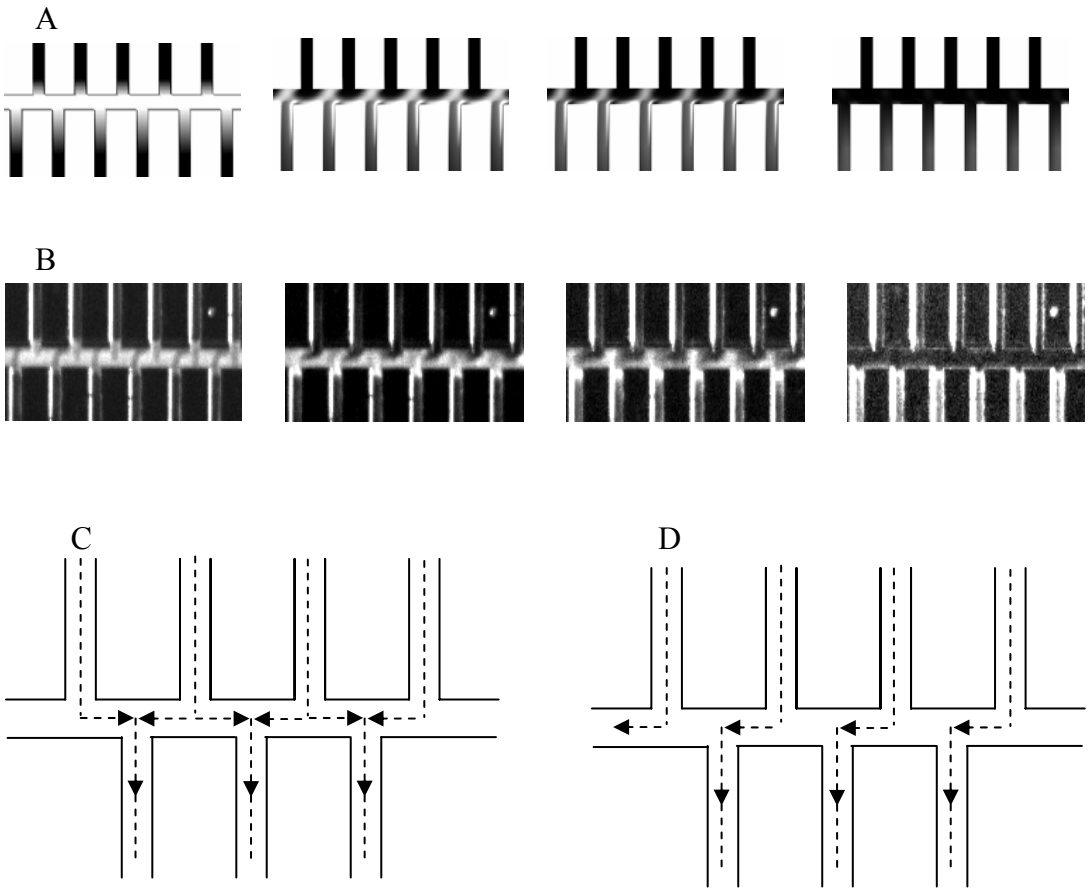

Figure 4-10. Transfer of negative species from cross channel to parallel channels due to an applied electric field of 100 V/cm. A) Numerical simulation showing gradual change of concentration gradient with time. B) Same phenomenon observed in experiments, here the cross channel is filled up with fluorescent proteins whereas parallel channels are polymerized with Acrylamide. C) Possible electric field flow path between parallel channels and cross channel. This configuration allows equal splitting of cross channel analytes. D) Another possible configuration of electric field orientation which allows preferential splitting of cross channel analytes.

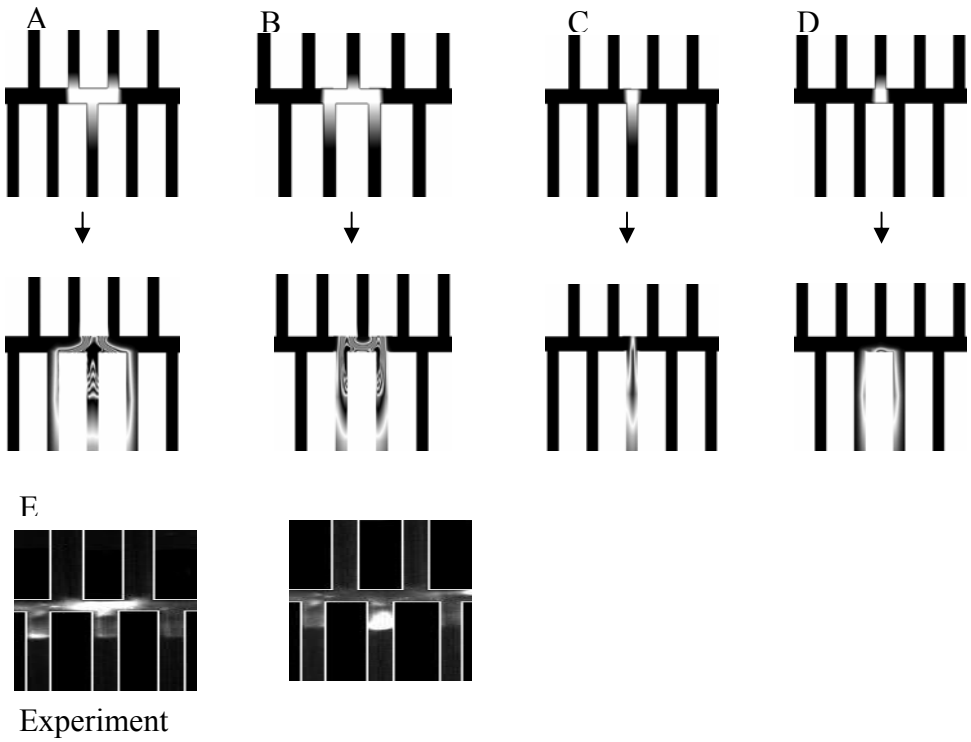

Figure 4-11. Transfer of protein plugs into parallel channel due to application of electric field. A) The plug is at center of two parallel channels and the size of plug is around 400 μm. The plug gets trifurcated into three parallel channels. B) The plug is before two parallel channels and gets bifurcated into two channels C) Plug is just above one channel and gets entirely transferred to that single channel. D) Similar to case B but the plug size is small and it still gets bifurcated in to channels. E) Experimental results for plug transfer from cross channel to parallel channel.

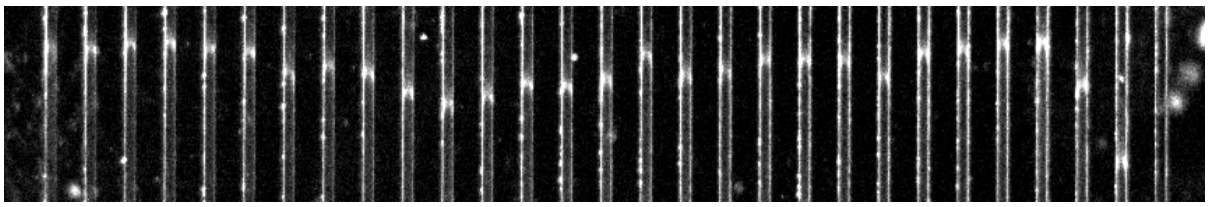

Figure 4-12. Protein migration pattern in all 29 parallel channels. As the protein migrates through the gel the protein peak location varies in different channel due to gel inconsistency and variation of electric field.

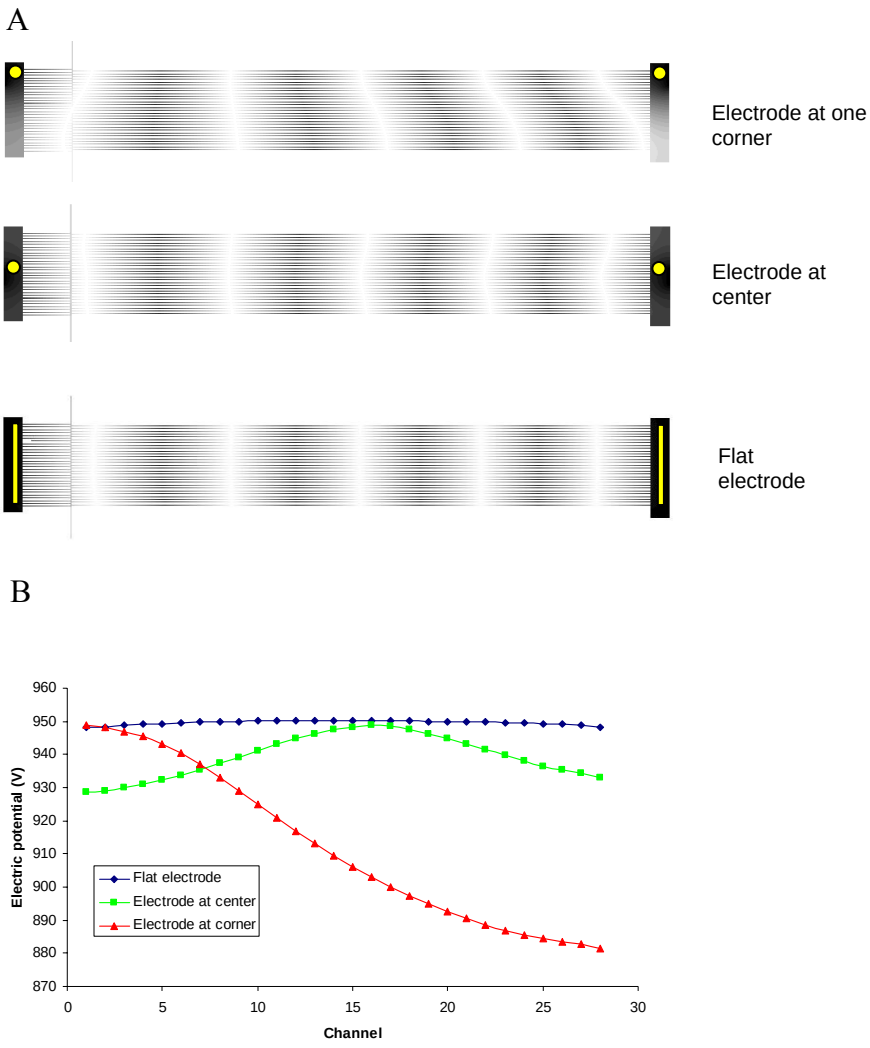

Figure 4-13. Electric field distributions at different location across the parallel channel. A) Different electrode configuration and position, B) plot of electric field across the entire 29 channels for all 3 cases measured halfway between the electrodes.

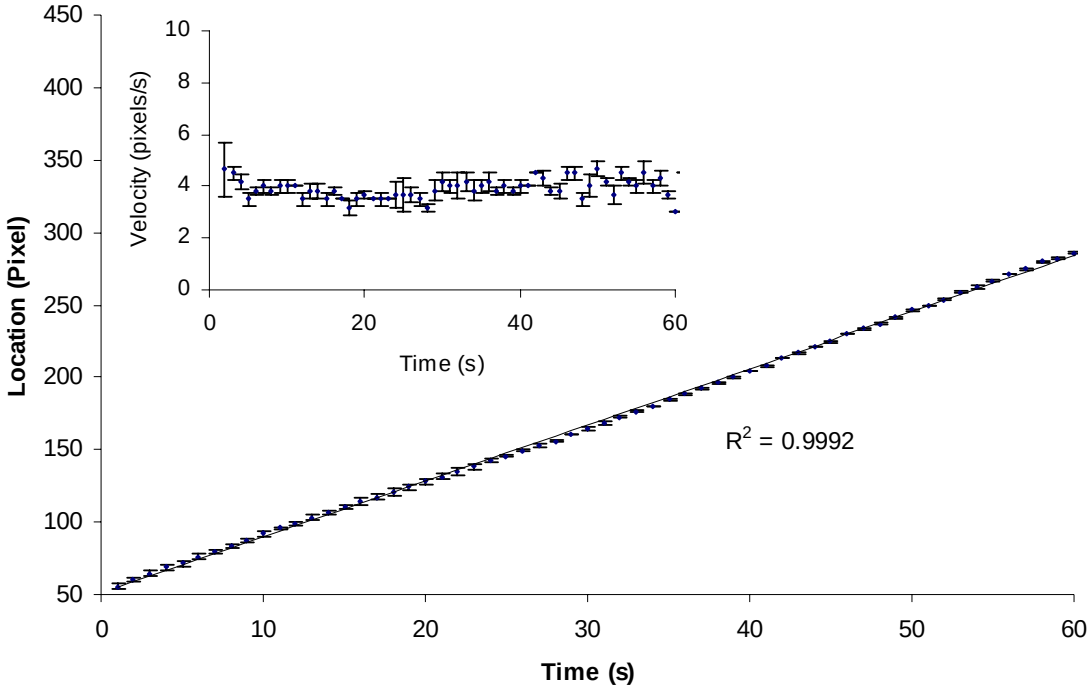

Figure 4-14. Experimental results of location of protein front with respect to time. The trend is linear indicating constant speed for the protein fronts inside the parallel channels.

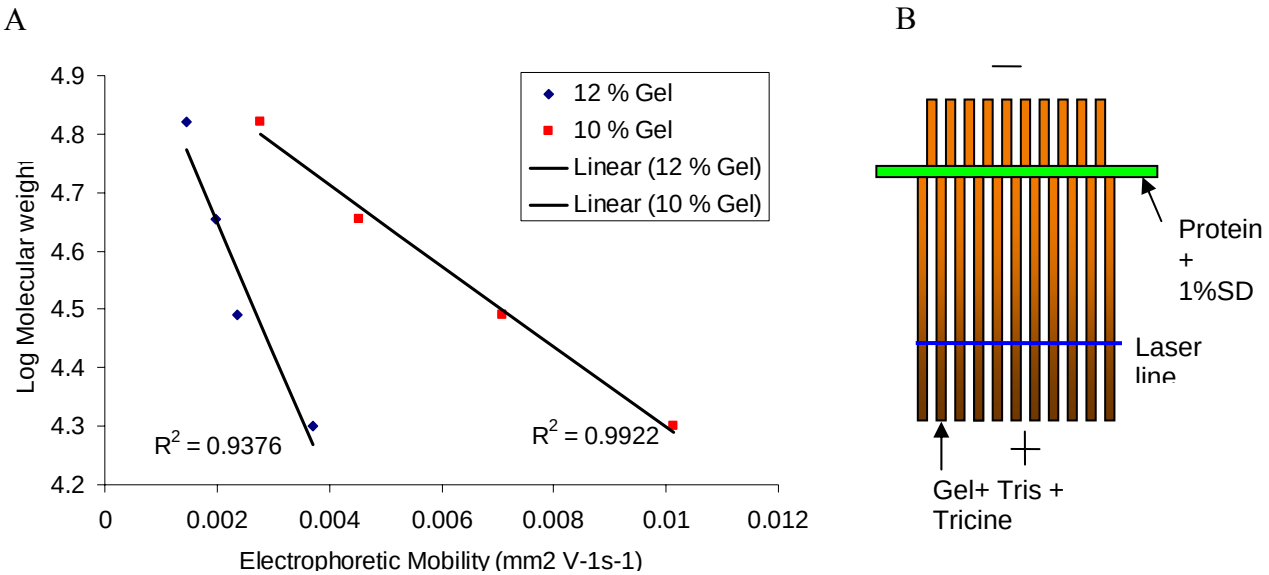

Figure 4-15. SDS-protein complex migration pattern in Gel due to application of electric field. A) Plot of Molecular weight of proteins vs. electrophoretic mobility. They show linear trend in both 10% and 12% gel. The data is obtained from 10-15th channels from left end B) Schematic of experiment for SDS-PAGE separation of 4 proteins in two dimensional devices.

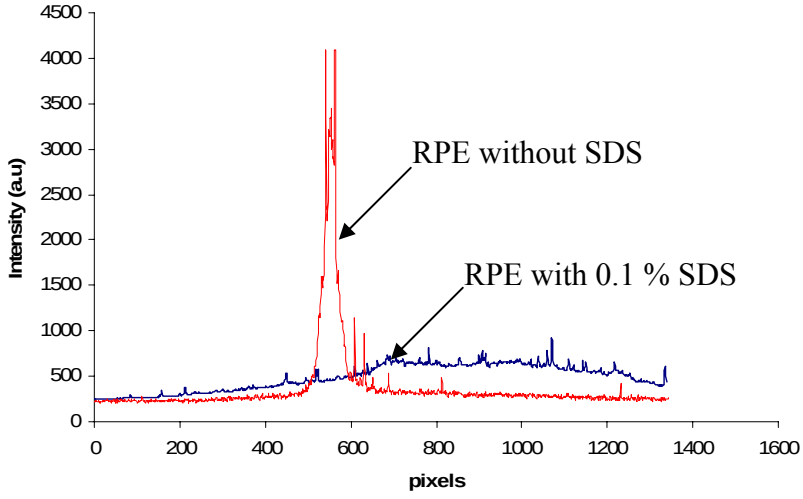

Figure 4-16. IEF for RPE with and without SDS in 5 cm channel. The electric field is 500 V and pH gradient is 3-10.

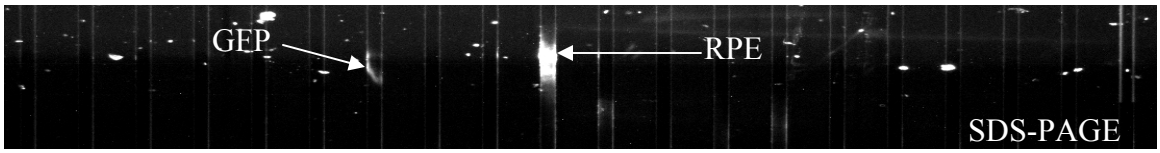

Figure 4-17. The transfer of GFP and RPE in second dimension after IEF is performed in first dimension. Electric field of 800 V is applied in parallel channels for separation second dimension. First dimension separation (IEF) is done in 3-10 pH gradient at 200 V.

A

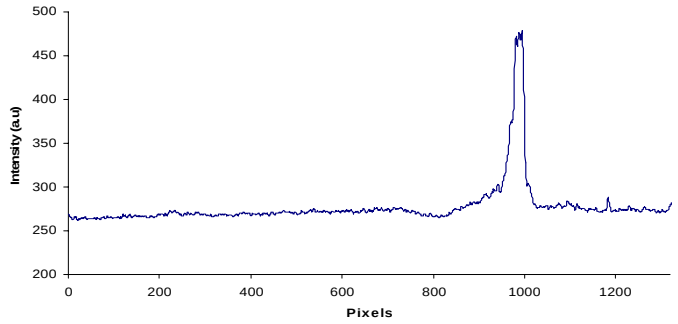

B

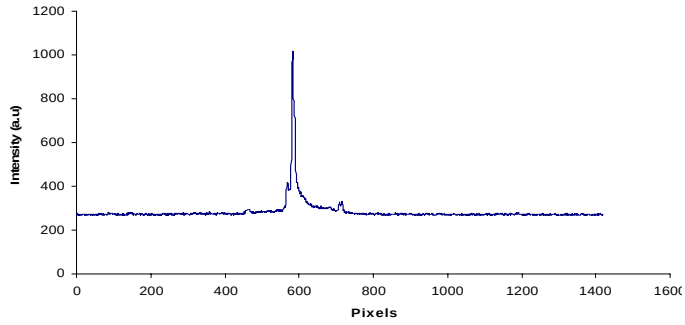

Figure 4-18. 2-Dimensional migration of a single protein. A) IEF of BSA in cross channel. The pH gradient is 3-10. The voltage applied is 200 V. B) SDS-PAGE of BSA in parallel channels after IEF is performed. The detection zone is 6 mm from the cross channel. The voltage applied is 1200 V across 6.5 cm parallel channels.

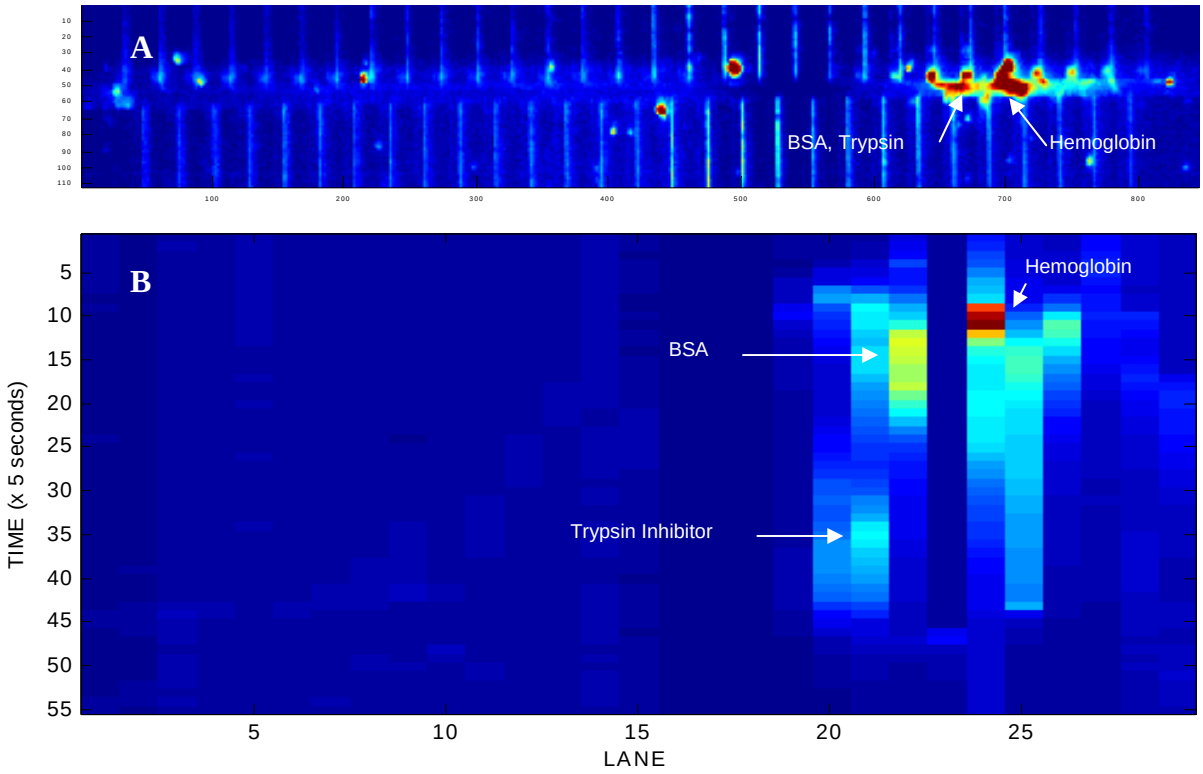

Figure 4-19. 2-Dimensional separation of three proteins. A) IEF of three proteins (BSA, hemoglobin and trypsin) in the cross channel. The pH gradient used is 3-10. BSA and trypsin has same isoelectric point of 4.6 whereas the Hemoglobin's isoelectric point is 7.1. Hence two broad peaks are visible in IEF. B) The proteins are further separated according to their molecular weight in parallel channels. Trypsin being the smallest (20 kDa) travels the fastest followed by hemoglobin (65.5 kDa) and BSA (66 kDa).

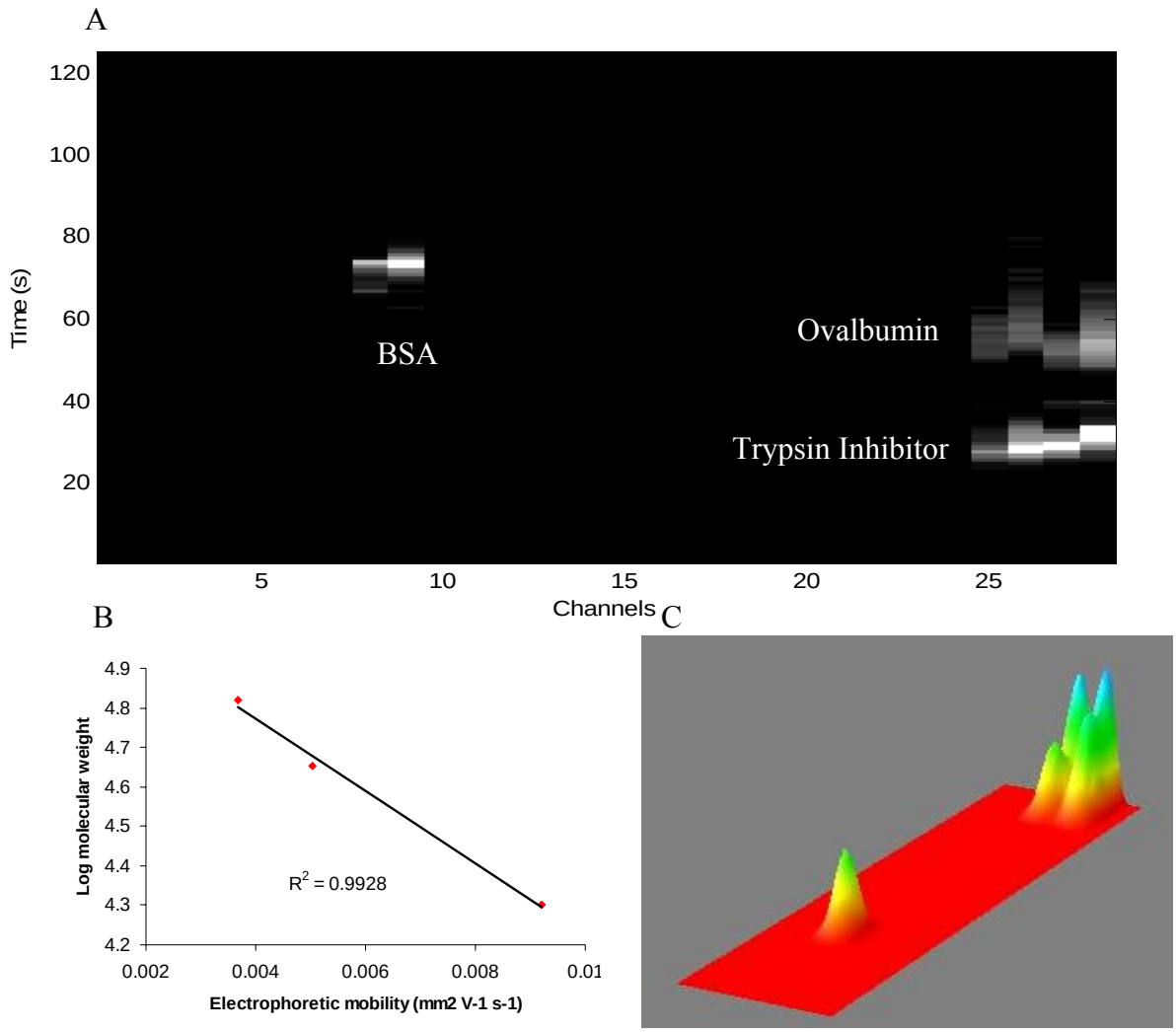

Figure 4-20. 2-Dimensional separation of three proteins (BSA, Ovalbumin and Trypsin) in lower pH gradient (3-5 pH) during IEF operation. A) 2-D map. B) The correlation between molecular weight and electrophoretic mobility show a linear trend. C) 3-D plot of A showing the signal Intensity of the proteins.

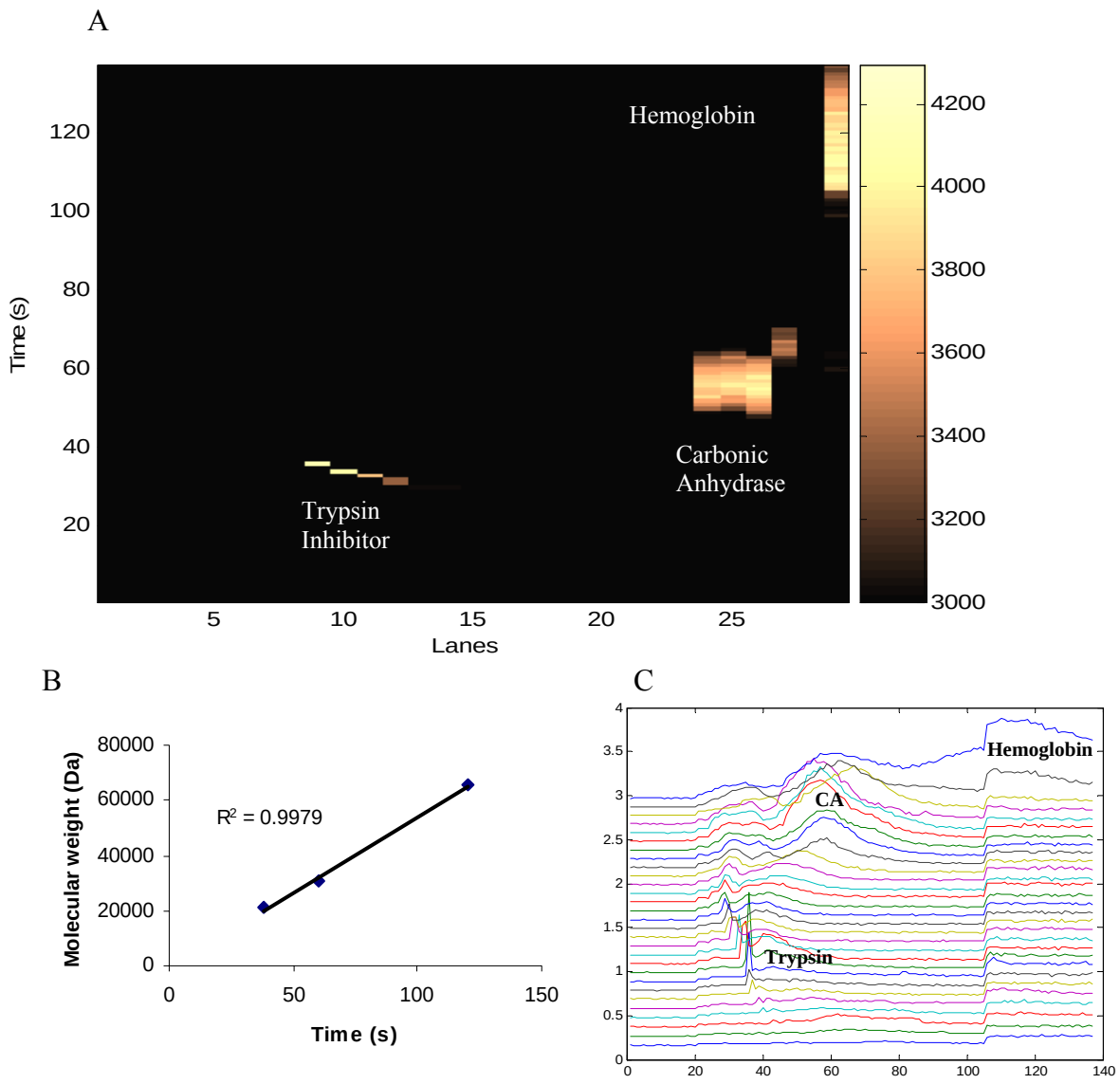

Figure 4-21. 2-Dimensional separations of three proteins (BSA, Ovalbumin and Hemoglobin) in 3-10 pH during IEF operation. A) 2-D time map. B) The correlation between molecular weight and electrophoretic mobility show a linear trend. C) Time profile plot for all 29 channels as recorded by the detector.

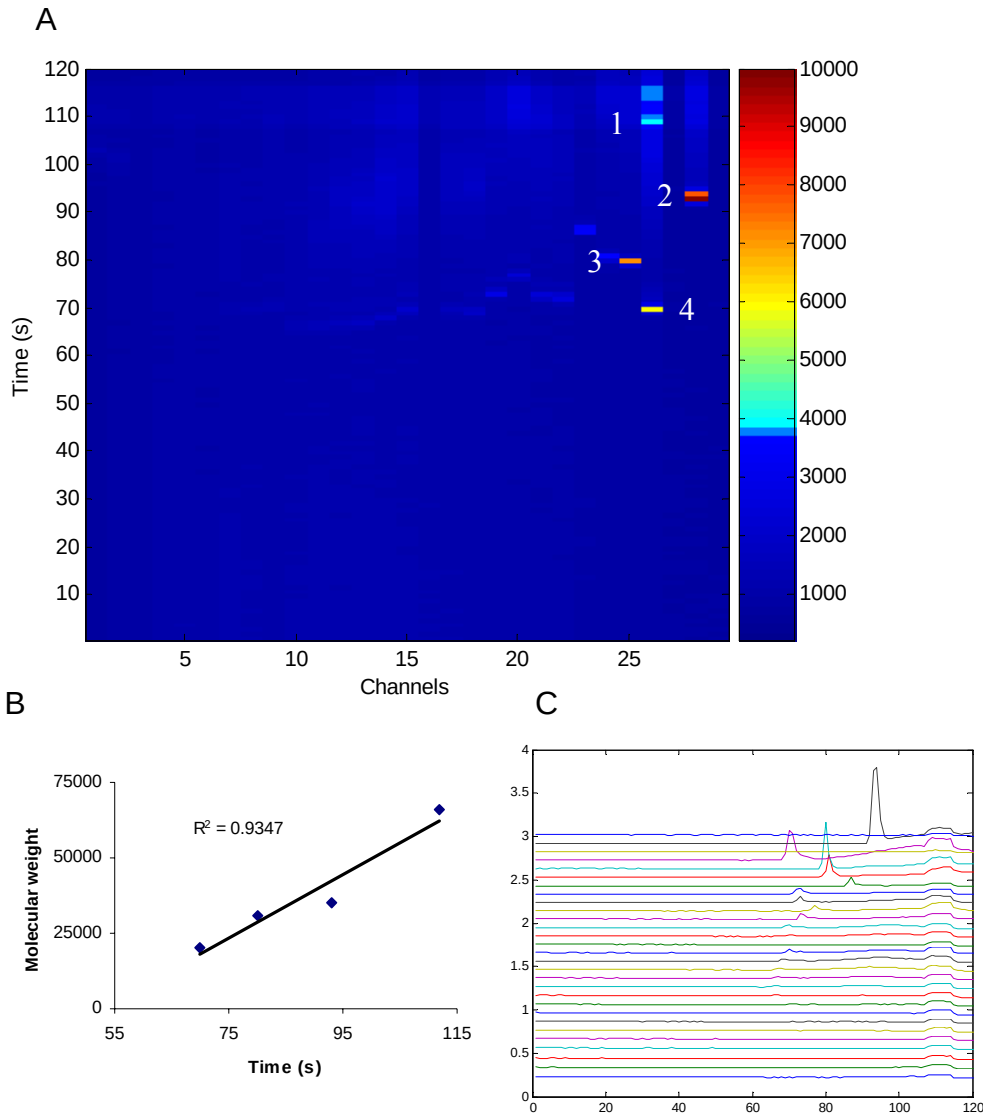

Figure 4-22. 2-Dimensional separation proteins for proteins BSA (1), carbonic anhydrase (2), ovalbumin(3) and trypsin (4). The pH gradient is 3-10 for IEF. The second dimension is carried out with 185 v/cm and the proteins got separated within 2 minutes.A) 2-D map. B) Correlation between molecular weight and time required to reach the detection point. C) The time profile plot for all 29 channels as recorded by the detector at 2 cm from cross channel. The data is normalized with maximum intensity value.

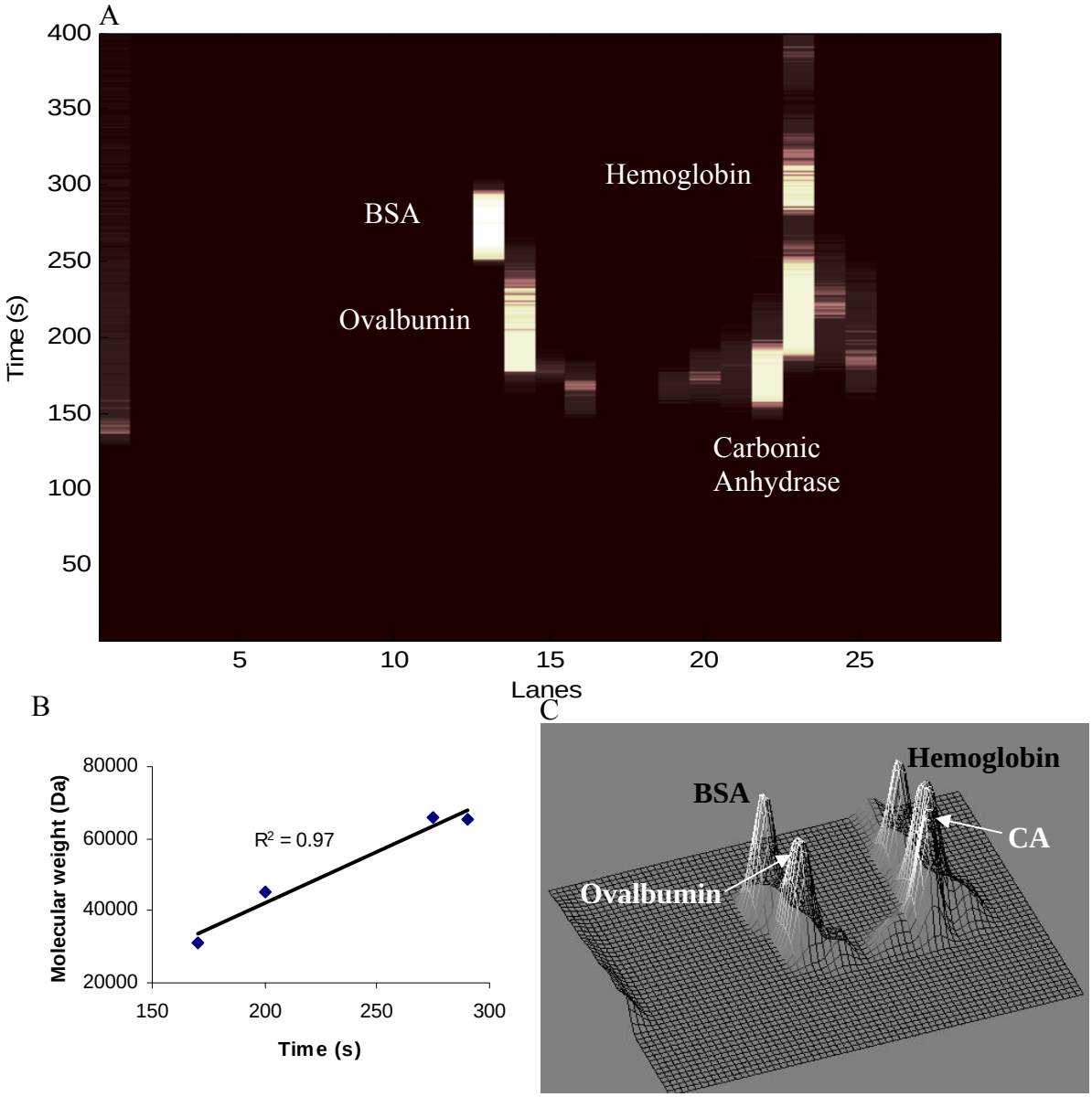

Figure 4-23. 2-D map for BSA, ovalbumin, hemoglobin and carbonic anhydrase in 10% acrylamide gel. The experiment is done at lower electric field (120 V/cm) and hence has taken more time for proteins to reach the detection point at 6.5 mm from the cross channel. A) 2-D map B) The time correlation with molecular weight. C) 3-D plot of A showing the signal Intensity of the proteins.

CHAPTER 5
CONCLUSION AND FUTURE DIRECTIONS

5.1 Conclusion

The main objective of this research is to miniaturize the two electrophoretic separation mechanism namely isoelectric focusing and SDS-PAGE and finally integrate them in a single microfluidic device. A whole channel imaging detection is assembled for detecting IEF. This system provides vital information about the dynamics of protein separation both in spatial and temporal mode and eliminates the need for mobilization of protein peaks after IEF, thereby preventing loss in resolution and time. IEF in microchannel proved to be quite successful in 6-channel devices. Proteins with as low as 0.1 pH difference in their pI could be separated. Resolution of IEF was found to be almost independent of channel length when the electric field was kept constant. This allows for miniaturization of device and rapid analysis.

One way of evaluating the performance of the separation system is to measure the peak capacity of the device. Peak capacity is a nondimensional quantity and is defined as a ratio of channel length and protein peak width. Since the peak capacity of a 2-dimensional separation system is the product of peak capacities of an individual separation in each dimension, the total peak capacity is higher and the system can be used for performing complex protein separation. The peak capacity of IEF in 6 channel device is around 125 (5 cm channel at 100 V/cm). The peak capacity of IEF in the cross channel in 2-D device, however, came down to around 90. The SDS-PAGE peak capacity in parallel channels is 68. Combined results are better than reported in literature[49, 109]. These peak capacities, however, depend on the peak width of the protein chosen. Different proteins have different peak width and the resultant peak capacity will vary. The most important component of 2-D separation is the presence of gel in the second dimension

separation. The gel effectively prevents proteins from diffusing into parallel channel before IEF is performed. The resultant 2-D separation is clean and precise.

5.2 Future Direction

There are still some issues of small amount of proteins leaking into extreme right parallel channels when an electric field is applied for IEF. This is mainly due to curved electric field in the junction of parallel channels with cross channel. This can be reduced by using a lower electric field at the beginning of experiment (IEF) and increasing the field when proteins are almost focused. Also redesigning the device such that higher concentration of gel is present near the cross channel which will further reduce the diffusion. Figure 5-1 shows a possible method to achieve the goal in the present design. The mask size is increased such that after polymerization, at least 500 μm on both the sides of the cross channel is not polymerized. The contents of the cross channel are then sucked out and higher concentration of monomer solution is pumped in. Since it is impossible to suck out the unpolymerized monomer solution in parallel channel, the only way to increase the concentration is by diffusion.

The new monomer solution with a higher concentration in the cross channel is then allowed to diffuse into the non-polymerised zone of parallel channel. Now the second polymerization is carried out with a mask with smaller trace width. The previously unpolymerized region in the parallel channels will now be polymerized. The device geometry can also be optimized by studying the diffusion phenomenon for different geometries in CFD-ACE. This will prevent costly and time consuming manufacturing steps.

In addition, the cross channel in the 2-D device is quite small in terms of length. The reason behind decreasing the length is to reduce separation time, smaller footprint and lower electric field requirements. But as the channel length is reduced electrosmotic and hydrostatic

flow starts playing a bigger role in the separation mechanism. Though it is difficult to accurately predict the right length of the cross channel for IEF, estimation can be done based on previous experimental results. Assuming the target separation resolution to be 0.1 pH for each parallel channels, total length required for resolving the full pH gradient (3-10 for our case) is 25.2 mm. But it is seen from experiments that both in 6 channel device and 2-D devices, the IEF has suffered extreme pH gradient compression (up to 60%). The length of cross channel should be increased to around 6.3 cm to take care of the pH gradient compression.

The hydrodynamic flow is also of important concern in cross channel. This hydrodynamic flow will drive the focused proteins out from the cross channel. The continuous flow will distort the IEF and will move the proteins from its isoelectric point. This flow usually happens due to unbalanced catholyte and anolytes in the reservoir. Assuming a variation of around 10% in pipetting the liquid, 2 mm diameter reservoir will have a resulting variation of 0.2 mm in height. This will in turn lead to a flow of 5 μm/s in cross channel (1.5 cm) from higher pressure to lower pressure region. IEF in first dimension is achieved in 180 seconds. This will lead to shift of peaks by about 900 μm from its original isoelectric point. Increasing the channel length will reduce this speed ($V \propto 1/L$) and hence reduce the peak shift. Now taking into account the pH gradient compression a cross channel of 6.3 cm will also reduce this peak shift variation due hydrostatic imbalance by more than 75% (1.2 μm/s).

As a result the channel length for IEF is suggested to increase to about 6.5 cm in order to take care of these problems. The main advantages of miniaturizing 2-D separation is the shorter time required to complete the operations. For a flat bed gel system it takes almost 10-12 hours to finish IEF and another 1 hr to finish SDS-PAGE. The same operation can be finished in less than

10 minutes. This is a huge improvement over the conventional system and at the same time it reduces the space requirement and labor intensive operations.

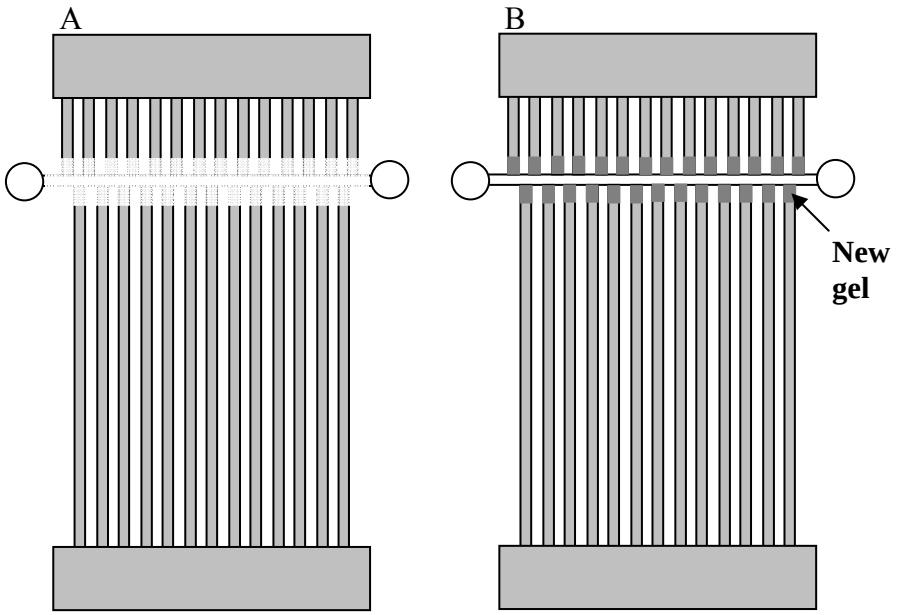

Figure 5-1. The mask size is increased such that 500 μm on both the sides of cross channel is left unpolymerized after UV exposure. The monomer solution from cross channel is replaced with another one with higher concentration. This higher concentration monomer solution will diffuse in to still unpolymerised part of parallel channel. Second exposure to UV with thinner mask will create a layer of higher concentration gel on both the sides of cross channel.

APPENDIX
TRANSIENT SOLUTION OF IEF

Standard transient electrophoretic process can be defined as[43, 78, 92, 110]

$$\frac{\partial C(x,t)}{\partial t} + \frac{\partial\left[C(x,t)u(x)\right]}{\partial x} = D\frac{\partial^2 C(x,t)}{\partial x^2} \qquad \text{[A-1]}$$

The transient state of the Equation [A-1] provides information about time and distance. It will define the velocity profile of macromolecules in pH gradient. The macromolecules here are assumed as spherical and non-spinning in nature. For a charged spherical particle moving in an electric field, the force balance yields

$$\textit{Viscous Drag} = \textit{Force due to electric field} \qquad \text{[A-2]}$$

Then from Stokes' result for drag on solid sphere.

$$Drag = 6\pi\eta\, u(x) r \qquad \text{[A-3]}$$

where η is the viscosity, r is the radius of the sphere and $u(x)$ is the velocity of sphere. The force on the particles (macromolecules) due to external electric field is $q(x)E$, where $q(x)$ is the charge on the sphere and E is the electric field. Hence

$$6\pi\eta r\, u(x) = q(x)E \qquad \text{[A-4]}$$

So the velocity of the particle is directly dependent on charge of particle in the solution.

$$u(x) = \left[\frac{q(x)}{6\pi\eta r}\right]E \qquad \text{[A-5]}$$

From Equation [1] of Chapter 1, the particle velocity is the product of μ_{ep} and electric field. Comparing with Equation [A-5], mobility can be written as

$$\mu = \frac{q(x)}{6\pi\eta r} \qquad \text{[A-6]}$$

The charge distribution in IEF is non-linear with respect to x. However the nonlinearity exists near the end of the channels. This non linear charge will give rise nonlinear distribution of mobility at different pH. The effective mobility for ionic species can be described as[111, 112]

$$\mu_{eff} = \frac{\mu_1 - \mu_2}{1 + e^{\frac{pH - pK_a}{c}}} + \mu_2 \qquad \text{[A-7]}$$

where μ_1 and μ_2 are the effective mobilities at low and high pH values respectively; c is a constant and pK_a is the dissociation constant. Since in IEF it is assumed that a pH gradient with respect to distance is established. So replacing pH by distance 'x' in Equation [A-7], we have.

$$\mu_{eff} = \frac{\mu_1 - \mu_2}{1 + e^{\frac{x - pK_a}{c}}} + \mu_2 \qquad \text{[A-8]}$$

So the mobility is now a function of distance. The charge distribution can be seen from Figure A-1

Equation [A-1] can be solved as a moving gaussian pulse in x-direction[96, 97].

$$C(x,t) = A(t)\exp\left[-\frac{(x - u(x)f(t))^2}{2s^2(t)}\right] \qquad \text{[A-9]}$$

where A(t) is the amplitude, s(t) is the half width of the pulse and $[u(x)f(t)]$ will give the position of center of mass of gaussian pulse.

At t=0, the analyte is assumed to have an initial concentration as a Gaussian distribution.

$$C(x,0) = \frac{c_0}{\sqrt{2\pi}\sigma}\exp\left[-\frac{x^2}{2\sigma^2(t)}\right] \qquad \text{[A-10]}$$

So comparing the initial conditions

$$A(0) = \frac{c_0}{\sigma\sqrt{2\pi}} \;;\; s(0) = \sigma \;;\; f(0) = 0 \qquad \text{[A-11]}$$

Now in Equation [A-1], *c(x,t)* and *u(x)* can be used to find out the constants *A(t)*, *s(t)* and *f(t)*. It is a lengthy procedure and the final form of s(t) and f(t) can be found out as:

$$f(t) = \left[\frac{1 - \exp\left(-\frac{du}{dx} t \right)}{\frac{du}{dx}} \right] \qquad \text{[A-12]}$$

$$s^2(t) = \sigma^2 + \frac{D}{\frac{du}{dx}} \left[\exp\left(2 \frac{du}{dx} t \right) - 1 \right] \qquad \text{[A-13]}$$

$$\text{where} \quad \frac{du}{dx} = \frac{E}{c} \left[\frac{\mu_2 - \mu_1}{\left[1 + \exp\left(\frac{x - pK_a}{c} \right) \right]^2} \right] \exp\left(\frac{x - pK_a}{c} \right) \qquad \text{[A-14]}$$

The functions found above is very complicated, with *f(t)* and *s(t)* having dependency on both *x* and *t*. The charge distribution, if carefully analyzed can be assumed to be essentially linear with non-linearity near the two extreme ends. This linear assumption makes the functions much simpler to evaluate. Figure A-2 shows such linear dependency of charge on distance.

So for the linear case the mobility can be assumed as:[97]

$$\mu = \left(\frac{x_{pI} - x}{x_{pI}} \right) \frac{q_0}{6\pi\eta r} \qquad \text{[A-15]}$$

where x_{pI} is the isoelectric point of that particle.

$$u(x) = \left(x_{pI} - x \right) \frac{E}{6\pi\eta r} \frac{q_0}{x_{pI}}; \qquad \text{[A-16]}$$

$$\text{Denoting } u_0 = \frac{q_0}{6\pi\eta r} E \ , \qquad \text{[A-17]}$$

u_0 is the initial velocity due to an applied field E and initial charge is q_0

Equation [A-16] can be rewritten as $u(x) = \left(x_{pI} - x\right)\frac{u_0}{x_{pI}}$ [A-18]

Assigning a typical time scale for electrophoretic process as t_0

$t_0 = \frac{x_{pI}}{u_0}$ [Assuming constant charge, t_0 is the time required to reach x_{pI}] [A-19]

Solving the Equation [A-1] as before using Equation [A-9], functions A(t), f(t) and s(t) can be found out as:

$$f(t) = \left[\frac{\exp(t/t_0) - 1}{1/t_0}\right] \quad \text{[A-20]}$$

$$A(t) = \frac{1}{s(t)\sqrt{2\pi}} \quad \text{[A-21]}$$

$$s(t) = \sqrt{Dt_0\left[1 - \exp\left(-2\frac{t}{t_0}\right)\left\{1 - \frac{\sigma^2}{t_0 D}\right\}\right]} \quad \text{[A-22]}$$

where σ is the initial gaussian distribution of the protein peaks.

So the final solution of concentration with respect to time and distance is:

$$C\left(x,t\right) = \frac{1}{s(t)\sqrt{2\pi}}\exp\left[-\frac{\left(x - \langle x(t)\rangle\right)^2}{2s^2(t)}\right] \quad \text{[A-23]}$$

$$\langle x(t)\rangle = x_{pI}\left[1 - \exp\left(-t/t_0\right)\right] \quad \text{[A-23]}$$

Here $\langle x(t)\rangle$ is the location of center of mass of the Gaussian pulse. The concentration plotted with respect to time and distance according to the Equation [A-23] is shown in Figure A-3 below.

Figure A-3 shows the IEF process. The x-axis is distance. The concentration is plotted at different times. The peak gradually sharpens as it approaches its pI point. The process asymptotically approaches towards completion.

Equation [A-23] can be analyzed for different conditions

At time t = 0, $s(t) = \sigma$, $\langle x(t) \rangle = 0$, the center of mass for the CA/protein is at x=0

$$C(x,0) = \frac{1}{\sigma\sqrt{2\pi}} \exp\left[-\frac{(x)^2}{2\sigma^2} \right] \qquad \text{[A-25]}$$

At time $t = \infty$, $g(t) = \sqrt{Dt_0}$, $\langle x(t) \rangle = x_{pI}$, So at very long time the CA/protein peaks center of mass will be exactly at their pI point.

$$C(x,\infty) = \frac{1}{\sqrt{2\pi Dt_0}} \exp\left[-\frac{(x - x_{pI})^2}{2Dt_0} \right] \qquad \text{[A-26]}$$

Equation [A-24] has the spatial location of center of mass of protein peak. Differentiating with respect to time will give the front velocity. The front speed thus can be defined as:

$$\langle v(t) \rangle = \frac{x_{pI}}{t_0} \exp\left(-\frac{t}{t_0} \right) \qquad \text{[A-27]}$$

This front speed can be monitored in real time by the imaging system developed for whole channel viewing and the numerical results can be experimentally verified. As seen from the Figure A-4, higher field gives a higher starting speed in focusing, but all of them approaches almost similar speed at about 1200s (20 minutes) from starting time.

So higher voltage will ensure faster focusing and will have faster reduction of speed near its pI point. As the CA/proteins are gradually getting focused, the conductivity of the system drops. This drop in conductivity however may be used to predict the degree of completion, thereby eliminating need for continuous monitoring of system dynamics by a CCD camera, if

final focused protein is the only requirement. So a theoretical development of conductivity model is required. The conductivity of the system can be found out in the following way. For a single ampholyte / protein species, the current density can be written as

$$\frac{\partial C(x,t)}{\partial t} + \frac{\partial J(x,t)}{\partial x} = 0 \qquad \text{[A-28]}$$

where '*j*' is the current density.

For large number of proteins, the total concentration can be written as $C^{All}{}_x = \sum_i C_x^i$, where i = 1,2,3…… Introducing Equation [A-1] in 28,

$$j(x,t) = C(x,t)u(x) - D\frac{\partial C}{\partial x} \qquad \text{[A-29]}$$

This can be analytically solved as

$$j(x,t) = C(x,t)\left[u_0\left(1 - \frac{x}{x_{pI}}\right) + D\left(\frac{x - \langle x(t)\rangle}{s^2(t)}\right)\right] \qquad \text{[A-30]}$$

Since conductivity σ_c is defined as current density per unit voltage. So $\sigma_c = j/E$, conductivity can be easily found out by dividing Equation [A-30] by *E*.

Now this conductivity is a function of both distance and time. In common IEF setup, usually the total voltage drop across the channel is measured. The conductivity thus measured in our experiment is only a function of time. Hence integration of conductivity with respect to distance *x* leads to a function which is only a function of time.

$$\sigma_c(t) = \left[\frac{E}{A}\int_0^L \frac{1}{\sigma_c(x,t)}dx\right]^{-1} \qquad \text{[A-31]}$$

There is no closed formed analytical solution for this integration and hence has to be integrated numerically. This conductivity value however is only for a particular protein (macromolecule). Hence for all different proteins taken together the total conductivity can be

assumed to have very similar characteristics with time though the absolute magnitude of conductivity will change.

The Figure A-5 shows the relationship of conductivity with applied electric field according to Equation [A-30]. As the field is increased the CA are more focused and hence the conductivity drop is more for higher voltage. As the CAs are focused faster, IEF time will be reduced.

Since the IEF process asymptotically approaches its completion, there must be a cut-off point say 95% of completion to define the time limit. Since from Equation [A-24], the position of the center of mass (C.M) of ampholyte / protein is known, it can be assumed the process is completed when front C.M is within 95% of it pI point.

$$x_{pI}\left[1-\exp(-\frac{t}{t_0})\right]=0.95x_{pI} \qquad \text{[A-32]}$$

$$\frac{t}{t_0}=\ln(20)\approx 3 \quad \rightarrow \; t=3\frac{x_{pI}}{u_0} \qquad \text{[A-33]}$$

But from Equation [A-17], $u_0 \propto E$, so from Equation [A-33], $t \propto 1/E$ [A-34]

Hence the time of completion is inversely proportional to applied field strength. So if the field strength is increased, the process can be achieved faster, but the field strength can not be increased indefinitely as it will have adverse effect of Joule heating and also increased electro-osmotic flow.

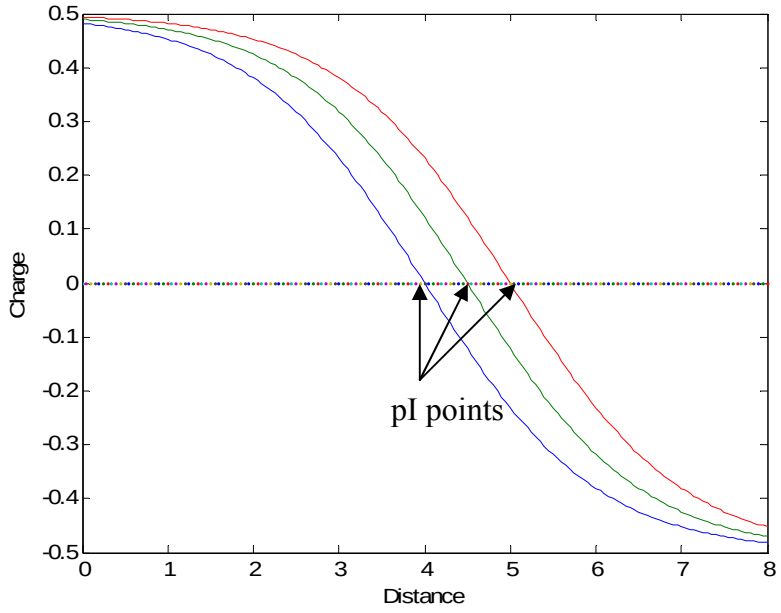

Figure A-1. Assumed charge distribution for different CA/ proteins in IEF focusing process for nonlinear case.

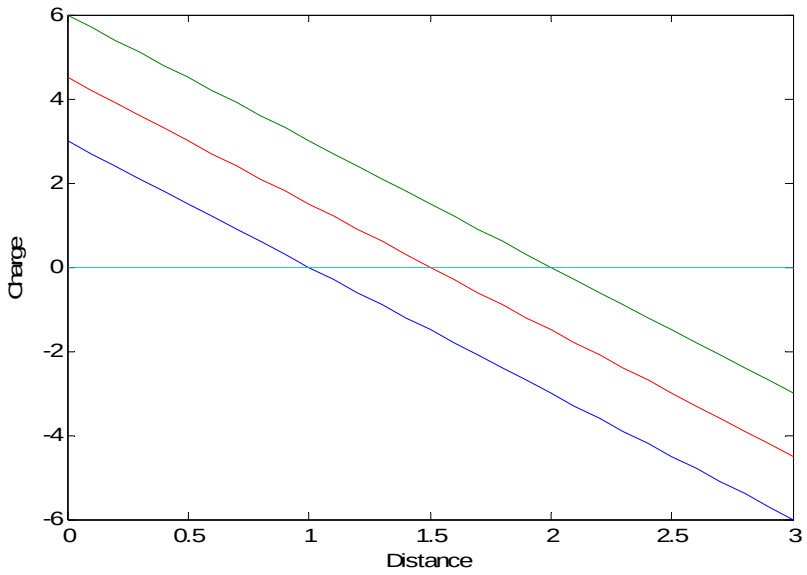

Figure A-2. Assumed charge distribution for different CA/ proteins in IEF focusing process

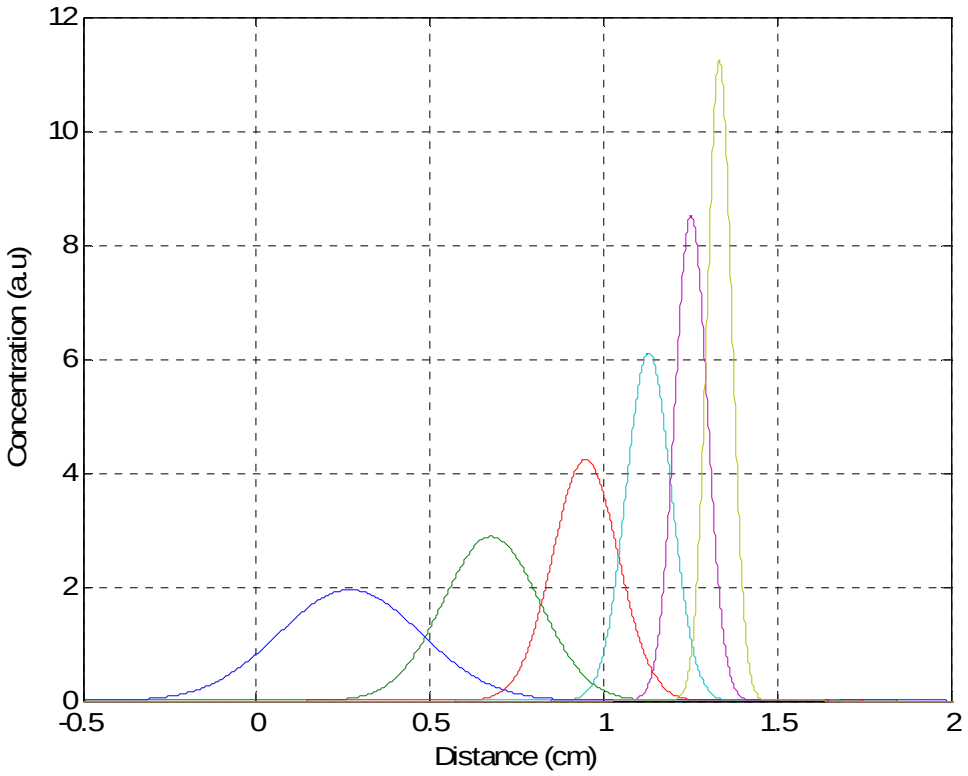

Figure A-3. Evolution of Gaussian peak with time for a particular ampholyte. As time progresses, the peak gets narrower and slows down and stops at pI point, exactly as observed in experiment. Using realistic diffusion constant $D=10^{-7}$ cm^2/s, E=500 V, $u_0=3x10^{-4}$cm/s, the protein front evolution is plotted with time at different applied field.

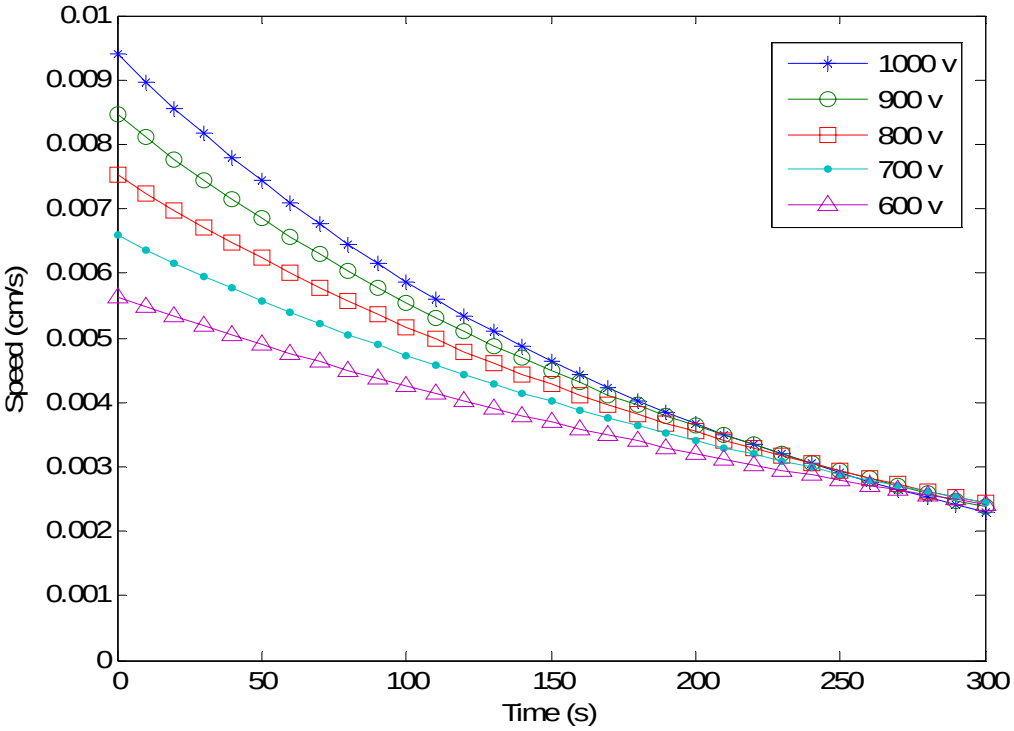

Figure A-4. Numerical results for front speed of CA/ proteins with time at different. applied electric field. The front speed is higher at higher electric field strength and tends to reduce speed faster. Faster reduction of font speed indicates faster approach towards its isoelectric point and hence faster process completion.

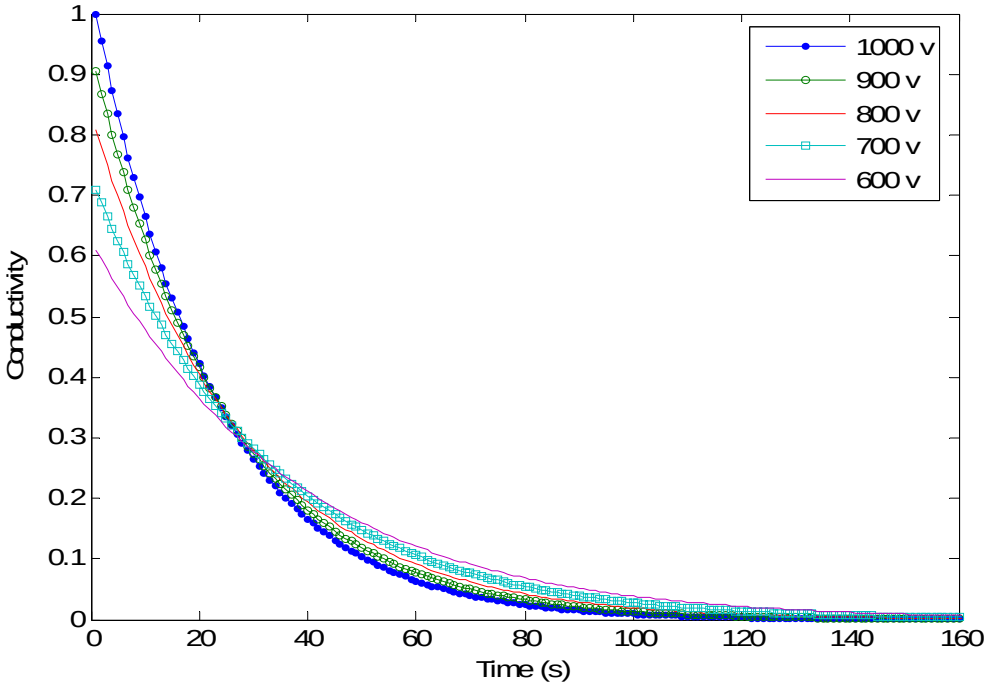

Figure A-5. Conductivity plotted with respect to time at different electric fields. The results shown is normalized. The length of the channel is 5 cm. The diffusion constant is 1e-7 cm^2/s. As the electric field is increased, the initial current density is high, but drops faster with time.

LIST OF REFERENCES

(1) Yazdi, N. A., F.; Najafi, K. *Proceeding of the IEEE* **1998**, *86*, 1640-1659.

(2) Schwarz, M. H., R.; Hosticka, B.J.; Huppertz, J., Kneip, T.; Kolnsberg, S.; Ewe, L.;Trieu, H.K.; *Ieee Trans. Circuits sys. II* **1999**, *46*, 870-877.

(3) De Gasperis, G. Y., Jun; Becker, Frederick F.; Gascoyne, Peter R. C.; Wang, Xiao-Bo *Biomedical Microdevices* **1999**, *2(1)*, 41-49.

(4) Wang, X.-B. Y., Jun; Huang, Ying; Vykoukal, Jody; Becker, Frederick F.; Gascoyne, Peter R. C. *Analytical Chemistry* **2000**, *72(4)*, 832-839.

(5) Barrie, G. P., R.; Kaler, K. V. I. S.; Jones, T. B. *Journal of Colloid and Interface Science* **1995**, *175(1)*, 97-107.

(6) Giddings, J. C. *Science* **1993**, *260*, 1456-1465.

(7) Wang, M. M. T., Eugene; Raymond, Daniel E.; Yang, Joon Mo; Zhang, Haichuan; Hagen, Norbert; Dees, Bob; Mercer, Elinore M.; Forster, Anita H.; Kariv, Ilona; Marchand, Philippe J.; Butler, William F. *Nature Biotechnology* **2005**, *23(1)*, 83-87.

(8) Yamada, M. S., Minoru *Lab on a Chip* **2005**, *5(11)*, 1233-1239.

(9) Terry, S. C.; Jerman, J. H.; Angell, J. B. *Ieee Transactions on Electron Devices* **1979**, *26*, 1880-1886.

(10) Shoji, S. S. B., V.; de Rooij, N.; Esashi, M.; *Tech. Digest IEEE Transducers (San Fransisco, CA, 1991)* **1991**, 1052-1055.

(11) Kim, J.-H. N., K-H.; Kang, C.J.; Jeon, D.; Kim, Y-S.; *Microelectronic engineering* **2004**, *73-74*, 864-869.

(12) Nguyen, N. T. S., S.; Richter, S.; Dotzel, W. *Sensors and Actuators, A: Physical* **1998**, *A69(1)*, 85-91.

(13) Xie, J. S., Jason; Lin, Qiao; Yang, Bozhi; Tai, Yu-Chong *Lab on a Chip* **2004**, *4(5)*, 495-501.

(14) Jackson, W. C. T., Hy D.; O'Brien, Michael J.; Rabinovich, Emmanuil; Lopez, Gabriel P. *ournal of Vacuum Science & Technology, B: Microelectronics and Nanometer Structures* **2001**, *19(2)*, 596-599.

(15) Yamahata, C. L., Frederic; Gijs, Martin A. M. *Microelectronic Engineering* **2005**, *78-79*, 132-137.

(16) Jerman, J. H. *Tech. Digest IEEE Transducers (San Fransisco, CA, 1991)* **1991**, 1045-1048.

(17) Darhuber, A. A. V. J. P. T., S.M.; Wagner, S. *Journal of microelectromechanical systems* **2003**, *12*, 873-879.

(18) Stone, H. A. S., A.D.; Ajdari, A. *Annu. Rev. Fluid Mech.* **2004**, *36*, 381-411.

(19) Wang, P.-J. C., Chia-Yuan; Chang, Ming-Lang *Biosensors & Bioelectronics* **2004**, *20(1)*, 115-121.

(20) Olsson, A. S., Goeran; Stemme, Erik *Sensors and Actuators, A: Physical* **1996**, *A57(2)*, 137-143.

(21) Olsson, A. S., Goeran; Stemme, Erik *Sensors and Actuators, A: Physical* **1995**, *A47(1-3)*, 549-556.

(22) Sethu, P. M., C. H. *Sensors and Actuators, A: Physical* **2003**, *A104(3)*, 283-289.

(23) Fuhr, G. H., R.; Muller, T.; Benecke, W.; Wagner, B.; *Proc. MEMS 92* **1992**, 25-30.

(24) Yao, S. H., D.E.; Mikkelsen, J.C.; Santiago, J.G. *Journal of Colloid and Interface Science* **2003**, *268*, 143-153.

(25) Sharp, K. V. A., R.J.; Santiago, J.G.; Molho, J.I. *The MEMS handbook*; CRC Press, 2002.

(26) Manz, A. G., N.; Widmer, H. M. *Sensors and Actuators, B: Chemical* **1990**, *B1(1-6)*, 244-248.

(27) Dunn, M. J. *Gel electrophoresis of proteins*; IOP Publishing Limited: Bristol, 1986.

(28) Righetti, P. G.; Drysdale, J. W. *Isoelectric Focusing*, First ed.; North-Holland Publishing: Amsterdam, 1976.

(29) Westermeier, R. *Electrophoresis in Practice*; VCH Publishers: Weinheim, Germany, 1993.

(30) Mosher, R. A.; Thormann, W. *Electrophoresis* **2002**, *23*, 1803-1814.

(31) Saravis, C. A.; O'Brien, M.; Zamcheck, N. *J Immunol Methods* **1979**, *29*, 97-100.

(32) Saravis, C. A.; Zamcheck, N. *J Immunol Methods* **1979**, *29*, 91-96.

(33) Rosen, A.; Ek, K.; Aman, P. *J Immunol Methods* **1979**, *28*, 1-11.

(34) Righetti, P. G.; Macelloni, C. *J Biochem Biophys Methods* **1982**, *6*, 1-15.

(35) Bjellqvist, B.; Ek, K.; Righetti, P. G.; Gianazza, E.; Gorg, A.; Westermeier, R.; Postel, W. *J Biochem Biophys Methods* **1982**, *6*, 317-339.

(36) Righetti, P. G.; Bossi, A. *Anal Biochem* **1997**, *247*, 1-10.

(37) O'Farrell, P. H. *J Biol Chem* **1975**, *250*, 4007-4021.

(38) Harrison, D. J. F., Karl; Seiler, Kurt; Fan, Zhonghui; Effenhauser, Carlo S.; Manz, Andreas *Science* **1993**, *261(5123)*, 895-897.

(39) Fan, Z. H. H., D. J.; *Analytical Chemistry* **1994**, *66*, 177-184.

(40) McDonald, J. C.; Metallo, S. J.; Whitesides, G. M. *Anal Chem* **2001**, *73*, 5645-5650.

(41) Duffy, D. C. M., J. Cooper; Schueller, Olivier J. A.; Whitesides, George M. *Analytical Chemistry* **1998**, *70(23)*, 4974-4984.

(42) Boone, T. D.; Fan, Z. H.; Hooper, H. H.; Ricco, A. J.; Tan, H.; Williams, S. J. *Anal Chem* **2002**, *74*, 78A-86A.

(43) Tan, W.; Fan, Z. H.; Qiu, C. X.; Ricco, A. J.; Gibbons, I. *Electrophoresis* **2002**, *23*, 3638-3645.

(44) Hofmann, O.; Che, D.; Cruickshank, K. A.; Muller, U. R. *Anal Chem* **1999**, *71*, 678-686.

(45) Liu, Z.; Pawliszyn, J. *J Proteome Res* **2004**, *3*, 567-571.

(46) Duong, T. T.; Kim, G.; Ros, R.; Streek, M.; Schmid, F.; Brugger, J.; Anselmetti, D.; Ros, A. *Microelectronic Engineering* **2003**, *67-8*, 905-912.

(47) Hatch, A. V. H., A.E.; Throckmorton, D.J.; Brennan, J.S.; Singh, A.S.; *Anal Chem* **2006**, *78*, 4976-4984.

(48) Chen, X.; Wu, H.; Mao, C.; Whitesides, G. M. *Anal Chem* **2002**, *74*, 1772-1778.

(49) Li, Y.; Buch, J. S.; Rosenberger, F.; DeVoe, D. L.; Lee, C. S. *Anal Chem* **2004**, *76*, 742-748.

(50) Baker, D. R. *Capillary Electrophoresis*; John Wiley and Sons Inc: New York: NY, 1995.

(51) Crimaldi, J. P. *Experiments in Fluids* **1997**, *23*, 325-330.

(52) Eggeling, C. J. W., R. Rigler, C.A. M. Seidel *Analytical Chemistry* **1998**, *70*, 2651.

(53) Pettit, G. H. E., M.N.; Hahn, D.W.; Brinson, B.E.; Saurbrey, R.; *Applied Physics A* **1994**, *58*, 573-579.

(54) Lukyanchuk, B. B., N.; Anisimov, S.; Arnld, N.; Bauerle, A.D. *Applied Physics A* **1996**, *62*, 397-401.

(55) Richards, D. P. S., C.; Polakowski, R.; Ahmadzadeh, H.; Dovichi, N. J. *Journal of Chromatography., A* **1999**, *853*, 21-25.

(56) Vogt, O.; Pfister, M.; Marggraf, U.; Neyer, A.; Hergenroder, R.; Jacob, P. *Lab Chip* **2005**, *5*, 205-211.

(57) McCormick, R. M.; Nelson, R. J.; Alonso-Amigo, M. G.; Benvegnu, D. J.; Hooper, H. H. *Anal Chem* **1997**, *69*, 2626-2630.

(58) Han, A.; Wang, O.; Graff, M.; Mohanty, S. K.; Edwards, T. L.; Han, K. H.; Bruno Frazier, A. *Lab Chip* **2003**, *3*, 150-157.

(59) Tan, W.; Fan, Z. H.; Qiu, C. X.; Ricco, A. J.; Gibbons, I. *Electrophoresis* **2002**, *23*, 3638-3645.

(60) Pugmire, D. L.; Waddell, E. A.; Haasch, R.; Tarlov, M. J.; Locascio, L. E. *Anal Chem* **2002**, *74*, 871-878.

(61) Lai, S.; Wang, S. N.; Luo, J.; Lee, L. J.; Yang, S. T.; Madou, M. J. *Analytical Chemistry* **2004**, *76*, 1832-1837.

(62) Juang, Y. J.; Lee, L. J.; Koelling, K. W. *Polymer Engineering and Science* **2002**, *42*, 539-550.

(63) Liu, R. H.; Yang, J. N.; Lenigk, R.; Bonanno, J.; Grodzinski, P. *Analytical Chemistry* **2004**, *76*, 1824-1831.

(64) Li, Y.; Buch, J. S.; Rosenberger, F.; DeVoe, D. L.; Lee, C. S. *Analytical Chemistry* **2004**, *76*, 742-748.

(65) Xu, Y.; Vaidya, B.; Patel, A. B.; Ford, S. M.; McCarley, R. L.; Soper, S. A. *Anal Chem* **2003**, *75*, 2975-2984.

(66) Koh, C. G.; Tan, W.; Zhao, M. Q.; Ricco, A. J.; Fan, Z. H. *Anal Chem* **2003**, *75*, 4591-4598.

(67) Kameoka, J.; Craighead, H. G.; Zhang, H. W.; Henion, J. *Analytical Chemistry* **2001**, *73*, 1935-1941.

(68) Mela, P.; van den Berg, A.; Fintschenko, Y.; Cummings, E. B.; Simmons, B. A.; Kirby, B. J. *Electrophoresis* **2005**, *26*, 1792-1799.

(69) Kim, D. S.; Lee, S. H.; Kwon, T. H.; Ahn, C. H. *Lab on a Chip* **2005**, *5*, 739-747.

(70) Esch, M. B.; Kapur, S.; Irizarry, G.; Genova, V. *Lab on a Chip* **2003**, *3*, 121-127.

(71) Rotting, O.; Ropke, W.; Becker, H.; Gartner, C. *Microsystem Technologies* **2002**, *8*, 32–36.

(72) McDonald, J. C.; Whitesides, G. M. *Acc Chem Res* **2002**, *35*, 491-499.

(73) Soper, S. A.; Ford, S. M.; Qi, S.; McCarley, R. L.; Kelly, K.; Murphy, M. C. *Analytical Chemistry* **2000**, *72*, 642A-651A.

(74) Becker, H.; Gartner, C. *Electrophoresis* **2000**, *21*, 12-26.

(75) Fredrickson, C., University of Florida, Gainesville, 2005.

(76) Hofmann, O.; Che, D. P.; Cruickshank, K. A.; Muller, U. R. *Analytical Chemistry* **1999**, *71*, 678-686.

(77) Macounova, K.; Cabrera, C. R.; Holl, M. R.; Yager, P. *Analytical Chemistry* **2000**, *72*, 3745-3751.

(78) Li, C.; Yang, Y.; Craighead, H. G.; Lee, K. H. *Electrophoresis* **2005**, *26*, 1800-1806.

(79) Cui, H.; Horiuchi, K.; Dutta, P.; Ivory, C. F. *Anal Chem* **2005**, *77*, 1303-1309.

(80) Xu, Y.; Zhang, C. X.; Janasek, D.; Manz, A. *Lab on a Chip* **2003**, *3*, 224-227.

(81) Herr, A. E.; Molho, J. I.; Drouvalakis, K. A.; Mikkelsen, J. C.; Utz, P. J.; Santiago, J. G.; Kenny, T. W. *Analytical Chemistry* **2003**, *75*, 1180-1187.

(82) Raisi, F.; Belgrader, P.; Borkholder, D. A.; Herr, A. E.; Kintz, G. J.; Pourhamadi, F.; Taylor, M. T.; Northrup, M. A. *Electrophoresis* **2001**, *22*, 2291-2295.

(83) Wang, Y. C.; Choi, M. H.; Han, J. *Anal Chem* **2004**, *76*, 4426-4431.

(84) Chen, X. X.; Wu, H. K.; Mao, C. D.; Whitesides, G. M. *Analytical Chemistry* **2002**, *74*, 1772-1778.

(85) Griebel, A.; Rund, S.; Schonfeld, F.; Dorner, W.; Konrad, R.; Hardt, S. *Lab on a Chip* **2004**, *4*, 18-23.

(86) Lee, H. G. *J Chromatogr A* **1997**, *790*, 215-223.

(87) Tian, H. J.; Landers, J. P. *Analytical Biochemistry* **2002**, *309*, 212-223.

(88) Shen, Y. F.; Smith, R. D. *Journal of Microcolumn Separations* **2000**, *12*, 135-141.

(89) Li, Y.; DeVoe, D. L.; Lee, C. S. *Electrophoresis* **2003**, *24*, 193-199.

(90) Harrison, D. J.; Fluri, K.; Seiler, K.; Fan, Z. H.; Effenhauser, C. S.; Manz, A. *Science* **1993**, *261*, 895-897.

(91) Fredrickson, C. K.; Fan, Z. H. *Lab Chip* **2004**, *4*, 526-533.

(92) Shimao *Electrophoresis* **1986**, *7*, 121-128.

(93) Bard, A. J.; Faulkner, L. R. *Electrochemical Methods: Fundamentals and Applications*; John Wiley & Sons: New York, 1980.

(94) Liu, Z. L., T.;Pawliszyn *Journal of Proteome Research* **2006**, *5*, 1246-1251.

(95) Svensson, H. *Acta Chemica Scandinavica* **1961**, *15*, 325-341.

(96) Zilberstein, G. V. B., Emmanuil M.; Bukshpan, Shmuel. *Electrophoresis* **2003**, *24(21)*, 3735-3744.

(97) Frumin, L. L. Z., G. V.; Peltek, S. E. *Journal of Biochemical and Biophysical Methods* **2000**, *45(2)*, 205-209.

(98) Herr, A. E.; Molho, J. I.; Santiago, J. G.; Kenny, T. W.; Borkholder, D. A.; Kintz, G. J.; Belgrader, P.; Northrup, M. A., Hilton Head, SC 2000; 115-119.

(99) Richards, D. P.; Stathakis, C.; Polakowski, R.; Ahmadzadeh, H.; Dovichi, N. J. *Journal of Chromatography A* **1999**, *853*, 21-25.

(100) Das, C.; Xia, Z.; Stoyanov, A.; Fan, Z. H. *Instrumentation Science and Technology* **2005**, *33*, 379-389.

(101) Baker, D. R. *Capillary Electrophoresis*; John Wiley and Sons Inc: New York, NY, 1995.

(102) Snyder, L. R.; Kirkland, J. J. *Introduction to modern liquid chromatography*, 2d ed.; Wiley: New York, 1979.

(103) Yang, C.; Zhu, G.; Zhang, L.; Zhang, W.; Zhang, Y. *Electrophoresis* **2004**, *25*, 1729–1734.

(104) Gao, L.; Liu, S. *Anal Chem* **2004**, *76*, 7179-7186.

(105) Lu, J. J.; Liu, S.; Pu, Q. *J Proteome Res* **2005**, *4*, 1012-1016.

(106) Das, C. F., Z.H.; *Electrophoresis* **2006**, *27*, 3619-3626.

(107) Viney, C. F., R.A. *Eur. J. Phys.* **1998**, *19*, 575-580.

(108) Ewing, A. G. W., R.A.; Olefirowicz, T.M.; *Analytical Chemistry* **1989**, *61*, 292-303.

(109) Herr, A. E.; Molho, J. I.; Drouvalakis, K. A.; Mikkelsen, J. C.; Utz, P. J.; Santiago, J. G.; Kenny, T. W. *Anal Chem* **2003**, *75*, 1180-1187.

(110) Macounova, K.; Cabrera, C. R.; Holl, M. R.; Yager, P. *Anal Chem* **2000**, *72*, 3745-3751.

(111) Poole, S. K.; Patel, S.; Dehring, K.; Workman, H.; Poole, C. F. *J Chromatogr A* **2004**, *1037*, 445-454.

(112) Chen, X. Z., J.; Zhai, H.; Chen, X; Hu, Z.; *Food Chemistry* **2005**, *92*, 381-386.

BIOGRAPHICAL SKETCH

Champak Das is currently pursuing his PhD in mechanical engineering from the University of Florida–Gainesville. Prior to joining University of Florida in 2003 he finished his M.S in mechanical engineering from Florida Institute of Technology, Melbourne in 2003 and B.S in mechanical engineering from Jadavpur University–Calcutta, India in 1998.After his B.S he joined Eveready Industries India Ltd. as a Development engineer and worked there for 3 years. His current research activities involve microfluidics, microscale electrophoresis and laser based diagnostics.